MATHEMATICAL MODELING OF A BUBBLING FLUIDIZED BED COMBUSTOR CO-FIRED WITH COTTON RESIDUE AND LIGNITE

A THESIS SUBMITTED TO
THE GRADUATE SCHOOL OF NATURAL AND APPLIED SCIENCES
OF
MIDDLE EAST TECHNICAL UNIVERSITY

BY

MEHMET SONER YAŞAR

IN PARTIAL FULFILLMENT OF THE REQUIREMENTS
FOR
THE DEGREE OF MASTER OF SCIENCE
IN
CHEMICAL ENGINEERING

DECEMBER 2018

Approval of the thesis:

MATHEMATICAL MODELING OF A BUBBLING FLUIDIZED BED COMBUSTOR CO-FIRED WITH COTTON RESIDUE AND LIGNITE

submitted by **MEHMET SONER YAŞAR** in partial fulfillment of the requirements for the degree of **Master of Science in Chemical Engineering Department, Middle East Technical University** by,

Prof. Dr. Halil Kalıpçılar
Dean, Graduate School of **Natural and Applied Sciences**

Prof. Dr. Pınar Çalık
Head of Department, **Chemical Engineering**

Prof. Dr. Görkem Külah
Supervisor, **Chemical Engineering Dept., METU**

Prof. Dr. Nevin Selçuk
Co-Supervisor, **Chemical Engineering Dept., METU**

Examining Committee Members:

Prof. Dr. Murat Köksal
Mechanical Engineering Dept., Hacettepe University

Prof. Dr. Görkem Külah
Chemical Engineering Dept., METU

Prof. Dr. Nevin Selçuk
Chemical Engineering Dept., METU

Asst. Prof. Dr. Özgür Ekici
Mechanical Engineering Dept., Hacettepe University

Asst. Prof. Dr. İnci Ayrancı
Chemical Engineering Dept., METU

Date: 14.12.2018

I hereby declare that all information in this document has been obtained and presented in accordance with academic rules and ethical conduct. I also declare that, as required by these rules and conduct, I have fully cited and referenced all material and results that are not original to this work.

Name, Surname: Mehmet Soner Yaşar

Signature:

ABSTRACT

MATHEMATICAL MODELING OF A BUBBLING FLUIDIZED BED COMBUSTOR CO-FIRED WITH COTTON RESIDUE AND LIGNITE

Yaşar, Mehmet Soner
M.Sc., Department of Chemical Engineering
Supervisor : Prof. Dr. Görkem Külah
Co-Supervisor: Prof. Dr. Nevin Selçuk

December 2018, 129 pages

A comprehensive system model, previously developed for prediction of combustion behaviors of Turkish lignites, lignite/hazelnut shell and lignite/olive residue blends in fluidized bed combustors, is extended for modeling of co-combustion of Turkish lignite and cotton residue in a bubbling fluidized bed combustor. Cotton residue has high nitrogen content (~ 4.1 wt. % a.r.) unlike lignite (~ 0.9 wt. % a.r.), olive residue (~ 1.6 wt. % a.r.) and hazelnut shell (~ 0.5 wt. % a.r.), which leads to relatively high emissions of nitric oxides (NO_x) and nitrous oxide (N_2O). For accurate prediction of emissions of NO and N_2O, a sufficiently detailed NO and N_2O formation and reduction reaction scheme is incorporated into the existing model. The assessment of the accuracy of the model is tested by comparing its predictions against the experimental data obtained in METU 0.3 MW_t atmospheric bubbling fluidized bed combustor (ABFBC) where a typical Turkish lignite is co-fired with limestone and cotton residue. Reasonable comparisons are obtained between the predicted and measured O_2, CO, CO_2, SO_2, NO and N_2O concentrations and temperature profiles. The results obtained in this study show that the addition of cotton residue increases emission of total nitrogenous species due to its high nitrogen content, but the main effect is observed in the increase of N_2O formation. Furthermore, determination of the fuel nitrogen partitioning into char and volatiles and distribution of volatile nitrogen species are found to be the most important parameters for modeling of NO and N_2O emissions in bubbling fluidized bed combustor.

Keywords: Co-combustion, lignite, cotton residue, mathematical modeling, NO and N_2O emission

ÖZ

PAMUK ARTIĞI VE LİNYİTİN KABARCIKLI AKIŞKAN YATAKLI YAKICIDA BİRLİKTE YAKILMASININ MATEMATİKSEL MODELLENMESİ

Yaşar, Mehmet Soner
Yüksek Lisans, Kimya Mühendisliği Bölümü
Tez Danışmanı : Prof. Dr. Görkem Külah
Ortak Tez Danışmanı: Prof. Dr. Nevin Selçuk

Aralık 2018, 129 sayfa

Bu çalışmada, daha önce, Türk linyitlerinin, linyiti/fındık kabuğu ve linyit/zeytin artığı (prina) karışımlarının yanma davranışlarının öngörülmesi için geliştirilmiş kapsamlı bir model Türk linyitinin pamuk küspesi ile kabarcıklı akışkan yataklı yakıcıda birlikte yakılmasının modellenmesi için genişletilmiştir. Linyitin (~ % 0,9 orijinalde), zeytin artığının (~ % 1,6 orijinalde) ve fındık kabuğunun (~ % 0,5 orijinalde) aksine pamuk küspesi yüksek azot içeriğine sahiptir (~ % 4,1 orijinalde), ve bu nispeten yüksek azot oksit (NO_x) ve azot protoksit (N_2O) emisyonlarına sebep olmaktadır. NO ve N_2O emisyonlarının doğru bir şekilde öngörülebilmesi için, yeterince detaylı bir NO ve N_2O oluşum ve indirgenme reaksiyon şeması mevcut modele dahil edilmiştir. Modelin doğruluğu, tipik bir Türk linyitinin kireç taşı ve pamuk küspesi ile birlikte yakıldığı, ODTÜ 0.3 MW_t atmosferik kabarcıklı akışkan yataklı yakıcıda (AKAYY) yapılan deneylerden elde edilen sonuçlarla kıyaslanarak test edilmiştir. Karşılaştırma sonucunda, O_2, CO, CO_2, SO_2, NO ve N_2O konsantrasyonları ve sıcaklık profilleri öngörüleri ile deneysel ölçümleri uyum içinde bulunmuştur. Bu çalışmada elde edilen sonuçlar, yakıta pamuk küspesi katılmasının, yüksek azot içeriğinden dolayı, toplam azotlu bileşik emisyonunu arttırdığını göstermiştir fakat ana etkinin N_2O'nun oluşumunun artmasında olduğu gözlemlenmiştir. Ayrıca, kabarcıklı akışkan yataklı yakıcılarda NO ve N_2O emisyonlarının modellenmesi için en önemli parametrelerin yakıt azotunun kok azotu ve uçucu azota bölünmesinin ve uçucu azot bileşiklerinin dağılımı olduğu bulunmuştur.

Anahtar Kelimeler: Beraber yanma, linyit, pamuk küspesi, matematiksel modelleme, NO ve N_2O emisyonları

To My Family

ACKNOWLEDGEMENTS

I wish to express my deepest gratitude to my supervisor Prof. Dr. Görkem Külah and my co-supervisor Prof. Dr. Nevin Selçuk for their guidance, advice, encouragements and insight throughout the research.

Financial supports provided by Middle East Technical University (METU) through BAP-07-02-2017-004-222 project is gratefully acknowledged.

I also thank to the Clean Combustion Laboratory members for their friendship and support during this study; Cihan Ateş, Özge Batır, Özge Şen and Batıkan Özdamar.

My special thanks go to my friends from undergraduate for their friendship; Göksu Kutlu, Aykut Yavuz, Can Yıldırım, M. Nur Aşkın and Doğan İlgün. I also would like to thank to friends from graduate for their endless support and friendship during this study; Nur Ber Emerce, Nisa Erişen, Aslı Karausta, Yağmur Çulhacıoğlu, Beril Dumanlılar, Berkan Atman; Fatma Şahin, Merve Sarıyer, Zeynep Karakaş, Selin Şahin, Merve Özkutlu, Berrak Erkmen, Ezgi Yavuzyılmaz, Seda Sivri, Neslin Güler, Almira Çaldıklıoğlu and Burak Akdeniz. Besides my dearest friends, I also would like to Songül the cat.

Last but not the least, I want to express my deepest pleasure to my mother Hatice Yaşar, my father Fettah Yaşar, my sisters Feza Demirarslan and Deniz Yaşar, my brother-in-law Ümit Demirarslan and my nieces Öykü Mercan & Aden Ela Demirarslan.

TABLE OF CONTENTS

CHAPTERS

LIST OF TABLES

TABLES

LIST OF FIGURES

FIGURES

LIST OF SYMBOLS

a	Decay constant, cm^{-1}
A	Cross-sectional area, cm^2
c_p	Specific heat capacity, $cal\ g^{-1}\ K^{-1}$
C	Concentration, $mol\ cm^{-3}$
C_D	Drag Coefficient
d	Diameter, cm
E	Activation energy, $cal\ mol^{-1}$
$E(r)$	Elutriation rate constant, s^{-1}
F	Mass flow rate of solid streams, $g\ s^{-1}$
F_z	Upward flow rate of entrained particles at any height in freeboard, $g\ s^{-1}$
$f(E)$	Activation energy distribution function for devolatilization, $mol\ cal^{-1}$
g	Gravitational acceleration, $cm\ s^{-2}$
h	Individual heat transfer coefficient, $cal\ cm^{-2}\ s^{-1}\ K^{-1}$
H	Height, cm
ΔH^0	Heat of reaction at standard state, $cal\ mol^{-1}$
k	Overall sulfation rate constant, $cm\ s^{-1}$; thermal conductivity, $cal\ cm^{-1}\ s^{-1}$
$k(E)$	First order reaction rate constant for devolatilization, s^{-1}
k_f	Film mass transfer coefficient, $cm\ s^{-1}$
k_s	First order surface reaction rate constant for char combustion, $cm\ s^{-1}$
K_{be}	Film mass transfer coefficient, $cm\ s^{-1}$
K_i^*	Total flux of entrained particles in size i, $g\ cm^{-2}\ s^{-1}$
$K_{i,h}^*$	Cluster flux of entrained particles in size i, $g\ cm^{-2}\ s^{-1}$
$K_{i,\infty}^*$	Dispersed non-cluster flux of entrained particles in size i, $g\ cm^{-2}\ s^{-1}$
L	Length, cm
m	Mass flow rate, $g\ s^{-1}$
M	Molecular or atomic weight, $g\ mol^{-1}$; hold-up in the bed, g

n	Index of the dimension; molar flow rate, $mol\ s^{-1}$; molar generation/ consumption rate, $mol\ s^{-1}$
$P_0(r)$	Size distribution of inlet fuel particles, cm^{-1}
$P_{bd}(r)$	Size distribution of bed drain particles, cm^{-1}
$P_{bed}(r)$	Size distribution of char particles in the bed, cm^{-1}
$P_{CO}(r)$	Size distribution of carry over char particles, cm^{-1}
$P_z(r)$	Size distribution of entrained char particles at any height in freeboard, cm^{-1}
Q	Volumetrix flow rate, $cm^3\ s^{-1}$; energy generation/loss rate, $cal\ s^{-1}$
r	Spatial independent variable, cm; rate of reaction, $mol\ cm^{-3}\ s^{-1}$
r_C	Carbon consumption rate on the surface of char particle, $mol\ cm^{-2}\ s^{-1}$
r_{HCN}	Rate of HCN oxidation in the gas phase, $mol\ cm^{-3}\ s^{-1}$
r_{SO_2}	Rate of sulfation reaction, $mol\ s^{-1}$
$r_{SO_2,elut}$	Rate of sulfation due to CaO particles carried by elutriation, $mol\ s^{-1}$
$r_{SO_2,ent}$	Rate of sulfation due to CaO particles carried by bubble eruption, $mol\ s^{-1}$
R	Ideal gas constant, $cal\ mol^{-1}\ K^{-1}$; radius, cm
$\mathbf{R}$	Energy generation/loss rate in freeboard, $cal\ cm^{-3}\ s^{-1}$
$\Re$	Species generation/depletion rate, $mol\ cm^{-3}\ s^{-1}$
$\Re(r)$	Shrinkage rate of particles, $cm\ s^{-1}$
S	External sorbent surface area, cm^2
t	Time, s
T	Temperature, K
u	Velocity, $cm\ s^{-1}$
u_0	Superficial gas velocity, $cm\ s^{-1}$
U	Overall heat transfer coefficient, $cal\ cm^{-2}\ s^{-1}\ K^{-1}$
V	Volume, cm^3
x	Mass fraction; spatial independent variable, cm
$x_{N,vol}$	Mass fraction of volatile nitrogen in the fuel nitrogen
x_{NH_3}	Molar ratio of NH_3 in the volatile nitrogen

x_{HCN}	Molar ratio of HCN in the volatile nitrogen
x_{N_2}	Molar ratio of N_2 in the volatile nitrogen
$X_{N \rightarrow NO}$	Fractional conversion of char nitrogen to NO
$X_{N \rightarrow N_2O}$	Fractional conversion of char nitrogen to N_2O
x_{vl}	Fraction of volatiles released in the bed
y	Mole fraction
z	Spatial independent variable, *cm*

Greek Letters

α	Thermal diffusivity, $cm^2\ s^{-1}$
δ	Bubble phase volume fraction
ε	Voidage; emissivity; convergence criterion
η	Contact efficiency
λ^0	Latent heat of vaporization at standard state, cal g^{-1}
μ	Viscosity, $g\ cm^{-1}\ s^{-1}$
v	Volatile released, %
v_∞	Ultimate yield of volatile releases, %
ρ	Density, $g\ cm^{-3}$
σ	Standard deviation of activation energy distribution, $J\ mol^{-1}$; Stephan-Boltzman constant, $cal\ cm^{-2}\ s^{-1}\ K^{-4}$; Fractional sorbent surface area
τ	Residence time
τ_{max}	
φ	Sphericity

Subscripts

0	Initial; feed
a	Air; ash
avg	Average
b	Bubble

bd	Bed drain
bed	Bed
bio	Biomass originated
bw	Bed wall
C	Carbon
CaO	Calcined limestone (CaO)
CO	Carry over
coal	Coal originated
cw	Cooling water
d	Char
e	Emulsion
elut	Elutriation
ent	Entrainment
f	Freeboard; feed fuel; fluidization
fc	Fixed carbon
fw	Freeboard wall
g	Gas
H	Hydrogen
het	Heterogeneous
i	Inert; inner
j	Species index
lst	Limestone
max	Maximum
maxe	Maximum elutriated
mf	Minimum fluidization
min	Minimum
N	Nitrogen
o	Outer
O	Oxygen
p	Particle
r	Reference

rxn	Reaction
S	Sulfur
s	Surface; solid
T	Tube
t	Terminal
tf	Through-flow
vm	Volatile Matter
w	Wall; water

Abbreviations

d.a.f.	Dry and ash free
ABFBC	Atmospheric Bubbling Fluidized Bed Combustor
BFBC	Bubbling Fluidized Bed Combustor
CFBC	Circulating Fluidized Bed Combustor
CFD	Computational Fluid Dynamics
FC	Fixed Carbon
FBC	Fluidized Bed Combustor
FTIR	Fourier Transform Infrared Spectroscopy
TGA	Thermogravimetric Analyzer
VM	Volatile Matter

CHAPTER 1

INTRODUCTION

Coal is the most abundant fuel in the world and its current reserves are approximately five times the reserves of oil and gas. It will therefore be used in the future for energy production, in an attempt to cope with the increasing energy demand. Turkey has widely spread reserves of lignite which is characterized by its high ash, moisture, volatile matter and sulfur content.

However, gradual introduction of increasingly restrictive legislations on emissions from fossil fuel combustion and necessity to increase the life of existing fossil fuel resources have been increasing the interest in combustion of alternative fuels such as biomass. Biomass can be considered as a renewable and green energy source due to the fact that it is CO_2-neutral and an effective remedy to reduce emissions of this greenhouse gas. In addition to that, biomass is the fourth largest energy source after fossil fuels and that about 10 % of the world's energy is produced by biomass [1]. On the other hand, utilization of biomass alone may cause severe operational problems and unscheduled shut-downs in the industry and utility boilers such as bed agglomeration, ash deposition and corrosion.

Among all alternatives, co-combustion of biomass with coal is the most promising option which compensates the drawbacks of burning biomass and coal as individual fuels. Biomass addition to coal-fired systems provides reduction in gaseous emissions whereas coal addition to biomass provides effective utilization of biomass. Fuel flexible feature of fluidized bed combustors (FBCs) makes it the best option, or sometimes the only option, for co-firing applications. The other attractive features of FBCs are high combustion efficiency, lower operational temperature, in-situ desulfurization and low NO_x emissions.

FBCs are commonly used for the combustion of low quality fuels such as lignite, which is a major indigenous energy source of Turkey with an estimated quantity of 15.7 billion tons of reserves [2]. Furthermore, olive residue, hazelnut shell and cotton residue are three of the most important sources of biomass in Turkey. Turkey is one of the main olive producers in the world with 846 000 ha of olive groves and 2 100 000 tons (1 640 000 tons for oil) olive production [3]. Olive residue is a specific type of biomass which is the remaining part of olives after pressing and extraction of olive oil. Annual production of olive residue is estimated as 656 000 tons [4]. Hazelnut production in Turkey accounts for 70 % of the worlds' total production with 707 000 ha of plantation and 675 000 tons of production [3,5]. Hazelnut shells have annual production of 338 000 tons [5]. Furthermore, Turkey is one of the leading producers of cotton with 502 000 ha of plantation and 2 450 000 tons (1 470 000 tons of seed) of cotton production [3]. The remaining part of cotton seed, which is produced by removal of cotton lint and fiber by ginning process, after extraction of cotton oil is called cotton residue. Annual production of cotton residue is predicted as 588 000 tons [6]. Consequently, significant amounts of these agricultural residues and indigenous lignite reserves are available to be used in co-combustion of lignite and biomass residues, and this necessitates a detailed understanding of co-firing of lignite and biomass. Such an objective requires mathematical modeling studies as well as experimental investigations.

Over the last few decades, comprehensive research, including both mathematical modeling studies [7–12] and experimental investigations in a pilot scale bubbling FBC [13–16], for the investigation of combustion, in-situ desulfurization and NO_x emission behaviors of Turkish lignites and Turkish lignite/biomass blends was conducted in Clean Combustion Laboratory in the Middle East Technical University. Among these studies, co-combustion of lignite/olive residue and lignite/hazelnut shell blends were simulated and successfully validated against the experimental data obtained in a pilot scale bubbling FBC [11–14]. Regarding the cotton residue, no modeling study for the co-combustion of lignite and cotton residue was carried out although experimental data was available for validation [14]. Cotton residue is a type of biomass characterized by its high nitrogen content (~ 4.1 wt. % in as-received basis) unlike lignite (~ 0.9 wt. % in as received basis), olive residue (~ 1.6 wt. % in as received basis) and hazelnut shell (~ 0.5 wt. % in as received basis). It is indeed this high nitrogen content that leads to relatively high emissions of nitric oxides (NO_x) and nitrous oxide (N_2O) [17,18]. Nitric oxides contribute to acid rain and photochemical smog in the atmosphere. On the other hand, nitrous oxide is known to be a greenhouse gas, and global warming potential of N_2O is about 298 times greater than that of that of CO_2 [19]. Furthermore, N_2O is involved in destruction of stratospheric ozone layer, which absorbs ultraviolet radiation [20]. Consequently, investigation of emissions of NO_x and N_2O is of prior importance.

Absence of a comprehensive mathematical model for co-combustion of cotton residue and lignite in a bubbling FBC on one hand, necessity for detailed understanding of NO and N_2O formation and reduction mechanisms in fluidized bed co-combustion of coal and cotton residue on the other, requires extension of a previously developed system model by incorporating N_2O formation and reduction mechanisms to predict the emissions of N_2O and also NO. To achieve this objective, a comprehensive system model, originally proposed by Selcuk and Sivrioğlu [21] and later improved, extended and validated against experimental data by Selcuk and her colleagues [7–12] is chosen as a basis. A sufficiently detailed NO and N_2O formation and reduction reaction scheme is developed for this high nitrogen content biomass. The fuel nitrogen split into char and volatiles and the distribution of volatile nitrogen species, which are unique to lignite and cotton residue, are determined by pyrolysis experiments. The accuracy of the model is tested by comparing its predictions with on-line temperature and concentration measurements of O_2, CO_2, CO, SO_2, NO_x, and N_2O obtained in METU 0.3 MW_t ABFBC where a typical Turkish lignite, with high VM/FC ratio (~ 1.2) and high ash content (~27 wt. %), with and without limestone is fired and Turkish lignite with limestone and cotton residue, with high nitrogen content (~ 4.1 wt. %), is co-fired in their own ashes.

CHAPTER 2

NO AND N_2O FORMATION AND REDUCTION IN FBCs

The formation and reduction of nitrous oxide (N_2O) and nitrogen oxides (NO_x), which are emitted mostly as nitric oxide (NO) with smaller amounts of nitrogen dioxide (NO_2), depend on the fuel type, fuel characteristics and the operation conditions of the combustor. NO_x and N_2O can originate from two main sources: from atmospheric nitrogen (by thermal and prompt processes) and from fuel nitrogen. The thermal process involves the direct oxidation of atmospheric nitrogen. This process is significant at high temperatures around 1700 K [22] and can be neglected in typical operation temperatures of fluidized bed combustors (FBCs). Similarly, prompt processes, which involve the reaction between hydrocarbon radicals that are produced mainly at high temperatures, do not contribute to NO_x and N_2O formation significantly at fluidized bed operation conditions.

Nitrogen in the solid fuels can be organically or inorganically bound to the fuel structure [23,24]. Nitrogen in coals and biomasses is largely organically bound in the fuel, although some inorganic nitrogen may be present as ammonium ions in high rank coals [24]. The nitrogen content of low rank coals typically ranges between 0.5 – 2.5 wt. % (d.a.f. basis) and increases with the increase in the carbon content. The nitrogen content of the biomass varies with the type of biomass. The typical nitrogen contents of some selected biomass and coal are presented in Table 2.1.

Table 2.1 Typical nitrogen contents of some selected biomasses and coals

Fuel	**N content (d.a.f. wt. %)**	**Ref.**
Bituminous Coal	1.0 – 2.7	[25–28]
Lignite	0.7 – 2.4	[27,29–33,16,34]
Brown Coal	0.5 – 0.9	[25,26,35,36]
Wood	0.05 – 1.0	[37]
Peat	1.7 – 3.6	[25,29]
Bark	0.2 – 0.6	[25,29]
Straw	0.04 – 0.7	[37]
Rice Straw	0.95	[37]
Olive Residue	0.3 – 1.8	[33,37]
Hazelnut Shell	0.2 – 1.3	[33,37]
Safflower Seed	3.1	[37]
Rapeseed	3.9	[37]
Cotton Stalk	0.3 – 1.4	[38–41]

Nitrogen in coal can be found mainly in the forms of pyridinic, pyrrolic and quaternary structures and small amounts are found in the amino groups especially in low rank coals [24,42,43] whereas the protein and amino structures are the main nitrogen functionalities in biomasses [26,44,45]. Although several studies have been conducted to correlate the functional forms of fuel nitrogen with the evolution of nitrogenous species such as NO, N_2O, NH_3 and HCN, the subject is still open to discussion as no clear dependence could be established due to insufficiency of quantitative methods used and wide range of fuel properties [24,43,46,47].

Conversion of fuel nitrogen into NO_x and N_2O is very complex. The process comprises of evolution of nitrogenous products during devolatilization and char combustion, and concurrent reactions among these species either in gas phase or solid phase over catalytic surfaces like char and ash. An overall reaction scheme illustrating the main formation and reduction paths, adopted from Svoboda et al. [48], is given in Figure 2.1. In this chapter, these paths will be explained in detail. Furthermore, the available information in the literature by taking fluidized bed combustion conditions and lignite and cotton residue as fuel types into consideration will be reviewed. Special emphasis will be placed on N_2O formation and reduction mechanisms since one of the objectives of this study is to incorporate these mechanisms into a previously developed model to be able to predict NO and N_2O emitted during combustion of lignite with and without limestone and co-combustion of lignite with limestone and cotton residue.

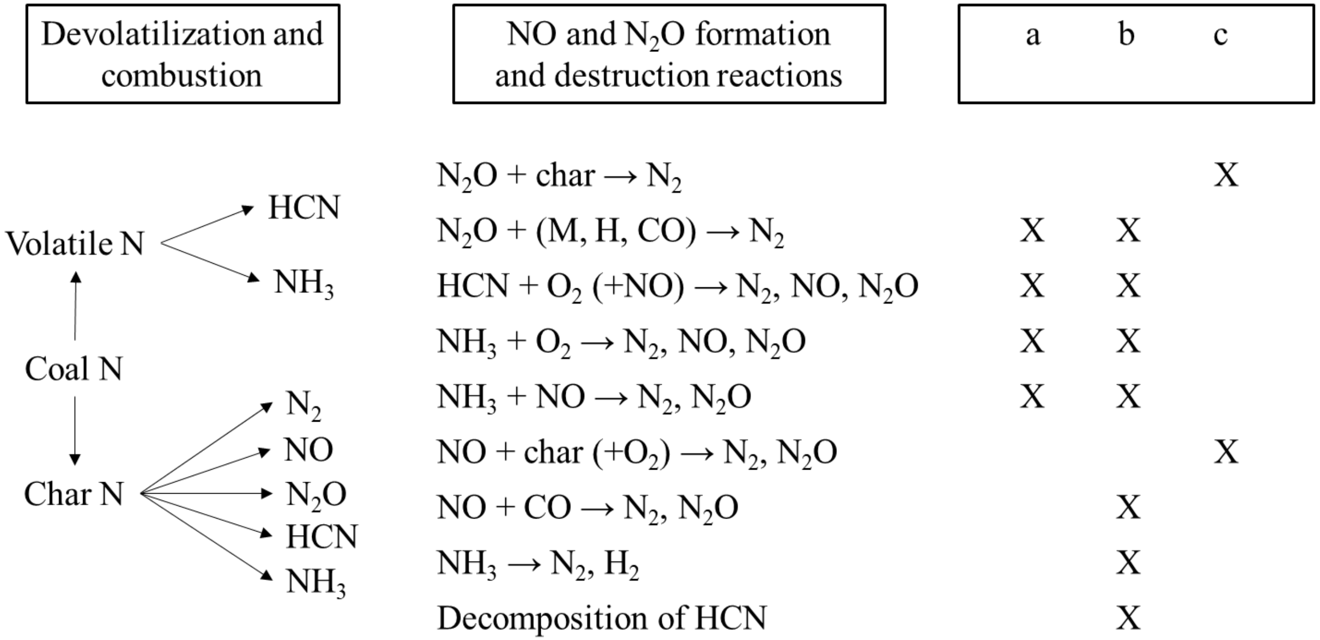

NO and N_2O formation and destruction reactions	a	b	c
N_2O + char → N_2			X
N_2O + (M, H, CO) → N_2	X	X	
HCN + O_2 (+NO) → N_2, NO, N_2O	X	X	
NH_3 + O_2 → N_2, NO, N_2O	X	X	
NH_3 + NO → N_2, N_2O	X	X	
NO + char (+O_2) → N_2, N_2O			X
NO + CO → N_2, N_2O		X	
NH_3 → N_2, H_2		X	
Decomposition of HCN		X	

a) Homogeneous reaction, b) heterogeneous reaction catalyzed, c) heterogeneous reaction non-catalyzed

Figure 2.1 The pathway of fuel-N conversion to NO and N_2O [48]

2.1 Devolatilization of Solid Fuels

Devolatilization is the thermal decomposition of a solid fuel. During devolatilization, fuel nitrogen is partitioned into volatile nitrogen and char nitrogen. The partitioning of nitrogen between volatiles and char as well as the volatile nitrogen composition depends mainly on fuel type and the temperature of the medium.

Primary devolatilization is the first step during combustion after moisture release. During primary devolatilization, which occurs at lower temperatures, the release of liquid (tar) and gaseous (light hydrocarbons, CO_x, H_2O, H_2S etc.) products and formation of char takes place [49,50]. At higher temperatures or long residence times, the secondary devolatilization takes place where the formed tar and char further decompose into light gases such as CO, H_2, CH_4, C_2H_4, HCN etc. [24,49]. Low rank coals release less tar and higher amounts of light gases [24]. Biomasses, on the other hand, are characterized by lower char yields and higher yields of tar and light gases [24]. However, tars from biomass are more reactive and decompose thermally at lower temperatures.

Wu and Ohtsuka [31,51] carried out pyrolysis studies with different types of coals including lignite at several heating rates, from 10 K/min and 1400 K/min. They observed that almost half of the fuel nitrogen was released as N_2 around temperatures of 800 °C. Furthermore, Yuan et al. [44,52] conducted rapid pyrolysis tests with several biomasses (rice straw, pine saw dust, chinar leaves, soy bean cake and two aquatic biomass) at 600 – 1200 °C using high frequency furnace. They concluded that nitrogen in all the biomass fuels is mainly converted to N_2, and only small part of nitrogen was retained in the char for all biomasses studied. They reported that, at 800 – 900 °C, 80 to 90 % of the fuel nitrogen was released as N_2.

The other nitrogenous species formed during devolatilization are HNCO, NH_3 and HCN. HNCO was found to be in minor amounts during devolatilization of coal and biomass [24,46].

The formation of NH_3 and HCN during pyrolysis of coal and biomass has been extensively studied in the literature [44,46,53–55]. It was concluded that HCN/NH_3 ratio is a function of chemical and physical properties of the fuel as well as the temperature and heating rate. Therefore, this ratio should be determined in a laboratory system such as TGA-FTIR, operating at conditions relevant to combustion system, for each fuel under investigation.

2.2 NO and N_2O Formation and Reduction Reactions

During combustion of coal and biomass, NO and N_2O are produced by volatile nitrogen and char nitrogen through homogeneous and heterogeneous reactions.

2.2.1 Homogeneous Reactions

2.2.1.1 Reactions of HCN

HCN is considered to be an important precursor for the formation of N_2O at typical FBC temperatures [56,57]. The following reaction scheme proposed by Desroches-Ducarne et al. [58] has been widely used in modeling of fluidized bed combustors [58–63].

$$HCN + \frac{1}{2}O_2 \rightarrow CNO \tag{2.1}$$

$$CNO + \frac{1}{2}O_2 \rightarrow NO + CO \tag{2.2}$$

$$CNO + NO \rightarrow N_2O + CO \tag{2.3}$$

In this scheme, HCN is first oxidized to CNO which is then converted to either NO or N_2O depending on the temperature of the medium and NO concentration.

2.2.1.2 Reactions of NH_3

Oxidation of NH_3 is considered to be an important source for NO and, at the same time, a strong reductant for NO under FBC conditions [57]. The principal reactions are:

$$NH_3 + \frac{5}{4}O_2 \rightarrow NO + \frac{3}{2}H_2O \tag{2.4}$$

$$NO + NH_3 + \frac{1}{4}O_2 \rightarrow N_2 + \frac{3}{2}H_2O \tag{2.5}$$

At FBC temperatures, NH_3 oxidation to N_2O was found to be of minor importance [57].

2.2.1.3 Reactions of N_2O

N_2O can be formed by oxidation of HCN or oxidation of char nitrogen. Reduction and decomposition of N_2O can take place by a large number of homogeneous and heterogeneous reactions. The following thermal decomposition reaction was suggested to be the most important route to homogeneous reduction of N_2O in fluidized bed combustors [64,65].

$$N_2O \rightarrow N_2 + \frac{1}{2}O_2 \tag{2.6}$$

Chen et al. [66] pointed out that, in the presence of water, reduction of N_2O by CO also takes place under FBC conditions:

$$N_2O + CO \rightarrow N_2 + CO_2 \tag{2.7}$$

2.2.2 Heterogeneous Reactions

Many heterogeneous reactions take place over surfaces of char, limestone and ash in fluidized bed combustors. These reactions are strongly influenced by particle size, carbon burnout for char, sulfation rate for limestone and the combustion environment. The important reactions will be reviewed in the following sections.

2.2.2.1 Oxidation of Char Nitrogen

During char combustion, NO is formed by direct oxidation. However, there is less agreement on the conversion mechanism of char nitrogen to N_2O. Several mechanisms were suggested in the literature and one of them is suggested by Goel et al. [67] to represent NO and N_2O formation during combustion of char in fluidized bed combustors.

In their mechanism, they postulated that oxygen breaks open the nitrogen containing aromatic rings. Oxygen then reacts with the nitrogen atoms to form an intermediate species, *I*, still bound to the char surface. The intermediate then splits to form NO or reacts with NO to form N_2O as shown below:

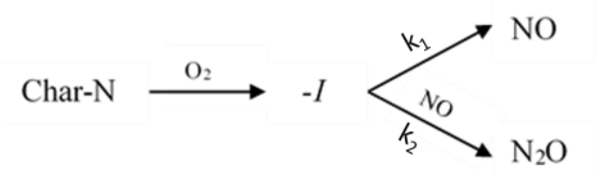

The fractional conversion of that intermediate species, *I*, into NO is $k_1/(k_1+k_2[NO])$ while that into N_2O is $k_2[NO]/(k_1+k_2[NO])$ where k_1 and k_2 are the rate constants for the reaction of the intermediate species, I, to produce NO and N_2O, respectively.

During char combustion, nitrogen retained in char is oxidized along with the oxidation of carbon. The oxidation rate is generally taken to be proportional to char combustion rate with a proportionality constant, N/C ratio, where N and C are the molar ratios of nitrogen and carbon content of the char [43].

2.2.2.2 Oxidation of Volatile Nitrogen

Volatile nitrogenous compounds, HCN and NH_3, oxidize over the catalytic surfaces of FBC solids such as char, limestone and ash [57]. The primary products of catalytic oxidation of volatile nitrogenous compounds are NO and N_2 which are formed by the following reactions:

$$NH_3 + \frac{5}{4}O_2 \rightarrow NO + \frac{3}{2}H_2O \qquad (2.8)$$

$$NH_3 + \frac{3}{4}O_2 \rightarrow \frac{1}{2}N_2 + \frac{3}{2}H_2O \qquad (2.9)$$

$$HCN + \frac{7}{4}O_2 \rightarrow NO + CO_2 + \frac{1}{2}H_2O \qquad (2.10)$$

$$HCN + \frac{5}{4}O_2 \rightarrow \frac{1}{2}N_2 + CO_2 + \frac{1}{2}H_2O \qquad (2.11)$$

Limestone: Calcined limestone is an extremely active catalyst for the oxidation of NH_3. Johnsson et al. [57] reported that the selectivity of NH_3 oxidation for NO formation was high (50 – 90 %) and increased with the medium temperature. In contrary, the selectivity of NH_3 oxidation for N_2O formation over calcined limestone was found to be negligible. Calcined limestone was also found to be an active catalyst for the oxidation of HCN. The selectivity of HCN oxidation for NO formation was reported to be 50 – 65 % [57]. On the other hand, the selectivity for N_2O formation was found to be negligible [57].

Although abovementioned studies reported the beneficial effect of limestone addition, several studies conducted in bubbling and circulating fluidized beds showed only marginal effect of limestone addition on NO [70] and N_2O [71–73] emissions. One reason for this outcome was reported to be due to the fact that part of the limestone present in the combustor is sulphated and relatively inactive [72].

Char: Char is also very active catalyst for the oxidation of both HCN and NH_3. Selectivity of NH_3 oxidation for NO was found to be between 80 – 90 % at 1123 K whereas selectivity of HCN oxidation for NO was found to be around 50 % [57].

However, catalytic effect of char on the HCN oxidation is not taken into consideration due to lack of appropriate kinetic data of char catalyzed HCN oxidation in the FBC conditions [58–61,74,75,18,76,77].

Ash: Catalytic activities of the ashes and bed materials depend on parent coal, and the activities of ashes of low rank coals were found to be higher for NH_3 oxidation possibly due to Ca and Fe contents [57]. Selectivity of NH_3 oxidation for NO formation was found to be around 60 – 70 % for ash [57]. In addition to that, Löffler et al. [78] reported that ashes of different type of fuels have strong catalytic effect on HCN oxidation, and formation of NO is favored. The activity might be due to CaO content of the ashes [78].

2.2.2.3 Reduction of NO

Interaction between NO and char extensively studied in the literature due to high potential of char particles for NO removal through gas solid reactions as well as the catalytic reaction in the presence of reductant species such as CO, NH_3 and H_2. Among them, gas-solid reaction between NO and char plays a key role in destruction of NO together with the catalytic reaction between NO and CO over char surface. Kinetics of NO-char reaction is influenced by char size and hold-up as well as the type of the parent fuel. Chars from reactive fuels such as lignite have high activity for NO reduction. The overall NO-char reaction can be taken as:

$$NO + Char \rightarrow \frac{1}{2}N_2 + CO \tag{2.12}$$

It is observed that the rate of NO reduction increases with increasing CO concentration [79,80] due to char catalyzed reduction of NO with CO, reaction (2.13):

$$NO + CO \xrightarrow{char} \frac{1}{2}N_2 + CO_2 \tag{2.13}$$

Furthermore, limestone is also found to be an active catalyst for the catalytic reduction of NO with CO [57] yet the presence of O_2 reduces the reaction rate and the catalytic activity is inhibited as the degree of sulfation increases.

The reduction of NO with H_2 and NH_3 occurs by the following catalytic reactions [57]:

$$NO + H_2 \rightarrow \frac{1}{2}N_2 + H_2O \tag{2.14}$$

$$NO + \frac{5}{2}H_2 \rightarrow NH_3 + H_2O \tag{2.15}$$

$$NO + \frac{2}{3}NH_3 \rightarrow \frac{5}{6}N_2 + H_2O \tag{2.16}$$

Char and limestone are very active catalysts for the catalytic reduction of NO with H_2. However, catalytic reduction of NO with H_2 is not significant in practical systems due to high conversion of H_2 into H_2O [48]. Calcined limestone, char and ash are the important catalysts for NO reduction with ammonia. However, for NO reduction with ammonia the activity of limestone is found to be relatively low compared to that for other limestone catalyzed reactions as the catalytic activity reduces with sulfation [57,81]. Furthermore, the influence of limestone is not significant in BFBCs as it was discussed in the previous section (*2.2.2.2*). Johnsson and Dam-Johansen [82] reported that catalytic reduction of NO with ammonia is only observed in the absence of oxygen, and that in the presence of oxygen ammonia is converted into NO and N_2 [82].

2.2.2.4 Reduction of N_2O

The possible products of the N_2O reduction by char are N_2, CO and CO_2 [83]. In a previous study [84], CO_2 and N_2 were the major products for the N_2O reduction over a lignite char with a product ratio of 1:2 at the temperature range between 650 – 950 K. Although CO was found at higher temperatures, the amount of CO never exceeded that of CO_2. Therefore, the overall reaction scheme can be taken as:

$$N_2O + Char \rightarrow \frac{1}{2}CO_2 + N_2 \tag{2.17}$$

Since the concentration of N_2O is generally much lower than that of CO and CO_2, neglection of CO as the N_2O reduction product will have negligible effect on CO and CO_2 concentrations.

Furthermore, in a previous study carried out in a FBC [65], activity of char on the N_2O decomposition is found to be 1000 times greater than that of bed material.

2.2.2.5 Decomposition of Volatile Nitrogen

NH_3 catalytically decomposes to give N_2 and H_2 over the surfaces of limestone and ash by the following reaction [57]:

$$NH_3 \rightarrow \frac{1}{2}N_2 + \frac{3}{2}H_2 \tag{2.18}$$

Decomposition of NH_3 was found not to take place over char [57]. Based on the FBC model calculation carried out by Johnsson [85], contribution of Reaction (2.18) to NH_3 consumption was found to be negligible.

Furthermore, HCN was found to react with calcined limestone to produce calcium cyanide ($CaCN_2$) mainly in the absence of O_2 or at very low concentrations [86].

$$2HCN + CaO(s) \rightarrow CaCN_2(s) + CO \tag{2.19}$$

2.3 Review of FBC Models Including NO and N_2O Emissions

2.3.1 Existing Models

In this chapter, the comprehensive mathematical models for fluidized bed combustors that incorporate NO and N_2O emission sub-model are critically reviewed. The details of the NO and N_2O sub-models presented in the literature are listed in Table 2.2. Assumptions deployed in Table 2.2 are detailed in Table 2.3. Although all these models were developed in order to predict the emissions of pollutant gaseous species NO and N_2O, there exist differences in the approaches to describe the nitrogen chemistry. Various methods were used for the determination of partitioning of fuel nitrogen into char and volatiles, and different volatile nitrogen species were taken into consideration. Furthermore, the homogeneous and heterogeneous reactions taken into consideration differ in the models presented in the literature. On the whole, these differences describe the diversity of the fluidized bed models including NO and N_2O emissions.

Table 2.2 Summary of models incorporates NO and N_2O formation and reduction

		A	**B**	**C**	**D**	**E**	**F**
Sung [76]	CFBC	n.i.	3	3	1 + 2b + 3e + 4 + 5c	1 + 2b + 3 + 4c	1a + 2a
Goel et al. [77]	BFBC	4a	3	3	1 + 2a + 4 + 5a	1 + 2a + 3 + 4c	3
Goel et al. [69]	CFBC	3	3	3/2	1 + 2a + 4 + 5a	1 + 2a + 3 + 4c	1a + 2a
Hannes [50]	CFBC	1	3	4	1 + 2b + 3e + 4 +5e	1 + 3 + 4b	1a + 2a
Desroches-Ducarne et al. [58]	CFBC	n.i.	1	3	1 + 2b + 3c + 4 + 5d	2b + 4a	1a + 2a
Chen et al. [66]	BFBC	4b	3	-	1 + 5a	1 + 3 + 4a	1b + 2b
Löffler et al. [74]	SFBC	3	1	3	1 + 2a + 3d + 4 + 5a	2a + 3	1b + 2b
Liu and Gibbs [59]	CFBC	2	3	3	1 + 2b + 3c + 4 + 5c	1 + 2b + 3 + 4d	1a
Zhou et al. [87,88]	BFBC	4b	3	-	1 + 5a	1 + 3 + 4a	3
Gungor and Eskin [62], **Gungor** [63]	CFBC	1	-	3	2b + 4 + 5a	2b + 3 + 4a	1a

n.i.: no information

Table 2.2 Summary of models incorporates NO and N_2O formation and reduction (continued)

		A	**B**	**C**	**D**	**E**	**F**
Gungor [89], **Gungor** [90]	CFBC	1	-	3	2b + 4 + 5a	2b + 3 + 4a	1b
Zhou et al. [75]	CFBC	3	1	1	1 + 4 + 5a	2b + 3	1b
Krzywanski et al. [91]	CFBC	n.i.	2	3	2a + 3c + 4 + 5e	1 + 2a + 3 + 4b	1b
Nikolopoulos et al. [60]	CFBC	1	3	1	1 + 2b + 4 + 5a	1 + 2b + 3 + 4a	1a + 2a
Xie et al. [92], **Zhong et al.** [61], **Xie et al.** [93]	CFBC	3	1	3	1 + 2b + 4 + 5a	2b + 3 + 4a	1b
Yu et al. [94]	CFBC	-	-	3	2b + 4 + 5a	2b + 3 + 4a	1b
Marias et al. [18]	BFBC	3	3	3	1 + 2b + 4 + 5a	1 + 2b + 3 + 4a	1b + 2b
Lu et al. [95]	BFBC	-	-	3	2b + 4 + 5a	2b	1b + 2b

n.i.: no information

Table 2.3 Nomenclature of Table 2.2

A) Partitioning into char nitrogen

1) Estimated based on empirical data or correlations based on bed temperature
2) Assumed to be proportional to total mass remained in the char
3) Estimated based on initial fuel properties
4) Fixed value
    a) 66 %
    b) 100 %

B) Char-N Oxidation Products

1) NO only
2) N_2O only
3) NO and N_2O

C) Volatile nitrogenous compounds

1) HCN only
2) NH_3 only
3) HCN and NH_3

D) Model for NO chemistry

1) Char nitrogen oxidation
2) Homogeneous volatile nitrogen oxidation
    a) Complex reaction mechanism with elementary reactions and radical species
    b) Simple reaction mechanism
3) Heterogeneous volatile nitrogen oxidation
    a) Char only
    b) Char and ash (or bed material)

Table 2.3 Nomenclature of Table 2.1 (continued)

    - c) Char, ash (or bed material) and CaO
    - d) Ash (or bed material) only
    - e) Char and CaO
  - 4) Homogeneous NO reduction
  - 5) Heterogeneous NO reduction
    - a) Char only
    - b) Char and ash (or bed material)
    - c) Char and CaO
    - d) Char, ash (or bed material) and CaO

E) Model for N_2O chemistry

  - 1) Char nitrogen oxidation
  - 2) Homogeneous HCN oxidation
    - a) Complex reaction mechanism with elementary reactions and radical species
    - b) Simple reaction mechanism
  - 3) Homogeneous N_2O reduction
  - 4) Heterogeneous N_2O reduction
    - a) Char only
    - b) Char and ash (or bed material)
    - c) Char and CaO
    - d) Char, ash (or bed material) and CaO

Table 2.3 Nomenclature of Table 2.1 (continued)

F) Model validation

1) NO concentration validation only
    - a) NO concentration profiles validation against experimental data
    - b) NO emission validation against experimental data

2) N_2O concentration validation only
    - a) N_2O concentration profiles validation against experimental data
    - b) N_2O emission validation against experimental data

3) No validation

The pioneering work in N_2O emission modeling studies for FBCs was carried out by Sung [76] in an attempt to verify their NO and N_2O measurements performed in CFBC test rig. NO and N_2O sub-model was incorporated into an overall comprehensive model which takes hydrodynamics, devolatilization, char combustion and NO and N_2O formation and reduction mechanisms to predict O_2, NO and N_2O concentration profiles. Volatile nitrogen was assumed to evolve as HCN and NH_3 only. Ash catalyzed reaction were excluded from the NO and N_2O formation and reduction sub-model. Furthermore, kinetic rate constants of oxidation of char-N to N_2O and reduction of NO and N_2O by char were adjusted to fit the predictions into measured NO and N_2O concentration profiles. A reasonable agreement was obtained between the prediction and measurements.

Another NO and N_2O modeling study for a BFBC and a CFBC was carried out by Goel et al. [69,77] by coupling nitrogen chemistry and fluid dynamics in an attempt to explain the effect of operational conditions on the nitric and nitrous oxide emissions. The fuel nitrogen was partitioned into both volatile and char nitrogen. A detailed kinetic mechanism for gas phase formation and reduction of NO and N_2O, including 340 elementary reactions and 55 chemical species, which contain both stable and radical species, was used. With regard to heterogeneous chemistry, a single particle model was utilized to include heterogeneous NO and N_2O formation and reduction. The predicted data was tested against a laboratory scale BFBC and a 12-

MW_{th} CFBC. Accuracy of the predictions of the CFBC and BFBC emission models were tested against measurements. Agreement for the CFBC and BFBC was found successful for the former and poor for the latter. Authors claimed that the poor agreement was due to the fact that the hydrodynamics of the laboratory scale BFBC, under investigation in the scope of this study, was based on the hydrodynamics of large-scale unit to observe the effect of operational conditions on NO and N_2O emissions in practical systems.

In the study carried out by Hannes [50], a comprehensive mathematical model that incorporates NO and N_2O formation and reduction mechanism for six different CFB boilers burning different types of coal was developed. The model considers hydrodynamics, volatile release and combustion, char combustion, particle size distribution, energy balance, SO_x retention and NO_x and N_2O formation and reduction. Split between NO and N_2O during char nitrogen oxidation was adjusted to fit the predictions into measured data. All volatile nitrogen was assumed to be evolved as NH_3. Therefore, HCN reactions were not taken into consideration. Moreover, catalytic activity of the ashes was only considered for N_2O decomposition. Although N_2O emission predictions were found to be in very good agreement with the measurements, it was pointed out that there exists a necessity for understanding of NO formation processes.

Desroches-Ducarne et al. [58] developed a comprehensive mathematical model for circulating fluidized bed combustion of municipal refuse collected from suburbs of Paris. Their model takes into consideration hydrodynamics, devolatilization, char and volatile combustion, acid and gas recapturing by Ca and NO and N_2O formation and reduction and is able to predict the gaseous pollutants (CO, NO, N_2O, SO_2, HCl) emission. Although, a simple description for the formation and reduction of nitrous oxide, including only homogeneous oxidation of HCN and reduction of N_2O by char, was considered, the model successfully predicted the effect of excess air, air staging and temperature on N_2O emission.

A single particle reaction-diffusion model, including NO and N_2O formation and reduction, for char combustion was integrated into a three-phase hydrodynamic description of a bubbling fluidized bed combustor by Chen et al. [66] in order to predict the batch experiments conducted in a bubbling fluidized bed combustor and to investigate the effect of some operational parameters on NO and N_2O emissions. The formation of volatile nitrogen species, NH_3 and HCN, and their subsequent oxidation were not taken into consideration. Char nitrogen was oxidized to both NO and N_2O, and the rate expression for the formation of N_2O from char nitrogen was adjusted to obtain good agreement between predictions and measurements of N_2O concentrations. A favorable agreement was obtained between the model calculations and measurements taken from batch combustion experiments with different operational conditions.

In an attempt to investigate and understand the formation of NO and N_2O during single particle combustion in a laboratory scale fluidized bed reactor operated at slugging regime, Löffler et al. [74] developed a detailed chemical kinetic model and combined it with a two-phase model. During devolatilization, it was assumed that elemental compositions of the parent coal remained constant. Furthermore, the volatile nitrogen species were assumed to be NH_3 and HCN only. N_2O was not considered as a product of direct oxidation of char. Instead, a mechanism, which includes the release of HCN during char combustion and its subsequent gas phase oxidation, was used to describe N_2O formation from char. A detailed reaction mechanism, which consists of 426 chemical reactions and 71 species, was used to describe homogeneous and heterogeneous chemistry. The model predictions were tested against concentration histories with respect to time and concentration profiles along reactor height obtained from a single particle combustion experiment conducted in a laboratory scale FBC. Good agreement was found between the predicted and measured data.

Another modelling study was carried out by Liu and Gibbs [59] in which a mathematical model for a CFBC firing pinewood chips was developed by considering NO and N_2O formation and reduction reactions. The nitrogen remained in the char was assumed to be proportional to total mass left in the char during devolatilization, and the volatile nitrogen was assumed to be only HCN and NH_3. Regardless of NO and N_2O formation mechanism, constant fuel particle size was assumed. The model was found to be able to predict the influence of main operational parameters on NO and N_2O emissions.

Development of a two-dimensional model for a CFBC is conducted by Gungor et al. [62,63,89,90]. In the model, hydrodynamics, volatile release and combustion, char combustion and size distribution, fragmentation and attrition, sulfur capture and NO and N_2O formation and reduction are taken into account. Char nitrogen oxidation was not taken into consideration. Although the fuels used in these studies were characterized by their high ash content, no ash catalyzed reaction was included. Predictions of NO_x emissions were validated against CFBC experiments carried out in industrial and pilot scale units whereas N_2O predictions were not validated against the measurements.

A modeling study for the co-combustion of lignite with biomass in CFB boiler was carried out by Krzywanski et al. [91]. The model considers hydrodynamics, devolatilization, char combustion and 43 chemical reactions including sulfation and NO and N_2O formation and reduction. NO and N_2O formation and reduction mechanism consists of 36 chemical reactions and includes both radical and stable species. However, formation of NO from char nitrogen was not included. No comparison between predicted and measured N_2O emissions was made in this study.

A 3-dimensional CFD model for CFB combustion of Rhenish lignite was developed by Nikolopoulos et al. [60]. The model considers hydrodynamics, drying, volatile release and combustion, char combustion and NO and N_2O formation and reduction. NO and N_2O sub-model is decoupled from the combustion model in order to minimize the computational cost. To achieve this, the velocity, solids and species distributions were taken from the combustion model, and transport equations for the nitrogenous species were solved separately by keeping those variables constant. The nitrogen remaining in the char was determined by using an empirical equation based on operational temperature. HCN was assumed to be the only volatile nitrogen species. Furthermore, two cases were investigated in the model. In the first case, 70 % of the nitrogen remained in the char was released as HCN as a product of secondary devolatilization, and the remaining was directly oxidized into NO and N_2O. In the second case, all nitrogen remained in the char was directly oxidized into NO and N_2O. Moreover, any ash catalyzed reaction was not taken into consideration. The results of this study indicate that the modeling with second case agrees better with the experimental measurements whereas the first case overestimates HCN and underestimates N_2O concentrations, and they concluded that the secondary conversion of char-N into HCN is not appropriate for the fuel and the reaction rates under consideration.

A comprehensive BFBC model incorporating NO and N_2O emissions was developed by Marias et al. [18] for the combustion of sewage sludge with high nitrogen content. The comprehensive model considers bed and freeboard hydrodynamics, devolatilization, char combustion and NO and N_2O formation and reduction mechanisms. The nitrogen bound within the fuel was assumed to be partitioned into char nitrogen and volatile nitrogen (HCN and NH_3 only). The catalytic effect of solids (ash, char or limestone) are not taken into consideration. The validity of the model was tested by comparing the simulated compositions of the species with the experimental ones at the reactor exit obtained from combustion tests operated at different operational conditions and the predictions were found to be accurate to describe the fate of nitrogen.

Recent studies [61,75,87,88,92–95] have focused on Computational Fluid Dynamics (CFD) analysis, in which equations of motion for both gas and solid phases are solved explicitly instead of using empirical correlations, to describe complex multiphase flow in fluidized bed combustors. Although this approach provides more detailed information in FBCs such as temporal and spatial distributions of temperature, species concentrations, gas and particle velocities, particle trajectories etc., there exist challenges in CFD analysis which consist of computational cost, modeling of particle shrinkage and incorporation of a detailed chemical reaction scheme. With regard to NO and N_2O formation and reduction mechanism, ash catalyzed reactions were discarded in all studies. Furthermore, for all studies except the one carried out by Zhou et al. [87,88], NO was the only product of char nitrogen oxidation. In all these CFD studies except Lu et al. [95] validity of predictions for N_2O emissions were not tested.

Lu et al. [95] accurately predicted the influence of temperature and MSW – coal mixing ratio on N_2O emissions.

2.3.2 Concluding Remarks

Incorporation of a sufficiently detailed N_2O formation and reduction mechanism into a comprehensive overall system model for bubbling fluidized bed combustion of coal and biomass is limited in literature. In those studies, major volatile nitrogen species are assumed to be NH_3 and/or HCN. However, based on the literature survey about pyrolysis of different types of fuel, N_2 is the major volatile nitrogen species during devolatilization which reduces the yields of NO and N_2O precursors such as NH_3, HCN and char nitrogen. As it was discussed earlier in section 2.1 and 2.2, distribution of the nitrogen species during devolatilization greatly influences the emissions of NO and N_2O in fluidized bed combustion of solid fuels.

Therefore, in this study, a previously developed system model will be extended to incorporate a sufficiently detailed N_2O formation and reduction mechanism. Fuel nitrogen partitioning into char and volatiles and formation of HCN and NH_3 during devolatilization, which are unique to fuel type, will be determined by pyrolysis experiments. The assessment of the accuracy of the model will be tested by comparing its predictions with experimental data obtained in METU 0.3 MW_t ABFBC Test Rig where a typical Turkish lignite with high ash content, is fired and co-fired with cotton residue.

CHAPTER 3

SYSTEM MODEL FOR ABFBC CO-FIRING LIGNITE AND COTTON RESIDUE

3.1 General

In this study, a comprehensive system model, originally proposed by Selcuk and Sivrioğlu [21] and later improved, extended and validated against experimental data by Selcuk and her colleagues [7–12] is chosen as basis for incorporation of N_2O formation and reduction for modelling of co-combustion of lignite and cotton residue. The model accounts for bed and freeboard hydrodynamics, volatile release and combustion, char particle combustion and size distribution, heat transfer, elutriation and entrainment, sulfur retention and NO and N_2O formation and reduction. The behavior of the fluidized bed combustor under consideration is described by a model based on conservation equations for energy and chemical species in conservative form for both bed and freeboard sections.

The main assumptions for the present model are illustrated in Figure 3.1 and Figure 3.2 for bed and freeboard section, respectively. The modifications required for the consideration of co-combustion of lignite with cotton residue are highlighted in the Figures 3.1 and 3.2. As can be seen from Figure 3.1, bed model assumptions, regarding hydrodynamics, heat transfer, combustion and sulfur retention sub-models, is not modified within the scope of this thesis study. However, the NO and N_2O formation and reduction sub-model in the bed section is updated to include both HCN formation during devolatilization and N_2O formation during char combustion for the incorporation of N_2O formation and reduction mechanism. As figure 3.2 illustrates, any modification for the consideration of hydrodynamics and heat transfer in freeboard is not carried out in this study. On the other hand, as highlighted in Figure

3.2, volatiles, not released to the bed, are assumed to be released with a logarithmic distribution to the freeboard instead of a linear distribution. Furthermore, freeboard sulfur retention sub-model is updated to include sulfation reaction due to course sorbent particles carried to freeboard by bursting bubbles. Finally, freeboard NO and N_2O formation and reduction sub-model is adjusted to comprise HCN formation during devolatilization to incorporate N_2O formation and reduction in freeboard section.

In the light of above-mentioned modifications, ten chemical species, O_2, CO, CO_2, H_2O, SO_2, NH_3, NO, HCN, CNO, N_2O are considered in the system model. Chemical reactions considered in the present model are listed in Table 3.1 and the correlations used in estimating important parameters in the model are listed in Table 3.2. In the model, it is assumed that the fuels follow their individual devolatilization and char combustion paths. Devolatilization and char combustion products are then combined throughout the combustor and undergo the same reaction path.

The components of the system model developed prior to this study are described in detail in the literature [7–10]. For the sake of integrity, a brief summary of the sub-models will be provided in the following section. Modifications carried out for the consideration of NO and N_2O formation and reduction will be explained in detail.

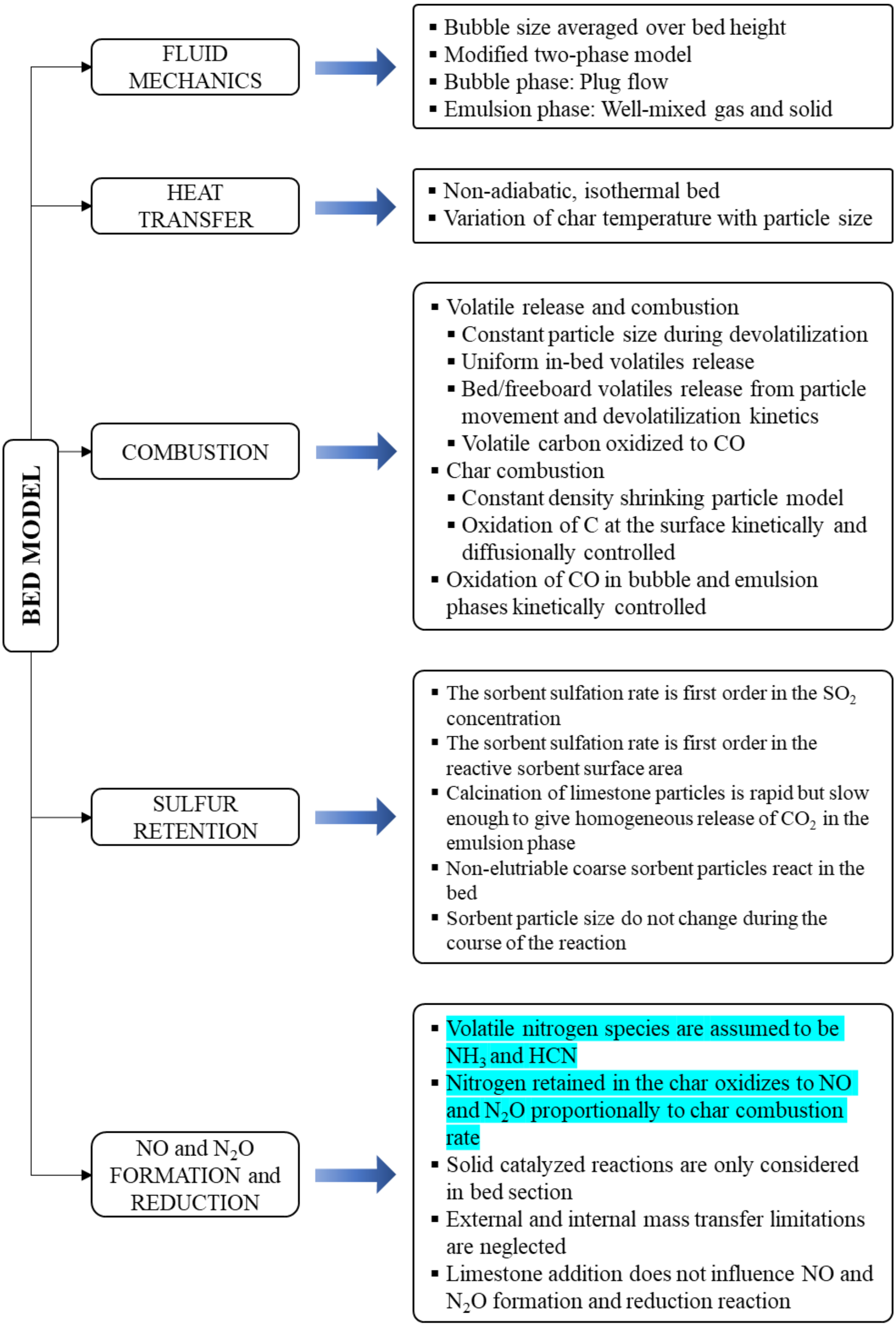

- Bubble size averaged over bed height
- Modified two-phase model
- Bubble phase: Plug flow
- Emulsion phase: Well-mixed gas and solid

- Non-adiabatic, isothermal bed
- Variation of char temperature with particle size

- Volatile release and combustion
  - Constant particle size during devolatilization
  - Uniform in-bed volatiles release
  - Bed/freeboard volatiles release from particle movement and devolatilization kinetics
  - Volatile carbon oxidized to CO
- Char combustion
  - Constant density shrinking particle model
  - Oxidation of C at the surface kinetically and diffusionally controlled
- Oxidation of CO in bubble and emulsion phases kinetically controlled

- The sorbent sulfation rate is first order in the SO_2 concentration
- The sorbent sulfation rate is first order in the reactive sorbent surface area
- Calcination of limestone particles is rapid but slow enough to give homogeneous release of CO_2 in the emulsion phase
- Non-elutriable coarse sorbent particles react in the bed
- Sorbent particle size do not change during the course of the reaction

- Volatile nitrogen species are assumed to be NH_3 and HCN
- Nitrogen retained in the char oxidizes to NO and N_2O proportionally to char combustion rate
- Solid catalyzed reactions are only considered in bed section
- External and internal mass transfer limitations are neglected
- Limestone addition does not influence NO and N_2O formation and reduction reaction

Figure 3.1 An overview of the steady state bed model assumptions

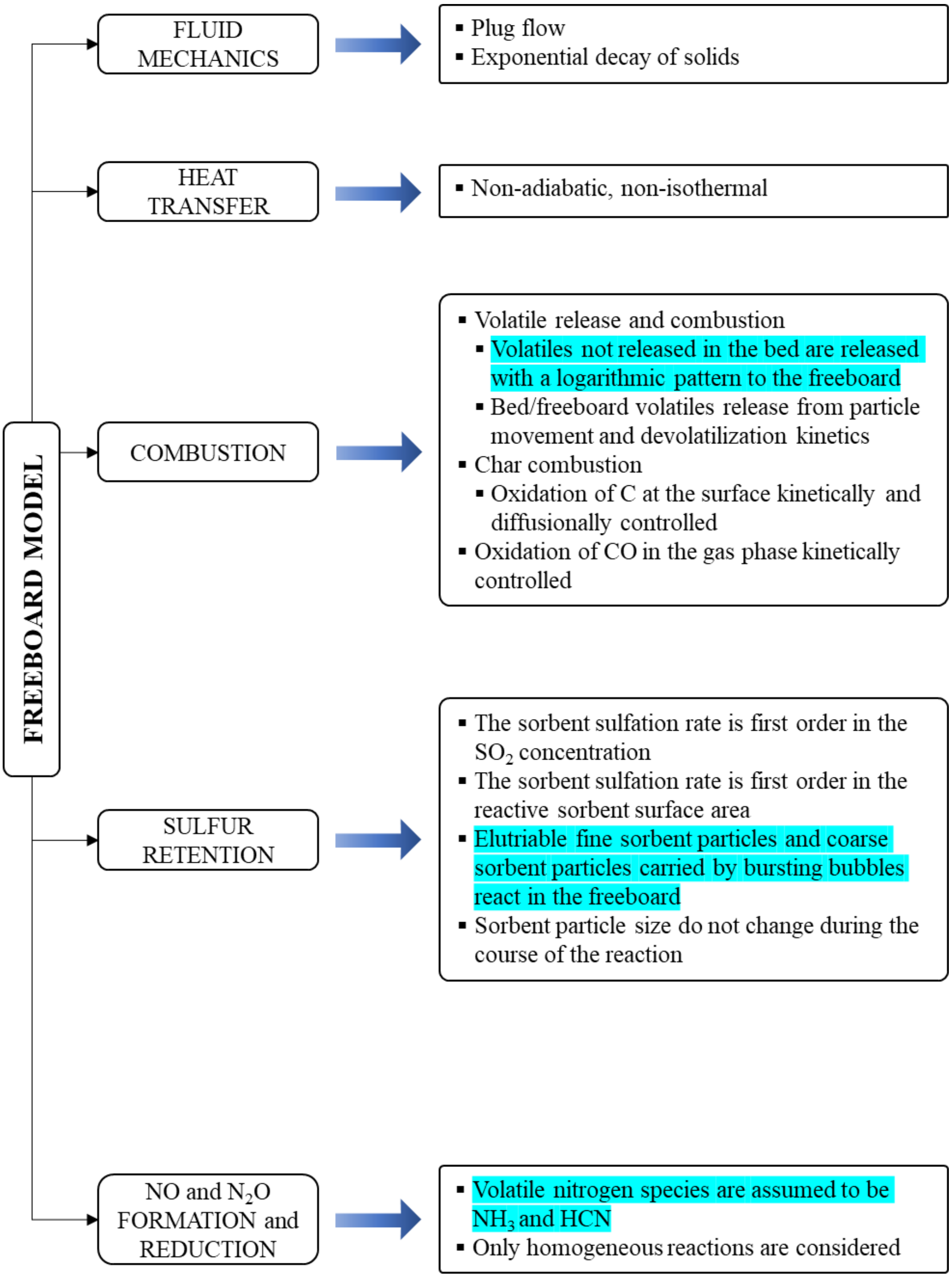

- Plug flow
- Exponential decay of solids

- Non-adiabatic, non-isothermal

- Volatile release and combustion
  - Volatiles not released in the bed are released with a logarithmic pattern to the freeboard
  - Bed/freeboard volatiles release from particle movement and devolatilization kinetics
- Char combustion
  - Oxidation of C at the surface kinetically and diffusionally controlled
- Oxidation of CO in the gas phase kinetically controlled

- The sorbent sulfation rate is first order in the SO_2 concentration
- The sorbent sulfation rate is first order in the reactive sorbent surface area
- Elutriable fine sorbent particles and coarse sorbent particles carried by bursting bubbles react in the freeboard
- Sorbent particle size do not change during the course of the reaction

- Volatile nitrogen species are assumed to be NH_3 and HCN
- Only homogeneous reactions are considered

Figure 3.2 An overview of the steady state freeboard model assumptions

Table 3.1 Reactions and rate expressions

	Reaction	Place	Rate Expression	Unit	Ref.
R1	$C_{vol}+1/2O_2 \rightarrow CO$	gas phase	Instantaneous	-	-
R2	$H_2+1/2O_2 \rightarrow H_2O$	gas phase	Instantaneous	-	-
R3	$S+O_2 \rightarrow SO_2$	gas phase	Instantaneous	-	-
R4	$N_{vol}+3/2H_2 \rightarrow NH_3$	gas phase	Instantaneous	-	-
R5	$N_{vol}+C_{vol}+1/2H_2 \rightarrow HCN$	gas phase	Instantaneous	-	-
R6	$C_{char,coal}+1/2O_2 \rightarrow CO$	char surface	$5.95\times10^4 T_d \exp(-17967/T_d)C_{O_2,s}$	$mol cm^{-3} s^{-1}$	[96]
	$C_{char,bio}+1/2O_2 \rightarrow CO$	char surface	$250 T_d \exp(-16013/T_d)C_{O_2,s}$	$mol cm^{-3} s^{-1}$	[97]
R7	$CO+1/2O_2 \rightarrow CO_2$	gas phase	$3.0\times10^{10} T_g \exp(-8052/T_g)C_{O_2}^{0.3} C_{CO} C_{H_2O}^{0.5}$	$mol cm^{-3} s^{-1}$	[98]
R8	$CaCO_3 \rightarrow CaO+CO_2$	sorbent surface	Instantaneous	-	-
R9	$CaO+SO_2+1/2O_2 \rightarrow CaSO_4$	sorbent surface	$23.9 C_{SO_2} S_0 \sigma_{avg}$	$mol s^{-1}$	-
R10	$N_{char}+1/2O_2 \rightarrow NO$	char surface	$r_C \dfrac{(1-x_{N,vol})x_N M_C}{x_{fc}\, M_N}\left(\dfrac{1}{1+9.02\times10^8 \exp(-3551/T_d)C_{NO}}\right)$	$mol cm^{-3} s^{-1}$	[67]
R11	$N_{char}+NO \rightarrow N_2O$	char surface	$r_C \dfrac{(1-x_{N,vol})x_N M_C}{x_{fc}\, M_N}\left(\dfrac{\mathrm{C}_{\mathrm{NO}}}{1/(9.02\times10^8 \exp(-3551/T_d)) + C_{NO}}\right)$	$mol cm^{-3} s^{-1}$	[67]
R12	$NH_3+5/4O_2 \rightarrow NO+3/2H_2O$	gas phase	$2.21\times10^{14} \exp(-38160/T_g)C_{NH_3}$	$mol cm^{-3} s^{-1}$	[99]

Table 3.1. Reactions and rate expressions (continued)

	Reaction	Place	Rate Expression	Unit	Ref.
R13	$NO+2/3NH_3 \rightarrow 5/6N_2+H_2O$	gas phase	$2.45\times10^{26}\exp(-27680/T_g)C_{NO}C_{NH_3}$	$mols^{-1}$	[99]
R14	$HCN+1/2O_2 \rightarrow CNO+1/2H_2$	gas phase	$2.14\times10^{11}\exp(-10000/T_g)C_{O_2}C_{HCN}$	$molcm^{-3}s^{-1}$	[58]
R15	$CNO+\frac{1}{2}O_2 \rightarrow NO+CO$	gas phase	$r_{HCN}(\frac{1}{1+1.02\times10^{15}\exp(-25460/T_g)C_{NO}})$	$molcm^{-3}s^{-1}$	[58]
R16	$CNO+NO \rightarrow N_2O+CO$	gas phase	$r_{HCN}(\frac{C_{NO}}{1/(1.02\times10^{15}\exp(-25460/T_g))+C_{NO}})$	$molcm^{-3}s^{-1}$	[58]
R17	$NO+Char \rightarrow 1/2N_2+CO$	char surface	$3.45\times10^{6}\exp(-22200/T_d)C_{NO}^{0.52}$	$molg^{-1}s^{-1}$	[82]
R18	$NO+CO \rightarrow 1/2N_2+CO_2$	char surface	$3.81\times10^{9}\exp(-22800/T_d)C_{NO}^{0.39}C_{CO}^{0.53}$	$molg^{-1}s^{-1}$	[82]
R19	$NH_3+5/4O_2 \rightarrow NO+3/2H_2O$	char surface	$3.4\times10^{10}C_{NH_3}C_{O_2}$	$molg^{-1}s^{-1}$	[82]
R20	$NH_3+5/4O_2 \rightarrow NO+3/2H_2O$	ash surface	$0.4C_{NH_3}^{0.57}C_{O_2}^{0.11}$	$molg^{-1}s^{-1}$	[82]
R21	$NH_3+3/4O_2 \rightarrow 1/2N_2+3/2H_2O$	char surface	$8.4\times10^{10}C_{NH_3}C_{O_2}$	$molg^{-1}s^{-1}$	[82]
R22	$NH_3+3/4O_2 \rightarrow 1/2N_2+3/2H_2O$	ash surface	$3.92\times10^{9}C_{NH_3}^{1.8}C_{O_2}^{0.07}$	$molg^{-1}s^{-1}$	[82]
R23	$N_2O+Char \rightarrow 1/2CO_2+N_2$	char surface	$7.0\times d_p^{-0.74}C_{N_2O}$	$molg^{-1}s^{-1}$	[65]
R24	$N_2O+CO \rightarrow N_2+CO_2$	gas phase	$2.51\times10^{14}\exp(-23163/T_g)C_{CO}C_{N_2O}$	$molcm^{-3}s^{-1}$	[100]
R25	$N_2O \rightarrow N_2+1/2O_2$	gas phase	$1.75\times10^{8}\exp(-23800/T_g)\mathrm{C}_{N_2O}$	$molcm^{-3}s^{-1}$	[101]

Table 3.2 Correlations used in the model

	Reference
Bubble size, d_b	[102]
Bubble to emulsion mass transfer, K_{be}	[103]
Bubble rise velocity, u_b	[103]
Emulsion phase gas velocity, u_e	[104]
Bubble phase volume fraction, δ	[104]
Minimum fluidization velocity, u_{mf}	[105]
Mass transfer to particles in the emulsion phase, k_f	[106]
Heat transfer to particles in the emulsion phase, h_p	[107]
Terminal velocity of the particles, u_t	[108]
Specific elutriation rate constant, $E(r)$	[109]
Exponential decay constant, a	[109]
Convective heat transfer coefficient of bed wall, h_{bw}	[110]
Convective heat transfer coefficient of cooling tubes, h_{cw}	[111]
Convective heat transfer coefficient of cooling water, h_i	[112]
Gas side heat transfer coefficient in freeboard, h_g	[107]

3.2 Model Description

The system model can be described in terms of bed hydrodynamics, freeboard solids distribution, volatile release and combustion, char particle combustion, particle size distribution, desulfurization and NO and N_2O formation and reduction.

3.2.1 Bed and Freeboard Hydrodynamics

The hydrodynamics of bubbling bed is described by modified two-phase theory suggested by Grace and Clift [113],

$$u_0 = \frac{Q_b}{A_{bed}} + u_{tf} + u_e(1 - \delta) \tag{3.1}$$

where throughflow velocity, u_{tf}, can be expressed in terms of emulsion phase velocity, u_e, using modified n-type type two phase theory of Grace and Harrison [114],

$$u_{tf} = (n + 1)u_e\delta \tag{3.2}$$

where $n = 2$ for three dimensional beds. Although Equation (3.1) explains the deviation from two-phase theory, correct implementation of this expression requires improved expressions for Q_b and u_e. An improved expression for the emulsion phase gas velocity was suggested by Gogolek and Becker [104],

$$u_e = \frac{u_{mf}}{1 - 1.5\delta^{2/3}} \tag{3.3}$$

The rise velocity of bubbles in the bubbling bed is obtained from Davidson and Harrison [103],

$$u_b = 0.711(gd_b)^{1/2} + u_0 - u_{mf} \tag{3.4}$$

An integrated average mean bubble size is found from bubble size expression proposed by Mori and Wen [102], in the sections unoccupied by the tube bank and from constant and uniform bubble size determined by the clearance between horizontal tube bank is utilized.

Bubbles are assumed to be free of solids and the gas interchange coefficient between bubble and emulsion phases, K_{be}, is defined as,

$$K_{be} = \frac{\begin{array}{c}\text{volume of gas going from bubbles}\\ \text{to emulsion or from emulsion to bubbles}\end{array}}{(\text{volume of bubbles in the bed})(\text{time})} \tag{3.5}$$

where the following relation suggested by Davidson and Harrison [103] is used:

$$K_{be} = 4.5 \frac{u_e}{u_b} \tag{3.6}$$

In the freeboard section, the hold-up of solid particles decreases exponentially as a function of distance from the surface of the bed or height in the freeboard with decay constant a,

$$\frac{\varepsilon_s}{\varepsilon_{s,0}} = \exp(-a \times z_f) \tag{3.7}$$

In a study of Choi et al. [109], an empirical correlation was presented to predict decay constant which was found by using empirical data obtained with variations in column size, gas velocity, temperature, particle size and density;

$$\begin{aligned} a = \frac{1}{d_p} \times \exp\left(-11.2 + 210 \frac{d_p}{d_{bed} - d_p}\right) \times \left(\frac{d_p \rho_g \left(u_0 - u_{mf}\right)}{\mu}\right)^{-0.492} \\ \times \left(\frac{d_p g \rho_p}{\rho_g \left(u_0 - u_{mf}\right)^2}\right)^{0.725} \times \left(\frac{\rho_p - \rho_g}{\rho_g}\right)^{0.731} \times C_D^{-1.47} \end{aligned} \tag{3.8}$$

The total volume fraction of solids just above the surface of bubbling bed, $\varepsilon_{s,0}$, is obtained from,

$$\varepsilon_{s,0} = 1 - \varepsilon_f \tag{3.9}$$

The volume fractions of char, inert and sorbent particles of size *r* at bed surface are obtained from the following equations, respectively:

$$\varepsilon_{d,0} = \frac{M_d \, P_{bed}(r) \Delta r / \rho_d}{M_i / \rho_i} \tag{3.10}$$

$$\varepsilon_{i,0} = \frac{M_i \, P_{bed,i}(r) \Delta r / \rho_i}{M_i / \rho_i} \tag{3.11}$$

$$\varepsilon_{CaO,0} = \frac{M_{CaO} \, P_{bed,CaO}(r) \Delta r / \rho_{CaO}}{M_i / \rho_i} \tag{3.12}$$

The entrainment flux of particles, K_i^*, is calculated by assuming that it consists of a cluster flux, $K_{i,h}^*$, and a dispersed, non-cluster flux, $K_{i,\infty}^*$, as suggested by Hazlett and Bergougnou [115],

$$K_i^* = K_{i,h}^* + K_{i,\infty}^* \tag{3.13}$$

and is obtained from the empirical correlations proposed by Choi et al. [109]. The elutriation rate constant, $E(r)$, used to calculate carry over flow rate, is then calculated from,

$$E(r) = \frac{A_{bed}}{M_d} K_{i,\infty}^* \tag{3.14}$$

The elutriated particles are assumed to rise at the superficial gas velocity in the freeboard.

Size distribution of entrained solid particles at any height in the freeboard is calculated by assuming that probability of finding particles of size *r* at any height is proportional to their presence in bed with proportionality constant being $K_{i,h}^*$.

$$F_{z,s} P_{z,s}(r) = K_{i,h}^* A_{bed} P_{bed,s}(r) \tag{3.15}$$

Multiplying both sides of Equation (3.15) by *dr* and integrating yields the flow rate of entrained particles and their size distribution as follows,

$$F_{z,s} = A_{bed} \int_{r_{min}}^{r_{max}} K_{i,h}^* P_{bed,s}(r) dr \tag{3.16}$$

$$P_{z,s}(r) = A_{bed} K_{i,h}^* P_{bed,s}(r) / F_{z,s} \tag{3.17}$$

3.2.2 Volatile Release and Combustion

In the system model, volatiles are assumed to be released uniformly in the emulsion phase for both fuels. The amount released in bed is determined by using the volatiles release model of Stubington et al. [116], and to describe the devolatilization kinetics, the parallel independent reaction model of Anthony and Howard [117] is used. In the presence of radial temperature profile and with the assumption of evenly distributed volatile matter in the particle, total amount of volatile matter released with respect to time is given by,

$$\frac{\nu_{avg}}{\nu_{\infty}} = \frac{3}{R^3}\int_0^R \left[1 - \int_0^{\infty} exp\left(-\int_0^t k(E)dt\right)f(E)dE\right]r^2dr \tag{3.18}$$

Devolatilization history of the particle yields the fraction of volatiles released in bed (x_{vl}). The remaining volatiles is assumed to be released to the freeboard with a logarithmic distribution with respect to distance from the surface of the bed. With regard to combustion of volatiles released, hydrocarbon species are eliminated due to their rapid oxidation to CO and H_2O [50], i.e., all carbon is assumed to burn instantaneously to CO (R1). Furthermore, all hydrogen and sulfur are assumed to burn instantaneously to produce water vapor (R2) and sulfur dioxide (R3) owing to rapid oxidation of sulfur (H_2S) and hydrogen (H_2 and hydrocarbons) containing species. In addition, volatile nitrogen can be released as ammonia (R4) and hydrogen cyanide (R5). Majority of the volatile nitrogen is converted to molecular nitrogen. The oxidation of CO takes place in both bubble and emulsion phases according to the rate expression of Hottel et al. [98]. Further details of the volatiles release sub-model can be found elsewhere [7,118].

3.2.3 Char Combustion

Char particles originating from both lignite and cotton residue are assumed to burn only to CO, as it is the major product of char combustion at typical FBC temperatures. Using the shrinking particle model and taking film mass transfer and kinetic resistances into consideration, the rate of carbon oxidation at the particle surface can be obtained as,

$$r_{C,e} = \frac{2}{\frac{1}{k_f} + \frac{2}{k_s}} \bar{C}_{O_2,e} \tag{3.19}$$

The film mass transfer coefficient, k_f, is obtained from the relation suggested by Jung and La Nauze [106]. In Eq. (3.19), average emulsion phase oxygen concentration is used to calculate the combustion rate. Kinetics of combustion for lignite and cotton residue are assumed to be represented by the rate laws suggested by Field et al. [96] and Adanez et al. [97], respectively.

Shrinkage rate of char particles, which is required for the calculation of particle size distribution, can be determined by noting that the rate of carbon removal from the surface of char must be equal to the rate of combustion of carbon at the particle surface.

$$\frac{d}{dt}\left[\frac{4}{3}\pi r^3 \rho_d \frac{x_{fc}}{x_{fc} + x_a}\right] = -4\pi r^2 M_C r_{C,e} \tag{3.20}$$

Rearranging Equation (3.20) yields the working form of the char particles shrinkage rate:

$$\Re(r) = -\frac{dr}{dt} = \frac{1}{\rho_d}\frac{x_{fc} + x_a}{x_{fc}} M_C r_{C,e} \tag{3.21}$$

Regarding the estimation of molar carbon consumption rate in the emulsion phase, which is required for the species conservation equations of the emulsion phase, the following expression can be used,

$$n_{C,e} = \frac{1}{M_C}\frac{x_{fc}}{x_{fc} + x_a}\frac{3M_d}{V_{bed}(1-\delta)\varepsilon_{mf}} \int_{r_{min}}^{r_{max}} \frac{P_{bed}(r)}{r} \Re(r) dr \tag{3.22}$$

With regard to char combustion in freeboard section, both elutriable fine char particles and coarse char particles carried due to bubble eruption are considered to burn without any shrinkage of particle. To be used in the species conservation equations in the freeboard section, the molar rate of carbon depletion for elutriable fines particles can be expressed as:

$$n_{C,elut} = \frac{3\eta}{M_C}\frac{x_{fc}}{x_{fc}+x_a}\frac{F_{CO}}{A_{bed}}\int_{r_{min}}^{r_{max,e}}\frac{P_{CO}(r)}{ru_p(r)}\Re(r)dr \tag{3.23}$$

That for coarse particles rise with bubble eruption can be written as:

$$n_{C,ent} = \frac{3\eta}{M_C}\frac{x_{fc}}{x_{fc}+x_a}\rho_d\int_{r_{min}}^{r_{max,e}}\frac{\varepsilon_d P_z(r)}{r}\Re(r)dr \tag{3.24}$$

Where, η is the contact efficiency in freeboard and can be estimated by the empirical correlation suggested by Kunii and Levenspiel [119].

$$\eta = 1 - \left(1 - \frac{u_e}{u_0}(1-\delta)\right)\exp(-6.62z_f) \tag{3.25}$$

The total molar carbon depletion rate in freeboard is the summation of char combustion rate of elutriable fines and coarse particles carried by bubbles;

$$n_{C,f} = n_{C,elut} + n_{C,ent} \tag{3.26}$$

The char particle temperature in the bed section is calculated by solving an energy balance around the particle, which is assumed to have uniform temperature,

$$\frac{\rho_d}{M_C}\frac{x_{fc}}{x_{fc}+x_a}\Delta H_{R1}^0\,\Re(r) - [h_p(T_d - T_{bed}) + \sigma\varepsilon(T_d^4 - T_{bed}^4)] = 0 \tag{3.27}$$

In addition, the freeboard char particle temperatures are assumed to be equal to the freeboard gas temperature.

3.2.4 Particle Size Distribution

The size distribution of char particles plays a key role in fluidized bed combustors since the total rate of char combustion is proportional to the char hold-up in the bed and external surface area provided by the char particles. The size distribution is calculated based on population balance in every particle size interval.

In this thesis study, char particle size distribution for lignite and cotton residue are determined separately by making population balance for each fuel. The steady state population balance on mass basis on char particle can be expressed as:

$$\begin{Bmatrix}\text{Char entering}\\ \text{in feed}\end{Bmatrix}_i - \begin{Bmatrix}\text{Char leaving}\\ \text{in bed drain}\end{Bmatrix}_i - \begin{Bmatrix}\text{Char leaving}\\ \text{in carry over}\end{Bmatrix}_i + \begin{Bmatrix}\text{Char shrinking into the}\\ \text{interval from a larger size}\end{Bmatrix}_i - \begin{Bmatrix}\text{Char shrinking out of the}\\ \text{interval to a smaller size}\end{Bmatrix}_i - \begin{Bmatrix}\text{Char depleted within the}\\ \text{interval due to combustion}\end{Bmatrix}_i = 0 \tag{3.28}$$

Where i represents the type of fuel: 1 for lignite, 2 for cotton residue. For the sake of clarity, subscript i is removed in the following equations.

In order to derive an equation based on the mass fractions in size intervals for shrinking char particles the following assumptions are made:

1. Char particles enter the bed at a rate of F_0 with size distribution of $P_0(r)$ which is expressed by Rosin-Rammler size distribution function.
2. As char particles are well-mixed, bed drain char size distribution represents the bed char size distribution:

$$P_{bd}(r) = P_{bed}(r) \tag{3.29}$$

3. The rate of elutriation of char particles of size r is directly proportional to their concentration in the bed, i.e.,

$$F_{CO}P_{CO}(r) = M_d P_{bed}(r) E(r) \tag{3.30}$$

   where $E(r)$ is the elutriation rate constant [109], M_d is the total mass of char in the bed and $P_{bed}(r)$ is the size distribution of char particles in the bed.

4. Densities of char particles do not change during the burn-out.
5. Char particles are considered to shrink by combustion according to shrinking particle model at a rate of

$$-\frac{dr}{dt} = \Re(r) = \frac{1}{\rho_d}\frac{x_{fc}+x_a}{x_{fc}}M_C r_{C,e} \tag{3.31}$$

Based on the assumptions, the working form of the population balance can be expressed as:

$$\frac{dW(r)}{dr} = -W(r)\left[\frac{F_{bd}}{M_d\Re(r)} + \frac{E(r)}{\Re(r)} - \frac{3}{r}\right] + F_0 P_0(r) \tag{3.32}$$

Eq. (3.32) is solved for both lignite and cotton residue to calculate the char hold-up of both species. Detailed derivation of Eq. (3.32) can be found elsewhere [118]. In eq. (3.32), $W(r)$ is defined as:

$$W(r) = M_d P_{bed}(r)\Re(r) \tag{3.33}$$

Equation (3.32) is subjected to the following boundary condition:

$$@ \quad r = r_{max} \qquad W(r) = 0 \tag{3.34}$$

as the probability of having solid particles of size r_{max} in the bed, i.e., P_{bed}, is practically zero, due to the shrinkage of maximum particle size in the bed.

Once the solution of $W(r)$ becomes available, the bed char hold-up, M_d, bed char size distribution, $P_{bed}(r)$, carry over flowrate, F_{CO}, and carry over char size distribution, $P_{CO}(r)$, can be calculated by the following equations:

$$M_d = \int_{r_{min}}^{r_{max}} W(r)dr \tag{3.35}$$

$$P_{bed}(r) = \frac{W(r)}{M_d\Re(r)} \tag{3.36}$$

$$F_{CO} = \int_{r_{min}}^{r_{max}} M_d P_{bed}(r)E(r)dr \tag{3.37}$$

$$P_{CO}(r) = \frac{M_d P_{bed}(r)E(r)}{F_{CO}} \tag{3.38}$$

With regard to the size distribution of inerts, it is assumed that the size distribution of inerts in the bed is equal to the measured bottom ash particle size distribution. Furthermore, the carry over flow rate and size distribution are calculated by the following equations:

$$F_{CO,i} = \int_{r_{min}}^{r_{max}} M_i P_{bed,i}(r) E(r) dr \tag{3.39}$$

$$P_{CO,i}(r) = \frac{M_i P_{bed,i}(r) E(r)}{F_{CO,i}} \tag{3.40}$$

3.2.5 Desulfurization Model

It is assumed that desulfurization involves two consecutive steps, instantaneous calcination of limestone followed by calcination reaction. The rate expression for the reaction between SO_2 and lime, reaction R7, is assumed to be first order in the SO_2 concentration and proportional to the reactive external surface area of the particles [9].

The sorbent fed has a wide particle size distribution and it is assumed that particle size of sorbent does not change during reaction. Attrition of limestone particles is not considered. Therefore, for any particle with size *r*, the rate equation takes the following form:

$$r_{SO_2} = k C_{SO_2} S(t) \tag{3.41}$$

During sulfation, sulfation reaction rate decreases with time due to pore blocking. Therefore, the reactive external surface area, $S(t)$, decays exponentially with time according to the following equation:

$$\frac{S(t)}{S_0} = \sigma(t) = exp\left[-\frac{6M_{CaCO_3} k C_{SO_2}}{x_{CaCO_3} \rho_{lst} d_p} t\right] \tag{3.42}$$

where total initial external surface area for spherical limestone particles, S_0, is expressed as:

$$S_0 = \frac{6M_{CaO}}{\rho_{CaO} d_p} \tag{3.43}$$

In order to model sulfation reaction at steady state, it is necessary to assess an average fractional external surface area, σ_{avg}, which is calculated from the solids residence time distribution function, and the fractional external surface area as a function of time $\sigma(t)$.

$$\sigma_{avg} = \frac{1}{\left[1 + \frac{6M_{CaCO_3} k C_{SO_2}}{x_{CaCO_3} \rho_{lst} d_p} \tau\right]} \left[1 - exp\left(-\left\{\frac{1}{\tau} + \frac{6M_{CaCO_3} k C_{SO_2}}{x_{CaCO_3} \rho_{lst} d_p}\right\} \tau_{max}\right)\right] \tag{3.44}$$

Calculation of average fractional external surface area, σ_{avg}, and determination of residence time of sorbent particles, τ, are given in detail elsewhere [120].

Finally, rate of sulfation reaction becomes:

$$r_{SO_2} = k C_{SO_2} S_0 \sigma_{avg} \tag{3.45}$$

Then the total reaction rate is the summation of the rates obtained at different sizes:

$$r_{SO_2} = \sum_{i=1}^{n} r_{SO_2,i} \tag{3.46}$$

In the freeboard section, sulfation reaction occurs due to both fine particles carried by elutriation and coarse particles carried by bubble eruption. The hold-up of sorbent particles in freeboard is described by exponential decay function of Choi et al. [109]. The sulfation rate for the sorbent particles carried to freeboard by bursting bubbles is expressed as:

$$r_{SO_2,ent} = k C_{SO_2} \left\{3(V_f \varepsilon_{CaO}) \left[\int_{r_{maxe}}^{r_{max}} \frac{P_{z,CaO}(r)}{r_p} dr\right]\right\} \sigma_{avg} \tag{3.47}$$

Moreover, sorbent particles with terminal velocities smaller than the superficial gas velocity are carried to the freeboard by the gas and the residence time of these particles, τ_{elut}, is calculated by,

$$\tau_{elut} = \frac{H_f}{u_0 - u_t} \tag{3.48}$$

The sulfation rate due to the sorbent particle with terminal velocities smaller than superficial gas velocity is expressed as:

$$r_{SO_2,elut} = kC_{SO_2} \frac{F_{CaO}}{\rho_{CaO} H_f} \left[\int_{r_{max}}^{r_{maxe}} \frac{P_{CaO}(r)(u_0 - u_t)}{r_p} dr \right] \sigma_{avg} \tag{3.49}$$

Finally, the total sulfation rate in freeboard is calculated with summation of sulfation rates due to sorbent particles carried by elutriation and bubble eruption:

$$r_{SO_2,f} = r_{SO_2,elut} + r_{SO_2,ent} \tag{3.50}$$

The detailed derivations of the freeboard sulfation rates can be found in the Appendix A.

3.2.6 NO and N_2O Formation and Reduction

In this thesis study, fuel nitrogen is assumed to be the only source for the formation of NO and N_2O due to low operational temperatures of FBCs. As it was explained in Chapter 2, nitrogen in solid fuels is partitioned into char nitrogen and volatile nitrogen during devolatilization stage. As the char nitrogen and volatile nitrogen undergo different reaction paths, estimation of partitioning factor, specific to the fuels under investigation within the scope of this study, must be preliminary step for the modeling of NO and N_2O emission. In order to determine this partitioning factor for cotton residue, nitrogen contents of the parent fuel and its own char are measured by elemental analysis. On the other hand, this factor for lignite is calculated by assuming that the mass fraction of nitrogen remained in the char to the total amount of nitrogen within the fuel is equal to the mass fraction of char (Ash + F.C.) in dry basis. The details of the estimation of the amount of char bound nitrogen is given in the Appendix B.

In order to decide about gases formed from devolatilization of lignite and cotton residue, pyrolysis experiments were carried out in TGA-FTIR system under N_2 atmosphere. Fuel samples were pre-dried at 60 °C for 30 min in order to prevent the overlap between moisture and nitrogenous species. Then, the samples were heated to 950 °C with 40 °C/min heating rate and kept isothermal at 950 °C for one hour. Pyrolysis gases were analyzed simultaneously by FTIR. Consequently, release of equal proportions of HCN and NH_3 is detected during pyrolysis experiments. Moreover, 80 % and 95 % of the volatile nitrogen for lignite and cotton residue are taken to be N_2 based on the literature data [31,52]. A clear representation of partitioning of the nitrogen within the fuel into char nitrogen and volatile gases is shown in the Figure 3.3.

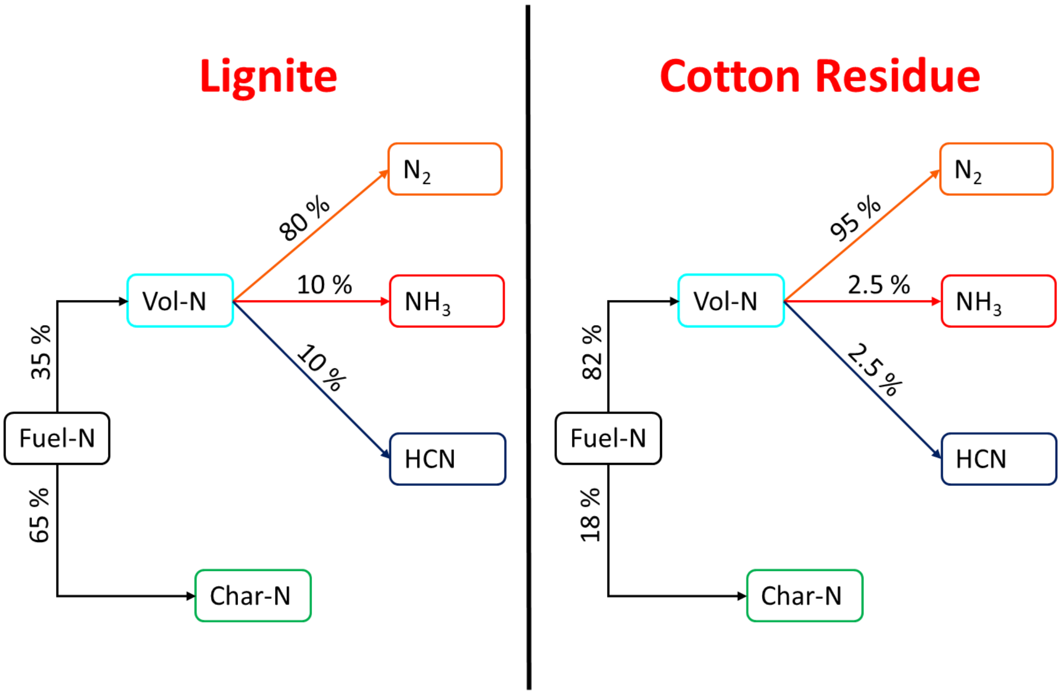

Figure 3.3 The representation of nitrogen within the fuel into char nitrogen and volatile gases

After the devolatilization stage is complete, the nitrogenous products of devolatilization undergo a reaction scheme consisting of 16 chemical reactions (R10 – R25 in Table 3.1). For the reactions regarding NH_3 oxidation and NO reduction, the reactions (R12, R13, R17 – R22 in Table 3.1) selected from the previous studies [50,121] and verified against the experimental data obtained in a pilot scale ABFBC firing lignite, lignite/olive residue and lignite/hazelnut shell blends [10–12], are utilized. With regard to N_2O formation and reduction reactions, a set of chemical reactions (R10, R11, R14 – R16, R23 – R25 in Table 3.1) is chosen based on extensive literature survey discussed in section 2.2.

For the gas phase oxidation of HCN, a global reaction scheme, with corresponding rate expressions, developed by Desroches-Ducarne et al. [58], is utilized in this study. However, catalytic effect of char on the HCN oxidation is not taken into consideration due to lack of appropriate kinetic data of char catalyzed HCN oxidation in the FBC conditions [18,58–61,74–77]. Therefore, catalytic effect of char is neglected in this study as HCN forms only a small amount of fuel nitrogen. A mechanism, developed by Goel et al. [67] for char nitrogen oxidation and further validated against experimental data obtained in a single particle combustion and a CFB combustion experiments [67,69], is used to describe char nitrogen oxidation. The products of the oxidation of char nitrogen are considered to be NO and N_2O. In addition to that, the oxidation of char nitrogen is assumed to be proportional with the char combustion rate, and the rate expression of the char nitrogen oxidation can be written as:

$$n_{N,e} = \frac{((1 - x_{N,vol})x_N/M_N)}{(x_{FC}/M_C)} n_{C,e} \tag{3.51}$$

The details of the derivation of Equation (3.51) can be found elsewhere [122]. The fractional conversion of each product, NO and N_2O, can be estimated by the following expressions suggested by Goel et al. [67],

$$X_{N \to NO} = \frac{1}{1 + \frac{k_2}{k_1} C_{NO}} \tag{3.52}$$

$$X_{N\rightarrow N_2O} = \frac{C_{NO}}{\frac{k_1}{k_2} + C_{NO}} \tag{3.53}$$

The details of the mechanism for the formation of NO and N_2O from char nitrogen oxidation is given in section 2.2.2.1.

Furthermore, N_2O reduction or decomposition is assumed to take place by homogeneous reaction with CO and thermal decomposition together with heterogeneous reduction by char particles as they are important paths for the reduction of N_2O as it was discussed in sections 2.2.1.3 and 2.2.2.4. CO_2 and N_2 are taken to be the only products of N_2O reduction by char owing to the fact that they were observed to be the major products over lignite chars [84].

CaO catalyzed reactions are not taken into consideration due to former findings that addition of limestone does not influence N_2O formation significantly in FBCs [71,72]. Moreover, since solid hold-up in the freeboard is negligible compared to that in the bed, heterogeneous reactions were only applied in bed section. In this study, external mass transfer effects on the heterogeneous NO formation and reduction reactions are omitted as Johnsson and Dam-Johansen [82] observed no external mass transfer limitations up to particles of 5 mm for solid catalyzed reactions and this was greater than the majority of the particles used in this study.

Char catalyzed reactions (R17, R18, R23) have Arrhenius type of rate expression including char particle temperature, T_d, or char particle diameter, d_p, so considering any char particle of size, r, rate of heterogeneous reaction, $r_{i,het}$, equals to

$$r_{i,het} = M_d P(r) r_i \tag{3.54}$$

Considering wide size distribution of particle in the bed, Equation (3.54) must be summed up for all particles.

$$r_{i,het} = M_d \int_{r_{min}}^{r_{max}} P(r) r_{i,het} dr \tag{3.55}$$

However, for the char catalyzed reactions does not include char particle diameter or temperature and ash catalyzed reaction (R19 – R22), rate of heterogeneous reaction, $r_{i,het}$, can be found by multiplying r_i with particle hold-up, M_s, directly.

$$r_{i,het} = M_s r_i \tag{3.56}$$

3.2.7 Mass Conservation Equations

Spatial variation of species concentrations is described by the conservation equations for chemical species in bubble phase, emulsion phase and freeboard section:

$$\frac{dn_{j,b}}{dz} = A_{bed}\delta\left[\Re_{j,b} + K_{be}\left(C_{j,e} - C_{j,b}\right)\right] \tag{3.57}$$

$$0 = n_{j,e}\big|_{z=0} - n_{j,e} + V_{bed}\delta\left[\frac{1-\delta}{\delta}\varepsilon_{mf}\Re_{j,e} - K_{be}\left(C_{j,e} - \bar{C}_{j,b}\right)\right] \tag{3.58}$$

$$\frac{dn_{j,f}}{dz} = A_f(1-\varepsilon_s)\Re_{j,f} \tag{3.59}$$

These equations are subject to the following boundary conditions:

$$@z = 0 \qquad n_{j,b} = y_{j,b}\frac{n_a}{1 + \frac{u_e}{u_b}\frac{1-\delta}{\delta}\varepsilon_{mf}} \tag{3.60}$$

$$@z = 0 \qquad n_{j,e} = y_{j,e}\frac{n_a}{1 + \frac{u_b}{u_e}\frac{\delta}{(1-\delta)\varepsilon_{mf}}} \tag{3.61}$$

$$@\, z = H_{bed} \qquad n_{j,f} = n_{j,e} + n_{j,b} \tag{3.62}$$

The expressions for the species generation or depletion terms appearing in Equations (3.57), (3.58) and (3.59), $\Re_{j,b}$, $\Re_{j,e}$ and $\Re_{j,f}$, take the following form for each species considered,

$j = 1\ (O_2)$

$$\Re_{1,b} = -\left\{0.5r_{R7} + \frac{5}{4}r_{R12} + 0.5r_{R14} + 0.5r_{R15} - 0.5r_{R25}\right\} \tag{3.63}$$

$$\begin{aligned}\Re_{1,e} = &-\frac{m_{vm,coal}x_{vl,coal}}{V_{bed}(1-\delta)\varepsilon_{mf}}\left\{\frac{1}{2}\frac{x_{C,vm}}{M_C} + \frac{1}{4}\frac{x_{H,vm}}{M_H} + \frac{x_{S,vm}}{M_S} - \frac{1}{2}\frac{x_{O,vm}}{M_O}\right\}_{coal} \\ &-\frac{m_{vm,bio}x_{vl,bio}}{V_{bed}(1-\delta)\varepsilon_{mf}}\left\{\frac{1}{2}\frac{x_{C,vm}}{M_C} + \frac{1}{4}\frac{x_{H,vm}}{M_H} + \frac{x_{S,vm}}{M_S} - \frac{1}{2}\frac{x_{O,vm}}{M_O}\right\}_{bio} \\ &-\left\{0.5r_{R7} + \frac{5}{4}r_{R12} + 0.5r_{R14} + 0.5r_{R15} - 0.5r_{R25}\right\} \\ &-\left\{0.5r_{R6} + 0.5\frac{r_{R9}}{V_{bed}(1-\delta)\varepsilon_{mf}} + 0.5r_{R10}\right\} \\ &-\frac{1}{V_{bed}(1-\delta)\varepsilon_{mf}}\left\{\frac{5}{4}r_{R19,het} + \frac{3}{4}r_{R21,het}\right\}_{coal} \\ &-\frac{1}{V_{bed}(1-\delta)\varepsilon_{mf}}\left\{\frac{5}{4}r_{R19,het} + \frac{3}{4}r_{R21,het}\right\}_{bio} \\ &-\frac{1}{V_{bed}(1-\delta)\varepsilon_{mf}}\left\{\frac{5}{4}r_{R20,het} + \frac{3}{4}r_{R22,het}\right\}_{ash}\end{aligned} \tag{3.64}$$

$$
\begin{aligned}
\Re_{1,f} = & -\frac{m_{vm,coal}\left(1 - x_{vl,coal}\right)}{V_f(1-\varepsilon_s)}\left\{\frac{1}{2}\frac{x_{C,vm}}{M_C} + \frac{1}{4}\frac{x_{H,vm}}{M_H} + \frac{x_{S,vm}}{M_S} - \frac{1}{2}\frac{x_{O,vm}}{M_O}\right\}_{coal} \\
& -\frac{m_{vm,bio}(1 - x_{vl,bio})}{V_f(1-\varepsilon_s)}\left\{\frac{1}{2}\frac{x_{C,vm}}{M_C} + \frac{1}{4}\frac{x_{H,vm}}{M_H} + \frac{x_{S,vm}}{M_S} - \frac{1}{2}\frac{x_{O,vm}}{M_O}\right\}_{bio} \\
& -\left\{0.5r_{R7} + \frac{5}{4}r_{R12} + 0.5r_{R14} + 0.5r_{R15} - 0.5r_{R25}\right\} \qquad (3.65) \\
& -\left\{0.5r_{R6} + 0.5\frac{r_{R9}}{V_f(1-\varepsilon_s)}\right\}
\end{aligned}
$$

$j = 2\ (CO)$

$$
\Re_{2,b} = \{-r_{R7} + r_{R15} + r_{R16} - r_{R24}\} \qquad (3.66)
$$

$$
\begin{aligned}
\Re_{2,e} = & \frac{m_{vm,coal}x_{vl,coal}}{V_{bed}(1-\delta)\varepsilon_{mf}}\left\{\frac{x_{C,vm}}{M_C}\right\}_{coal} \\
& + \frac{m_{vm,bio}x_{vl,bio}}{V_{bed}(1-\delta)\varepsilon_{mf}}\left\{\frac{x_{C,vm}}{M_C}\right\}_{bio} \\
& + \{-r_{R7} + r_{R15} + r_{R16} - r_{R24}\} + r_{R6} \qquad (3.67) \\
& + \frac{1}{V_{bed}(1-\delta)\varepsilon_{mf}}\left\{r_{R17,het} - r_{R18,het}\right\}_{coal} \\
& + \frac{1}{V_{bed}(1-\delta)\varepsilon_{mf}}\left\{r_{R17,het} - r_{R18,het}\right\}_{bio}
\end{aligned}
$$

$$
\begin{aligned}
\Re_{2,f} = & \frac{m_{vm,coal}\left(1 - x_{vl,coal}\right)}{V_f(1-\varepsilon_s)}\left\{\frac{x_{C,vm}}{M_C}\right\}_{coal} \\
& + \frac{m_{vm,bio}(1 - x_{vl,bio})}{V_f(1-\varepsilon_s)}\left\{\frac{x_{C,vm}}{M_C}\right\}_{bio} \qquad (3.68) \\
& + \{-r_{R7} + r_{R15} + r_{R16} - r_{R24}\} + r_{R6}
\end{aligned}
$$

$j = 3\ (CO_2)$

$$\Re_{3,b} = \{r_{R7} + r_{R24}\} \tag{3.69}$$

$$\begin{aligned}\Re_{3,e} = \{r_{R7} + r_{R24}\} \\ &+ \frac{F_{lst} x_{CaCO_3}}{M_{CaCO_3} V_{bed}(1-\delta)\varepsilon_{mf}} \\ &+ \frac{1}{V_{bed}(1-\delta)\varepsilon_{mf}}\{r_{R18,het,coal} + r_{R18,het,bio}\} \\ &+ \frac{0.5}{V_{bed}(1-\delta)\varepsilon_{mf}}\{r_{R23,het,coal} + r_{R23,het,bio}\}\end{aligned} \tag{3.70}$$

$$\Re_{3,f} = \{r_{R7} + r_{R24}\} \tag{3.71}$$

$j = 4\ (H_2O)$

$$\Re_{4,b} = \left\{1.5 r_{R12} + \frac{r_{R13}}{V_{bed}\delta}\right\} \tag{3.72}$$

$$\begin{aligned}
\Re_{4,e} = {} & \frac{m_{vm,coal} x_{vl,coal}}{V_{bed}(1-\delta)\varepsilon_{mf}} \left\{\frac{1}{2}\frac{x_{H,vm}}{M_H}\right\}_{coal} + \frac{m_{vm,bio} x_{vl,bio}}{V_{bed}(1-\delta)\varepsilon_{mf}} \left\{\frac{1}{2}\frac{x_{H,vm}}{M_H}\right\}_{bio} \\
& + \left\{\frac{m_f x_{H_2O}}{V_{bed}(1-\delta)\varepsilon_{mf}} \frac{1}{M_{H_2O}}\right\}_{coal} + \left\{\frac{m_f x_{H_2O}}{V_{bed}(1-\delta)\varepsilon_{mf}} \frac{1}{M_{H_2O}}\right\}_{bio} \\
& + \left\{1.5 r_{R12} + \frac{r_{R13}}{V_{bed}(1-\delta)\varepsilon_{mf}}\right\} \\
& + \frac{1}{V_{bed}(1-\delta)\varepsilon_{mf}} \left\{1.5 r_{R19,het} + 1.5 r_{R21,het}\right\}_{coal} \\
& + \frac{1}{V_{bed}(1-\delta)\varepsilon_{mf}} \left\{1.5 r_{R19,het} + 1.5 r_{R21,het}\right\}_{bio} \\
& + \frac{1}{V_{bed}(1-\delta)\varepsilon_{mf}} \left\{1.5 r_{R20,het} + 1.5 r_{R22,het}\right\}_{ash}
\end{aligned} \tag{3.73}$$

$$\begin{aligned}
\Re_{4,f} = {} & \frac{m_{vm,coal}\left(1 - x_{vl,coal}\right)}{V_f(1-\varepsilon_s)} \left\{\frac{1}{2}\frac{x_{H,vm}}{M_H}\right\}_{coal} \\
& + \frac{m_{vm,bio}\left(1 - x_{vl,bio}\right)}{V_f(1-\varepsilon_s)} \left\{\frac{1}{2}\frac{x_{H,vm}}{M_H}\right\}_{bio} \\
& + \left\{1.5 r_{R12} + \frac{r_{R13}}{V_f(1-\varepsilon_s)}\right\}
\end{aligned} \tag{3.74}$$

$j = 5\ (SO_2)$

$$\Re_{5,b} = 0 \tag{3.75}$$

$$\Re_{5,e} = \frac{m_{vm,coal} x_{vl,coal}}{V_{bed}(1-\delta)\varepsilon_{mf}} \left\{\frac{x_{S,vm}}{M_S}\right\}_{coal} + \frac{m_{vm,bio} x_{vl,bio}}{V_{bed}(1-\delta)\varepsilon_{mf}} \left\{\frac{x_{S,vm}}{M_S}\right\}_{bio} - \left\{\frac{r_{R9}}{V_{bed}(1-\delta)\varepsilon_{mf}}\right\} \tag{3.76}$$

$$\Re_{5,f} = \frac{m_{vm,coal}(1 - x_{vl,coal})}{V_f(1-\varepsilon_s)} \left\{\frac{x_{S,vm}}{M_S}\right\}_{coal} + \frac{m_{vm,bio}(1 - x_{vl,bio})}{V_f(1-\varepsilon_s)} \left\{\frac{x_{S,vm}}{M_S}\right\}_{bio} - \left\{\frac{r_{R9}}{V_f(1-\varepsilon_s)}\right\} \tag{3.77}$$

$j = 6\ (NH_3)$

$$\Re_{6,b} = -\left\{ r_{R12} + \frac{2}{3}\frac{r_{R13}}{V_{bed}\delta} \right\} \tag{3.78}$$

$$\begin{aligned}
\Re_{6,e} = &\frac{m_{vm,coal}x_{vl,coal}}{V_{bed}(1-\delta)\varepsilon_{mf}} \left\{ \frac{x_{N,vm}x_{N,vol}}{M_N} x_{NH_3} \right\}_{coal} \\
&+ \frac{m_{vm,bio}x_{vl,bio}}{V_{bed}(1-\delta)\varepsilon_{mf}} \left\{ \frac{x_{N,vm}x_{N,vol}}{M_N} x_{NH_3} \right\}_{bio} \\
&- \left\{ r_{R12} + \frac{2}{3}\frac{r_{R13}}{V_{bed}(1-\delta)\varepsilon_{mf}} \right\} \\
&- \frac{1}{V_{bed}(1-\delta)\varepsilon_{mf}} \left\{ r_{R19,het} + r_{R21,het} \right\}_{coal} \\
&- \frac{1}{V_{bed}(1-\delta)\varepsilon_{mf}} \left\{ r_{R19,het} + r_{R21,het} \right\}_{bio} \\
&- \frac{1}{V_{bed}(1-\delta)\varepsilon_{mf}} \left\{ r_{R20,het} + r_{R22,het} \right\}_{ash}
\end{aligned} \tag{3.79}$$

$$\begin{aligned}
\Re_{6,f} = &\frac{m_{vm,coal}(1-x_{vl,coal})}{V_f(1-\varepsilon_s)} \left\{ \frac{x_{N,vm}x_{N,vol}}{M_N} x_{NH_3} \right\}_{coal} \\
&+ \frac{m_{vm,bio}(1-x_{vl,bio})}{V_f(1-\varepsilon_s)} \left\{ \frac{x_{N,vm}x_{N,vol}}{M_N} x_{NH_3} \right\}_{bio} \\
&- \left\{ r_{R12} + \frac{2}{3}\frac{r_{R13}}{V_f(1-\varepsilon_s)} \right\}
\end{aligned} \tag{3.80}$$

$j = 7\ (NO)$

$$\Re_{7,b} = \left\{ r_{R12} - \frac{r_{R13}}{V_{bed}\delta} + r_{R15} - R_{R16} \right\} \tag{3.81}$$

$$\begin{aligned}\Re_{7,e} = {} & \left\{ r_{R12} - \frac{r_{R13}}{V_{bed}(1-\delta)\varepsilon_{mf}} + r_{R15} - r_{R16} \right\} \\ & + r_{10} + r_{11} \\ & - \frac{1}{V_{bed}(1-\delta)\varepsilon_{mf}} \left\{ r_{R17,het} + r_{R18,het} - r_{R19,het} \right\}_{coal} \\ & - \frac{1}{V_{bed}(1-\delta)\varepsilon_{mf}} \left\{ r_{R17,het} + r_{R18,het} - r_{R19,het} \right\}_{bio} \\ & + \frac{1}{V_{bed}(1-\delta)\varepsilon_{mf}} \left\{ r_{R20,het} \right\}_{ash}\end{aligned} \tag{3.82}$$

$$\Re_{7,f} = \left\{ r_{R12} - \frac{r_{R13}}{V_f(1-\varepsilon_s)} + r_{R15} - r_{R16} \right\} \tag{3.83}$$

$j = 8\ (HCN)$

$$\Re_{8,b} = -r_{R14} \tag{3.84}$$

$$\begin{aligned}\Re_{8,e} = {} & \frac{m_{vm,coal} x_{vl,coal}}{V_{bed}(1-\delta)\varepsilon_{mf}} \left\{ \frac{x_{N,vm} x_{N,vol}}{M_N} x_{HCN} \right\}_{coal} \\ & + \frac{m_{vm,bio} x_{vl,bio}}{V_{bed}(1-\delta)\varepsilon_{mf}} \left\{ \frac{x_{N,vm} x_{N,vol}}{M_N} x_{HCN} \right\}_{bio} - r_{R14}\end{aligned} \tag{3.85}$$

$$\begin{aligned}\Re_{8,f} = {} & \frac{m_{vm,coal}(1 - x_{vl,coal})}{V_f(1-\varepsilon_s)} \left\{ \frac{x_{N,vm} x_{N,vol}}{M_N} x_{HCN} \right\}_{coal} \\ & + \frac{m_{vm,bio}(1 - x_{vl,bio})}{V_f(1-\varepsilon_s)} \left\{ \frac{x_{N,vm} x_{N,vol}}{M_N} x_{HCN} \right\}_{bio} - r_{R14}\end{aligned} \tag{3.86}$$

$j = 9\ (CNO)$

$$\Re_{9,b} = \{r_{R14} - r_{R15} - r_{R16}\} \tag{3.87}$$

$$\Re_{9,e} = \{r_{R14} - r_{R15} - r_{R16}\} \tag{3.88}$$

$$\Re_{9,f} = \{r_{R14} - r_{R15} - r_{R16}\} \tag{3.89}$$

$j = 10\ (N_2O)$

$$\mathfrak{R}_{10,b} = \{r_{R16} - r_{R24} - r_{R25}\} \tag{3.90}$$

$$\mathfrak{R}_{10,e} = \{r_{R16} - r_{R24} - r_{R25}\} \\ + r_{11} - \frac{1}{V_{bed}(1-\delta)\varepsilon_{mf}}\left\{r_{R23,het,coal} + r_{R23,het,bio}\right\} \tag{3.91}$$

$$\mathfrak{R}_{10,f} = \{r_{R16} - r_{R24} - r_{R25}\} \tag{3.92}$$

3.2.8 Energy Conservation Equations

3.2.8.1 Energy Balance in Bed

Based on the assumption that the gas and the inert particles are at the same temperature and that the mass of combustion gases and char particles are negligible compared to the mass of inerts, a combined gas/solid phase energy balance for bed can be written as,

$$n_a \int_{T_r}^{T_a} c_{p,a} dT - \alpha \frac{A_T}{L_T} \int_0^{L_T} U_{cw}(T_{bed} - T_{cw}) dx \\ -A_{bw} h_{bw}\left(T_{bed} - T_{bw,s}\right) - m_{CO} c_{p,i}(T_{bed} - T_r) \\ -m_{bd} c_{p,i}(T_{bed} - T_r) - n_g \sum_{j=1}^{n} y_j \int_{T_r}^{T_{bed}} c_{p,g_j} dT \\ -(m_{coal} x_{H_2O} + m_{bio} x_{H_2O})\lambda^0 + Q_p + Q_{rxn} = 0 \tag{3.93}$$

where heat generated from chemical reaction, Q_{rxn}, and energy transferred from burning char particles, Q_p, are obtained from the following equations,

$$
\begin{aligned}
Q_{rxn} = {} & m_{vm,coal} x_{vl,coal} \left\{ \begin{matrix} \dfrac{x_{C,vm}}{M_C} \Delta H_{R1}^0 + \dfrac{1}{2} \dfrac{x_{H,vm}}{M_H} \Delta H_{R2}^0 + \dfrac{x_{S,vm}}{M_S} \Delta H_{R3}^0 \\ + \dfrac{x_{N,vm} x_{N,vol}}{M_N} x_{NH_3} \Delta H_{R4}^0 + \dfrac{x_{N,vm} x_{N,vol}}{M_N} x_{HCN} \Delta H_{R5}^0 \end{matrix} \right\}_{coal} \\
& + m_{vm,bio} x_{vl,bio} \left\{ \begin{matrix} \dfrac{x_{C,vm}}{M_C} \Delta H_{R1}^0 + \dfrac{1}{2} \dfrac{x_{H,vm}}{M_H} \Delta H_{R2}^0 + \dfrac{x_{S,vm}}{M_S} \Delta H_{R3}^0 \\ + \dfrac{x_{N,vm} x_{N,vol}}{M_N} x_{NH_3} \Delta H_{R4}^0 + \dfrac{x_{N,vm} x_{N,vol}}{M_N} x_{HCN} \Delta H_{R5}^0 \end{matrix} \right\}_{bio} \\
& + A_{bed} \delta \Delta H_{R7}^0 \int_0^{H_{bed}} r_{R7} dx + A_{bed} \delta \Delta H_{R12}^0 \int_0^{H_{bed}} r_{R12} dx \\
& + A_{bed} \delta \frac{\Delta H_{R13}^0}{V_{bed} \delta} \int_0^{H_{bed}} r_{R13} dx + A_{bed} \delta \Delta H_{R14}^0 \int_0^{H_{bed}} r_{R14} dx \\
& + A_{bed} \delta \Delta H_{R15}^0 \int_0^{H_{bed}} r_{R15} dx + A_{bed} \delta \Delta H_{R16}^0 \int_0^{H_{bed}} r_{R16} dx \\
& + A_{bed} \delta \Delta H_{R24}^0 \int_0^{H_{bed}} r_{R24} dx + A_{bed} \delta \Delta H_{R25}^0 \int_0^{H_{bed}} r_{R25} dx \\
& + V_{bed} (1 - \delta) \varepsilon_{mf} \Delta H_{R7}^0 r_{R7} + V_{bed} (1 - \delta) \varepsilon_{mf} \Delta H_{R12}^0 r_{R12} \\
& + V_{bed} (1 - \delta) \varepsilon_{mf} \frac{\Delta H_{R13}^0 r_{R13}}{V_{bed} (1 - \delta) \varepsilon_{mf}} + V_{bed} (1 - \delta) \varepsilon_{mf} \Delta H_{R25}^0 r_{R25} \\
& + V_{bed} (1 - \delta) \varepsilon_{mf} \Delta H_{R10}^0 r_{R10} + V_{bed} (1 - \delta) \varepsilon_{mf} \Delta H_{R14}^0 r_{R14} \\
& + V_{bed} (1 - \delta) \varepsilon_{mf} \Delta H_{R11}^0 r_{R10} + V_{bed} (1 - \delta) \varepsilon_{mf} \Delta H_{R15}^0 r_{R15} \\
& + V_{bed} (1 - \delta) \varepsilon_{mf} \Delta H_{R16}^0 r_{R16} + V_{bed} (1 - \delta) \varepsilon_{mf} \Delta H_{R24}^0 r_{R24} \\
& + \left\{ \begin{matrix} \Delta H_{R17}^0 r_{R17,het} + \Delta H_{R18}^0 r_{R18,het} + \Delta H_{R19}^0 r_{R19,het} \\ + \Delta H_{R21}^0 r_{R21,het} + \Delta H_{R23}^0 r_{R23,het} \end{matrix} \right\}_{coal} \\
& + \left\{ \begin{matrix} \Delta H_{R17}^0 r_{R17,het} + \Delta H_{R18}^0 r_{R18,het} + \Delta H_{R19}^0 r_{R19,het} \\ + \Delta H_{R21}^0 r_{R21,het} + \Delta H_{R23}^0 r_{R23,het} \end{matrix} \right\}_{bio} \\
& + \left[\Delta H_{R20}^0 r_{R20,het} + \Delta H_{R22}^0 r_{22,het} \right]_{ash} - \frac{F_{lst} x_{CaCO_3}}{M_{CaCO_3}} \Delta H_{R8}^0 + \Delta H_{R9}^0 r_{R9}
\end{aligned}
\tag{3.94}
$$

$$Q_p = \frac{3M_d}{\rho_d} \int_{r_{min}}^{r_{max}} [h(T_d - T_{bed}) + \sigma\epsilon(T_d^4 - T_{bed}^4)] \frac{P_{bed}(r)}{r} dr \tag{3.95}$$

Energy loss through the bed walls is taken into account by making a one-dimensional heat transfer analysis. For a combustor with square cross-section and wall thickness of L_{bw}, the temperature profiles inside the wall of variable cross-section is given by the following equation,

$$\frac{d^2T_{bw}}{dx^2}\left(x + \frac{A_{bed}^{0.5}}{2}\right) + \frac{dT_{bw}}{dx} = 0 \tag{3.96}$$

Equation (3.96) is subjected to the following boundary conditions:

$$@x = 0 \qquad h_{bw}(T_{bed} - T_{bw}) = \; -k_{bw}\frac{\partial T_{bw}}{\partial x} \tag{3.97}$$

$$@x = L_{bw} \qquad\qquad T_{bw} = \qquad T_{bw,o} \tag{3.98}$$

In order to account for the energy absorbed by the in-bed heat exchanger, a separate energy balance is performed on the cooling water. Neglecting the heat transfer resistance of the tubes, the spatial variation of the temperature of the cooling water is given by the following equation:

$$\frac{m_{cw}}{\pi}\frac{dT_{cw}}{dx} - \frac{d_{T,o}}{c_{p,cw}} h_{cw}(T_{bed} - T_w) = 0 \tag{3.99}$$

The inlet temperature of the cooling water is set as boundary condition to 3.98. Surface temperature of the tube wall, T_w, is calculated by solving a surface energy balance:

$$h_{cw}d_{T,o}(T_{bed} - T_w) - h_i d_{T,i}(T_w - T_{cw}) = 0 \tag{3.100}$$

3.2.8.2 Energy Balance in Freeboard

The gas temperature profile in freeboard is obtained by solving an energy balance which considers convective transport and, generation and loss of energy:

$$\frac{dT_f}{dz_f} = \frac{A_f(1-\varepsilon_s)}{n_f c_{p,g}} \boldsymbol{R} \tag{3.101}$$

Equation (3.101) has the following boundary condition:

$$@\ z_f = 0 \qquad T_f = T_{bed} \tag{3.102}$$

$\boldsymbol{R}$ in Equation (3.101) is the combined energy generation and loss rate per unit volume of freeboard and defined as:

$$\boldsymbol{R} = \boldsymbol{R_{rxn}} + \boldsymbol{R_{fw}} + \boldsymbol{R_p} \tag{3.103}$$

$\boldsymbol{R_{rxn}}$, $\boldsymbol{R_{fw}}$ and $\boldsymbol{R_p}$ terms in Equation (3.103) are energy generated by chemical reactions, energy loss from freeboard walls and energy exchange between solid particles and the gaseous medium, respectively. These terms can be expressed as follows:

$$\boldsymbol{R_{rxn}} = m_{vm,coal}(1 - x_{vl,coal}) \left\{ \begin{array}{c} \frac{x_{C,vm}}{M_C}\Delta H_{R1}^0 + \frac{1}{2}\frac{x_{H,vm}}{M_H}\Delta H_{R2}^0 \\ + \frac{x_{S,vm}}{M_S}\Delta H_{R3}^0 + \frac{x_{N,vm}x_{N,vol}}{M_N} x_{NH_3}\Delta H_{R4}^0 \\ + \frac{x_{N,vm}x_{N,vol}}{M_N} x_{HCN}\Delta H_{R5}^0 \end{array} \right\}_{coal}$$

$$m_{vm,bio}(1 - x_{vl,bio}) \left\{ \begin{array}{c} \frac{x_{C,vm}}{M_C}\Delta H_{R1}^0 + \frac{1}{2}\frac{x_{H,vm}}{M_H}\Delta H_{R2}^0 \\ + \frac{x_{S,vm}}{M_S}\Delta H_{R3}^0 + \frac{x_{N,vm}x_{N,vol}}{M_N} x_{NH_3}\Delta H_{R4}^0 \\ + \frac{x_{N,vm}x_{N,vol}}{M_N} x_{HCN}\Delta H_{R5}^0 \end{array} \right\}_{bio}$$

$$+\Delta H_{R7}^0 r_{R7} + \frac{\Delta H_{R9}^0 r_{R9}}{V_f(1 - \varepsilon_s)} + \Delta_{R12}^0 r_{R12} + \frac{\Delta H_{R13}^0 r_{R13}}{V_f(1 - \varepsilon_s)} \tag{3.104}$$

$$+\Delta H_{R14}^0 r_{R14} + \Delta H_{R15}^0 r_{R15} + \Delta H_{R16}^0 r_{R16}$$

$$+\Delta H_{R24}^0 r_{R24} + \Delta H_{R25}^0 r_{R25}$$

$$\boldsymbol{R_{fw}} = -\frac{4d_{bed}}{A_{bed}(1 - \varepsilon_s)} h_{fw}(T_f - T_{fw}) \tag{3.105}$$

$$\boldsymbol{R_p} = \frac{3F_{CO,i}}{A_{bed}\rho_d} \int_{r_{min}}^{r_{max,e}} \frac{P_{z,i}(r)}{r u_p(r)} \left\{ h_p(T_i - T_f) + \sigma\varepsilon(T_i^4 - T_f^4) \right\} dr$$

$$+3\varepsilon_i \int_{r_{max,e}}^{r_{max}} \frac{P_{z,i}(r)}{r} \left\{ h_p(T_i - T_f) + \sigma\varepsilon(T_i^4 - T_f^4) \right\} dr \tag{3.106}$$

It is assumed that in freeboard, inert particles temperatures remain at T_{bed}. A surface energy balance is formulated to solve for temperature of freeboard wall,

$$h_f(T_f - T_{fw}) - \frac{(T_{fw} - T_{fw,o})}{R_w} = 0 \tag{3.107}$$

where h_f is calculated by using the approach of Kunii and Levenspiel [119]:

$$\frac{h_f - (h_r + h_g)}{h_{z,f=0} - (h_r + h_g)} = \exp(-\frac{a z_f}{2}) \tag{3.108}$$

3.3 Solution Procedure

The input data required by the system model are the configuration of the test rig and its internals, air, coal and biomass flow rates, coal and biomass analyses, all solid and gas properties, inlet temperature of air, cooling water and feed solids and the size distribution functions of feed solids and bottom ash deduced from sieve analyses.

Apart from these input data, application of the model necessitates empirical and semi-empirical correlations for heat and mass transfer coefficients, combustion kinetics, elutriation and entrainment rates etc., listed in Table 3.2. However, these expressions contain empirical and semi-empirical constant which may not always comply with the experimental system to be modeled. Therefore, it is the usual practice to adjust some of these constants until a compromise is found to reproduce the measured data as accurate as possible [50]. In this study, minimum number of fitting parameters were utilized. These were exponential decay constants for particle hold-up, elutriation rate constant, CO oxidation rate, overall sulfation rate constant and the expression for the fractional conversion of NO and N_2O.

Direct use of elutriation rate constant of Choi et al. [109] yielded higher carry over flow rates at combustor exit. To match the measured carry over flow rates, elutriation rate constants of char particles are multiplied with 0.11, 0.53, 0.09 and 0.45 and elutriation rate constants of ash particles are multiplied with 0.42, 0.17, 0.07 and 0.10 for Run 1, Run 2, Run 9 and Run 10 respectively. Fine-tuning for the carry over flow rate at the cyclone exit was the simplest approach since carry over flow rate was only a function of elutriation.

With regard to entrainment, direct use of the particle hold-up distribution of Choi et al. [109] in the model resulted in incorrect particle loads at the freeboard exit. To match the predicted and measured particle loads at the freeboard exit, the decay constants of the inert ash hold-up expression of Choi et al. [109] is multiplied by 0.4, 3.5, 3.9 and 4.2 for Run 1, Run 2, Run 9 and Run 10, respectively. The decay constants of the limestone hold-up expression of Choi et al. [109] is multiplied by 6.0, 4.2 and 4.6 for Run 2, Run 9 and Run 10, respectively.

CO concentration predicted in freeboard by using rate expressions of Hottel et al. [98] were found to be an order of magnitude lower than the measurements. To match the measured CO concentrations at the freeboard, the rate constant from Hottel et al. [98] was multiplied by 0.1 and this value was used for model validation.

Regarding overall sulfation rate constant, which is a function of the stone properties as well as the fluidization conditions, its value is adjusted so that predicted SO_2 emission agrees well with the experimentally observed SO_2 emission in a once-through operation of the test rig and is estimated as 23.9 cm/s.

The expression for the fractional conversion of char-N to NO and N_2O were adopted from Goel et al. [67] who produced the expression for a bituminous coal. Direct adoption of the expression for cotton residue yielded higher NO and lower N_2O concentrations for the co-firing runs. To match the NO and N_2O concentration at the freeboard exit, the expression of Goel et al. [67] is multiplied with 5.0 for cotton residue.

Figures 3.4 to 3.6 show the algorithm of the steady state model code in compact form. The solution starts with making initial guesses for T_{bed}, $\bar{y}_{O_2,e}$, $M_{d,coal}$, $M_{d,bio}$, F_a, $T_{bw,o}$ and $f_{3,bio}/f_3$. This is followed by computation of $\bar{T}_d$ by using estimated parameters. There are seven loops of iterations to be converged for $M_{d,coal}$, $M_{d,bio}$, F_a, $\bar{y}_{O_2,e}$, $\bar{T}_{d,coal}$, $\bar{T}_{d,bio}$ and T_{bed}.

For each loop, a convergence criterion, ε, is set as the absolute difference between calculated and estimated values of the parameters. The predictions reported in this study were obtained with the values of 5×10^{-3}, 5×10^{-3}, 5×10^{-3}, 0.0025, 5×10^{-3}, 1, 1 and 1 for iterations on $M_{d,coal}$, $M_{d,bio}$, F_a, $f_{3,bio}/f_3$, $\bar{y}_{O_2,e}$, $\bar{T}_{d,coal}$, $\bar{T}_{d,bio}$ and T_{bed}.

The integration of ODEs is carried out by Backward-Differentiation Formula (BDF) method embedded in the ODE solver LSODES. Solution of the non-linear algebraic equations is performed by using the subroutines ZERO and HYBRID. Details of the solution procedure of steady state code for coal combustion can be found elsewhere [118].

The total CPU time for the complete model is about 140 seconds on 2.9 GHz Intel Core i5-4210H computer.

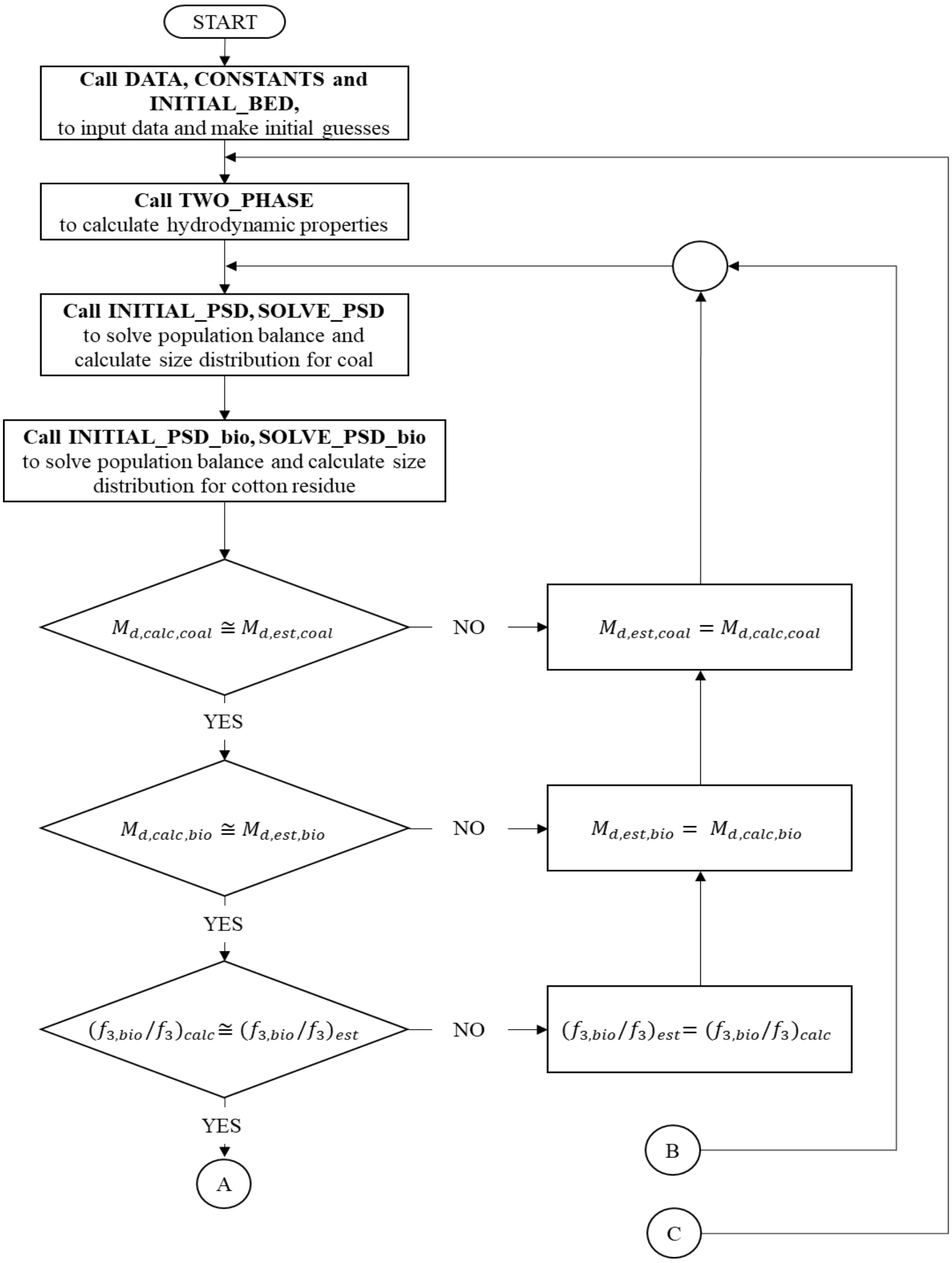

Figure 3.4 Flowchart for the steady state code for bed section (The shade area shows the modified sections of this study)

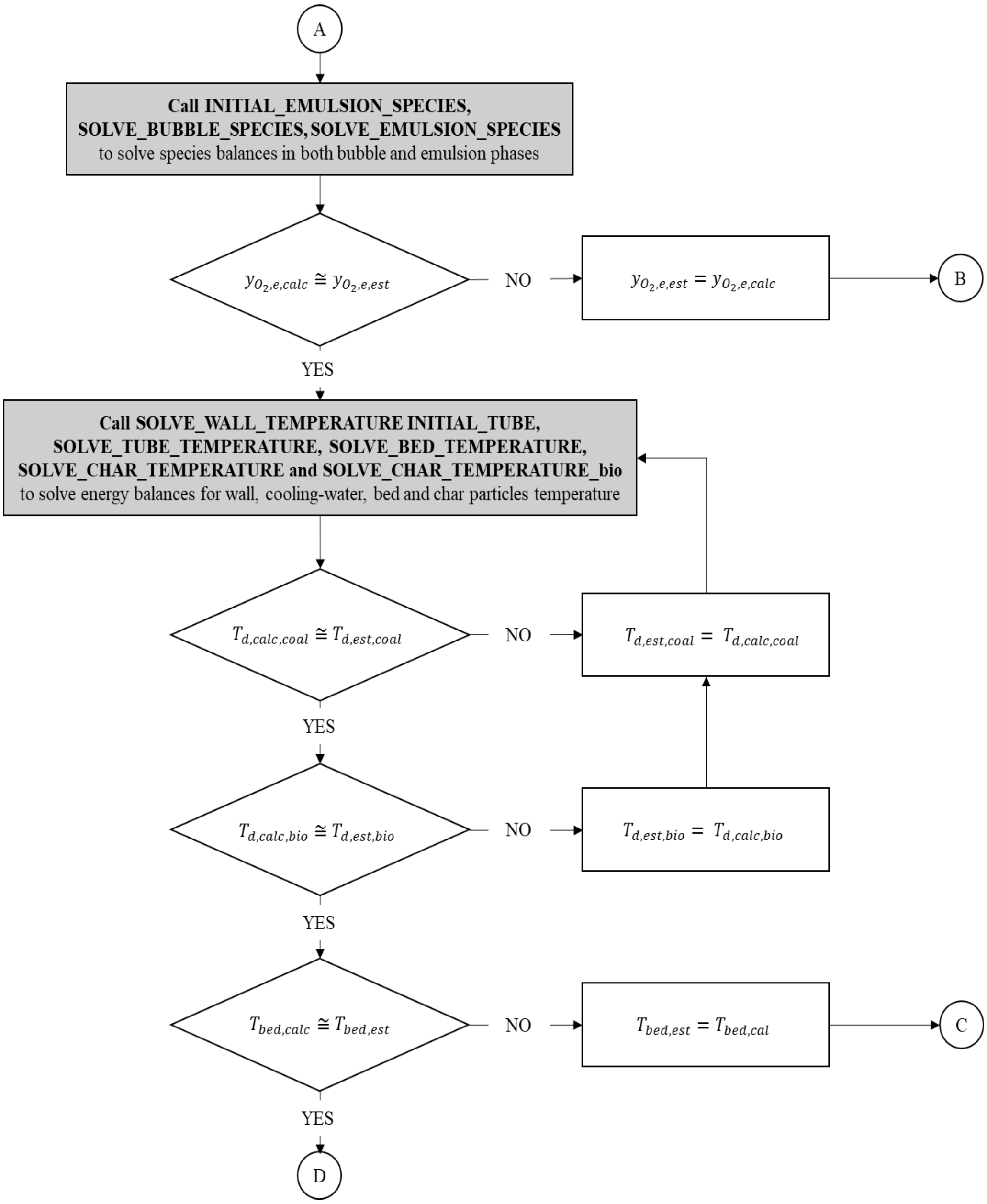

Figure 3.5 Flowchart for the steady state code for bed section (The shade area shows the modified sections of this study)

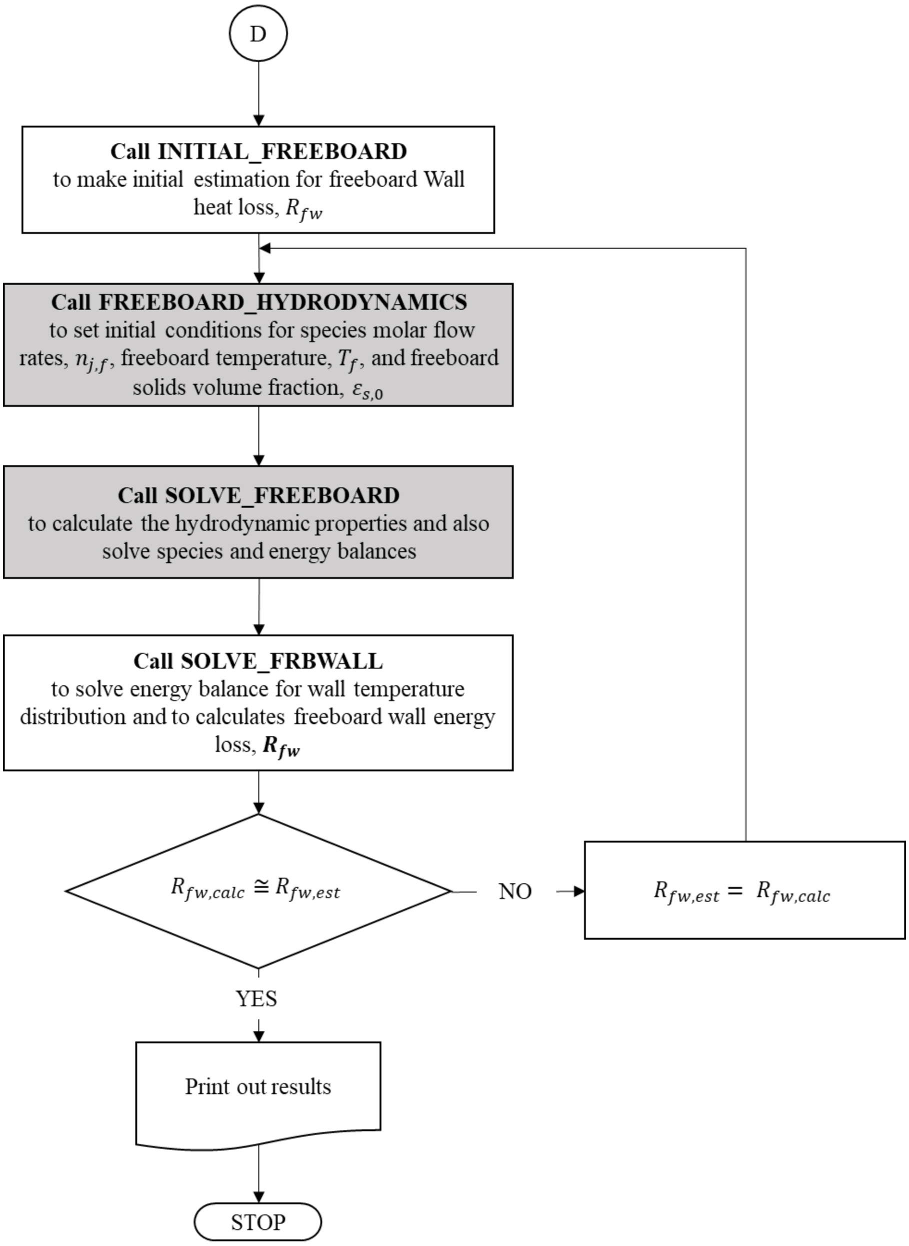

Figure 3.6 Flowchart for the steady state code for freeboard section (The shade area shows the modified sections of this study)

CHAPTER 4

EXPERIMENTAL SET-UP AND CONDITIONS

4.1 0.3 MWt Atmospheric Bubbling Fluidized Bed Combustion (ABFBC) Test Rig

Experimental work was carried out by Gogebakan et al. [13–15,33,123] in a former Ph.D. study on a 0.3 MW_t ABFBC Test Rig designed and constructed within the scope of a cooperation agreement between Middle East Technical University (METU), Babcock & Wilcox GAMA (BWG) under the auspices of Canadian Development Agency (CIDA). The test rig was originally constructed and operated for the investigation of combustion and in-situ desulfurization characteristics of low quality Turkish lignites. It was then modified for co-firing of lignite and biomass within the scope of a research project, MAG 104M200, financed by The Scientific and Technical Research Council of Turkey (TÜBİTAK). The modified test rig is shown schematically in Figure 4.1. As can be seen from the figure, the test rig basically consists of a forced draft (FD) fan, a windbox with an ash removal system, a modular combustor, a cyclone with recycle leg, a baghouse filter, an induced draft (ID) fan and a fuel and limestone feeding system.

4.1.1 The Combustor

The main body of the test rig is the modular combustor formed by five modules of equal dimensions. Each module has an internal cross-section of 0.45 m x 0.45 m and height of 1 m. Inner walls of each module are refractory lined with firebricks with a thickness of 6 cm. Outer walls of the refractory bricks are insulated with insulation bricks with thickness of 20 cm. Further insulation is provided by leaving an air gap of

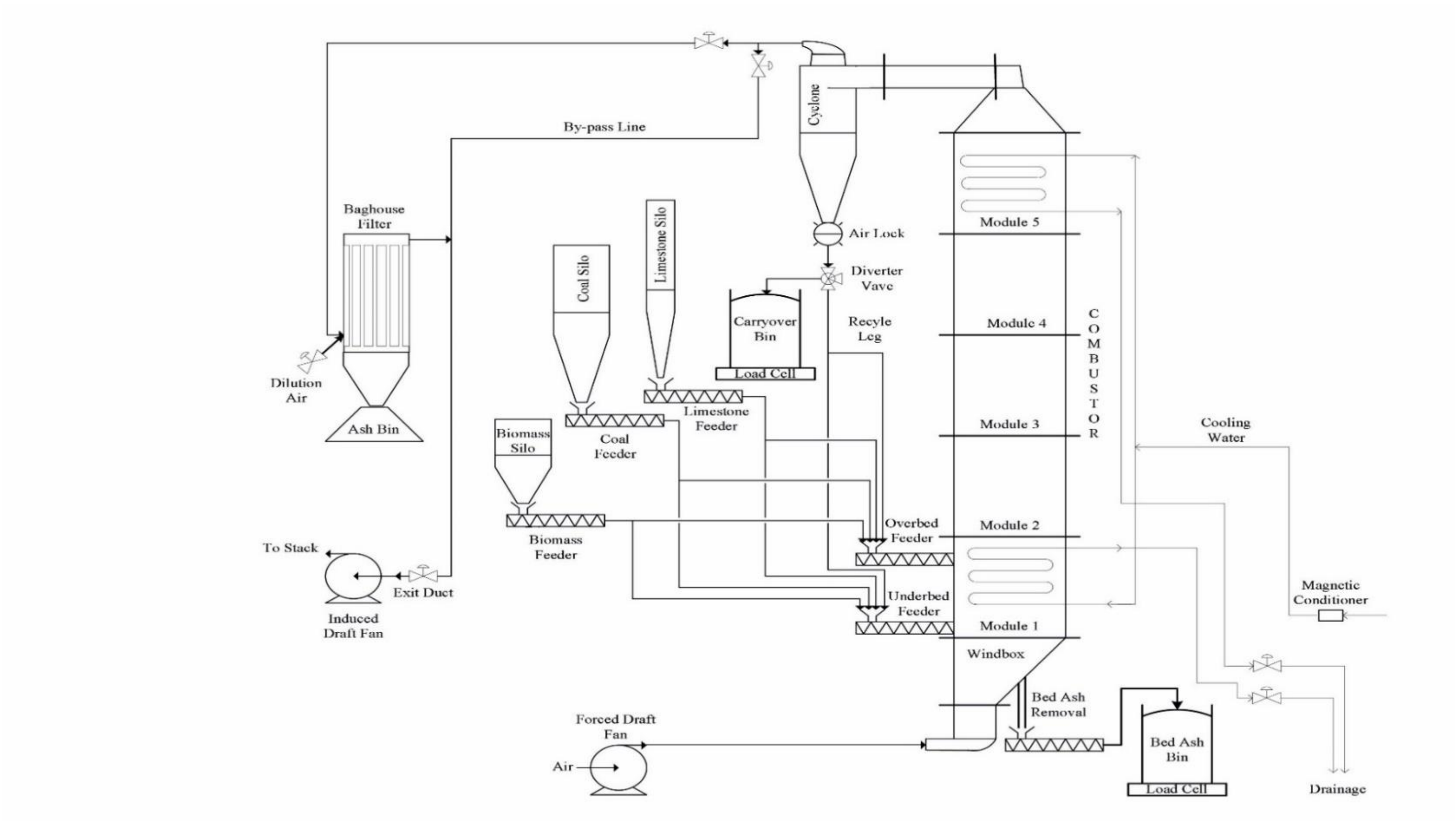

Figure 4.1 Schematic representation of METU 0.3 MW_t ABFBC test rig

6 mm between the outer wall of insulation brick and the inner wall of steel construction of each module.

The first and fifth modules from the bottom are referred as bed and cooler, respectively, and the ones in between are referred as freeboard modules. The bed module provides an expanded bed height of 1 m. It contains 6 water-cooled U-tubes (25 mm OD, stainless steel) for cooling purposes, 5 ports for thermocouples, 4 ports for gas sampling probes, one port for LPG distributor, one port for ignitor and two ports for feeding fuel/limestone mixture. One of the feeding port is 22 cm and the other is 85 cm above the distributor plate. In freeboard and cooling modules, there are 6 ports for gas sampling probes and 9 ports for thermocouples. There exists a water-cooled tube bundle consisting of 11 tubes (26.7 mm OD, carbon steel) with 14 passes installed across the cross-section of the cooler module for cooling the stack gases before leaving the combustor.

4.1.2 Air and Gas System

The fluidizing air fed by FD fan enters the bottom of the windbox through a pipe of 6.5 m long and 7.8 cm ID on which a manual gate valve, an automatic butterfly valve and a vortex flowmeter are installed. The design of the windbox allows the installation of bed ash removal system as shown in Figure 4.1. Air supplied to the windbox by means of the pipe of 7.8 cm ID diverges to the full cross-section of the combustor at the distributor plate located 1.4 m above the entrance port. Sieve type distributor plate contains 412 holes, each 4.5 mm in diameter, arranged in a triangular pattern.

Flue gases pass through the cooler module before they enter the cyclone. They then enter the baghouse filter to leave the elutriated particles before passing through ID fan to exit from the stack. As the temperature of the flue gases entering baghouse filter is limited by the maximum operating temperature of the bag material (P84-Polyimide) which is 260 °C, two alternative systems are provided for the safe operation of the bag house filter: A bypass line between the cyclone and the ID fan and an air dilution system to reduce the flue gas temperature at the inlet to the filter through a slide valve if the temperature exceeds the upper operating limit of the bag material.

An orifice meter with a bore diameter of 8.05 cm is installed at the stack gas line before ID fan to measure the flow rate of the flue gases. The pressure drop across the orificemeter is measured by means of a pressure transmitter. Knowing the temperature and pressure of the flue gases passing through the orificemeter, the signal from the transmitter is interpreted in the control system to yield molar flow rate.

4.1.3 Solids Handling System

Lignite, biomass and limestone are stored in three separate silos and conveyed into the hoppers of feeders at controlled flow rates via pre-calibrated volumetric feeders placed under their respective silos. The lignite/biomass/limestone mixture can be continuously fed to the bed through water-cooled screw feeders either 22 cm or 85 cm above the distributor plate.

Bed ash is withdrawn from the bed through 5 cm ID, 1.1 m long water-cooled ash removal pipe. Some of the bed ash is disposed and the rest is stored to provide bed inventory when required. Bed ash drain rate is adjusted from the computer to obtain the desired bed pressure drop and hence the expanded bed height. Bed ash particles are collected in a continuously weighted ash storage bin.

The majority of the elutriable fines produced from solid in the bed and those fed within the solid streams are captured by the cyclone. Particles caught in the cyclone pass through an air lock (i.e. a rotary valve) and fall onto a diverter. Depending on the position of the diverter, particles are either discharged from the system to a continuously weighted ash storage bin for experiments without recycle or recycled to the combustor for re-firing. In order to catch fine particles of fly ash leaving the cyclone, a pulse-jet type baghouse filter with a 100 % collection efficiency for particles greater than 1 μm is utilized.

4.1.4 Cooling Water System

Cooling water required for the test rig is passed through a magnetic conditioner and is then divided into two streams, one for the in-bed tube bundles, the other for the tube bundle in the cooler module. Heat transfer areas provided by the bed and cooler modules are 0.30 m^2 and 4.3 m^2, respectively. The cooling water in bed enters lower header and leaves the bed through the upper header. The cooling water for the cooler module enters the upper header and flows downward to provide counter-current flow to the up flowing flue gases. Water flow rates are adjusted by means of either a manual or a pneumatic control valve located at the drain of each stream to maintain maximum exit temperature of about 60°C.

4.1.5 Gas Sampling and Analysis System

In order to measure the concentrations of O_2, CO, CO_2, SO_2, NO and N_2O along the combustor and also downstream of cyclone, combustion gas is sampled by gas sampling probes which are fabricated for in-situ extractive gas sampling. The positions of the gas sampling probes are given in Table 4.1. Gas is sampled at a rate of 13 cm^3/s at STP which is small enough to cause minimal interference to the combustion system. After passing through the probe, sample gas is transported through the heated stainless-steel line to gas drier. The sample line itself is maintained at 150°C by means of variable DC power supply so that no water, sulfuric acid or hydrocarbons would condense along the sampling interface. In addition, all lines and fittings in contact with the gas sample are made of Teflon or stainless steel to prevent interferences due to gas adsorption or heterogeneous reactions. Once through the drier, the gas is cooled, filtered and pumped to the analyzers.

The online continuous gas analyzers with which the test rig is equipped are listed in Table 4.2. Sampled gas passes through two analyzers in series, ABB Advanced Optima 2000 and Siemens Ultramat 6. In ABB Advanced Optima 2000, O_2 concentration is measured by a magnetomechanical analyzer module Magnos 106, whereas CO, CO_2, NO and N_2O concentrations are measured by an infrared analyzer module Uras 14. In Siemens Ultramat 6, SO_2 concentration is measured by nondispersive infrared module. Bailey SMA 90 measures temporal variation of O_2 and CO on wet basis at the combustor exit.

Table 4.1 Relative positions of gas sampling probes

Probe No	**Distance above the distributor plate, cm**
P10	26
P9	56
P8	69
P7	85
P6	123
P5	183
P4	291
P3	344
P2	419
P1	500

Table 4.2 On-line gas analyzers

Instrument	**Gas Species**
Bailey SMA 90	O_2, CO
Siemens Ultramat 6	SO_2
ABB Advanced Optima 2000 (Magnos 106)	O_2
ABB Advanced Optima 2000 (Uras 14)	CO, CO_2, NO, N_2O

4.1.6 Instrumentation and Control Systems

The test rig is extensively equipped with instrumentation and control systems for research purposes. These systems can be divided into following categories:

- Data acquisition and control system
- Solid flow control and monitoring
- Air and gas flow control and monitoring
- Cooling-water flow control and monitoring
- On-line continuous gas analyzers
- Pressure sensors
- Temperature sensors

The test rig is equipped with a data acquisition and control system namely Bailey INFI 90. Real time process data is monitored, manipulated, collected and analyzed with the aid of a control software called Bailey LAN-90 Process Control View installed on an IBM compatible PC 486 computer running under QNX operating system. The control system scans the signal coming from all of the instruments attached to it in a fraction of a second and reports and logs their averages discretely for 30 seconds of intervals. An uninterruptible power supply is connected to Bailey INFI 90 and PC in order to enable proper shut-down in case of an electricity cut-off by preventing corruption of data logged.

Fuel and sorbent feed rates are controlled manually by adjusting the fuel feeder or sorbent feeder control dial from the computer. The flow rates of fuel and sorbent are normally set to such values that provide desired excess air and Ca/S molar ratio, respectively. Bed ash drain rate can also be adjusted from the computer to obtain the desired bed pressure drop and hence the expanded bed height. The interface between the controller and driving motors of fuel and sorbent feeders and bed ash drain are provided with three speed transmitters. Cyclone ash and bed ash are collected in respective bins and their flow rates are followed by load cells placed under respective bins.

The volumetric flow rate of air is measured by a vortex flow meter and adjusted with an automatic butterfly valve driven by a computer controlled pneumatic actuator. In order to achieve conversion from volumetric to molar flow rate, a static pressure tap, and a temperature sensor is placed downstream of the vortex flow meter. The flow rate of air is normally set to a value to achieve the desired superficial velocity in the combustor. In order to achieve almost neutral pressure on the bed surface, the flow rate of exhausted gases is adjusted with an automatic butterfly valve driven by a computer controlled pneumatic actuator.

In order to measure flow rates of cooling-water flowing through bed and cooler bundles, two orifices are located up streams of their lower and upper headers, respectively. The pressure drops across the orificemeters are measured by means of pressure transmitters. The signal from the transmitters are interpreted in the control system to yield mass flow rate of the cooling-water flowing through in-bed and cooler bundles. There exist two manual control valves installed on the downstream of upper and lower headers of bed and cooler bundles, respectively, to adjust the cooling-water flow in each bundle. The flow rates of cooling-water in bed and cooler bundles are normally set to a value which provide exit water temperature in the range 40-60°C.

Pressure sensors are used for measuring differential and gauge pressures at various positions on the test rig. Measured differential pressures are the pressure drops over orificemeters, bed and distributor plate pressure drop, and gauge pressures are the pressure at the bed surface and pressure of air feed at the downstream of the vortex flow meter. Also, an orifice meter is placed before the ID fan ensuring that the flow rate of stack gas is determined.

Spatial and temporal variations of gas temperatures along the height of the combustor are measured by means of thermocouples of K type (Chromel-Alumel) with grounded junction to minimize their response time. The tips of the thermocouples are on the symmetry axis of the combustor. The axial positions of thermocouples are given in Table 4.3. The temperature of air feed at the downstream of vortex flow meter and temperatures of cooling water at the exits of bed and cooler bundles are measured by resistance thermocouples of type Pt-100. Further details of the test rig and operating procedures such as procedures before cold start-up, during runs, after shut down can be found elsewhere [33].

Table 4.3 Relative positions of thermocouples

Thermocouple No	**Distance above the distributor plate, cm**
TC1	25
TC2	44
TC3	73
TC4	73
TC5	97
TC6	133
TC7	154
TC8	226
TC9	257
TC10	285
TC11	330
TC12	361
TC13	425
TC14	500

4.2 Experimental Conditions

4.2.1 Operating Conditions

Results of four combustion tests which were conducted in an earlier study [33] was used within the scope of this thesis study. The operation conditions of the combustion tests are tabulated in Table 4.4. In Run 1, lignite was burned without limestone and cotton residue addition whereas in Run 2, lignite was burned with limestone addition. In Runs 9 and 10, lignite was co-fired with the cotton residue with a share of 30 and 41 % on weight basis and with limestone addition. In all the runs, the lignite was burned in its own ash due to its high ash content. Feed point location was 0.22 m above the distributor plate for all runs.

Table 4.4 Operating conditions of the experiments

	Run 1	**Run 2**	**Run 9**	**Run 10**
Coal flow rate, kg/h	76.5	68.7	46.0	35.7
Biomass flow rate, kg/h	0.0	0.0	19.7	25.2
Limestone flow rate, kg/h	0.0	22.4	16.7	12.9
Ca/S molar ratio	0.0	2.7	2.7	2.7
Bed drain flow rate, kg/h	6.9	8.3	5.5	0.0
Cyclone ash flow rate, kg/h	14.2	19.4	17.3	18.0
Baghouse filter ash flow rate, kg/h	0.4	1.2	0.0	0.0
Excess air, %	23	21	10	21
Superficial velocity, m/s	2.2	1.9	1.9	2.0
Average bed temperature, ^{o}C	894	848	860	857
Average freeboard temperature, ^{o}C	866	817	849	843
Bed height, m	1.02	1.12	1.15	1.15
Bed cooling water flow rate, kg/h	3629	2842	3301	4802
Freeboard cooling water flow rate, kg/h	1792	2767	3281	3170

4.2.2 Fuel and Sorbent Characteristics

The characteristics of Çan lignite and cotton residue used in the experiments are summarized in Table 4.5. As can be seen from the table, lignite used in the experiments is characterized by its high VM/FC ratio (~1.2), high ash content (~27 %), high total sulfur content (~3.5 %) and low nitrogen content (~ 0.9 %). On the other hand, cotton residue almost contains no ash and sulfur. Its VM/FC ratio (~6.2) and nitrogen content (~ 4.1 %) are much higher than that of lignite.

Table 4.5 Fuel analyses

	Lignite				**Cotton Residue**
	Run 1	Run 2	Run 9	Run 10	
Proximate Analysis (As Received Basis, wt. %)					
Moisture	16.35	16.48	17.05	17.47	6.93
Ash	28.78	26.74	27.06	24.29	5.38
Volatile Matter	29.79	31.05	30.97	31.44	75.57
Fixed Carbon	25.17	25.74	24.93	26.80	12.14
Ultimate Analysis (Dry Basis, wt. %)					
Carbon	44.60	44.93	39.87	40.04	46.79
Hydrogen	3.95	4.09	3.89	3.84	6.48
Nitrogen	1.09	1.14	0.88	0.98	4.40
Oxygen	11.97	13.96	18.28	21.42	36.23
Combustible Sulphur	3.98	3.86	4.46	4.29	0.32
Ash	34.41	32.02	32.62	29.43	5.78
Total Sulphur	4.17	4.07	4.46	4.35	0.32
Calorific Value					
LHV, MJ/kg	12.3	13.3	12.5	13.4	17.4

Ash constituents of lignites and cotton residue are shown in Table 4.6. With regard to ash compositions, lignite ash is mainly composed of acidic oxides whereas cotton residue ash is mainly composed of basic oxides.

Table 4.6 Fuel ash compositions

As oxides, %	**Lignite**				**Cotton Residue**
	Run 1	Run 2	Run 9	Run 10	
Silica, SiO_2	57.29	56.56	55.55	50.11	0.00
Aluminum, Al_2O_3	19.67	17.49	21.35	22.57	0.81
Ferric, Fe_2O_3	12.05	10.99	11.71	11.46	4.95
Calcium, CaO	4.85	9.21	5.42	7.79	10.83
Magnesium, MgO	0.82	0.57	0.53	0.55	14.77
Sulfur, SO_3	2.00	2.05	2.71	4.24	0.00
Sodium, Na_2O	1.58	1.45	1.05	1.51	10.29
Potassium, K_2O	0.21	0.31	0.20	0.18	57.51
Titanium, TiO_2	1.53	1.38	1.48	1.58	0.85

For the tests with limestone additions, limestone with physicochemical properties shown in Table 4.7 was utilized. Limestone was supplied by Park Thermic, Electric Industry and Trade, Inc. and originates from Acıbaşı limestone quarry, 10 km away from the Çayırhan Thermal Power Plant.

Table 4.7 Characteristics of Beypazarı limestone

Size Distribution		**Chemical Analysis (wet)**	
Size (mm)	Weight (%)	Component	Weight (%)
1.180 - 1.000	14.80	Moisture	0.69
1.000 - 0.850	5.29	$CaCO_3$	88.92
0.850 - 0.710	6.26	$MgCO_3$	6.44
0.710 - 0.600	10.66	SiO_2	2.91
0.600 - 0.500	3.84	Na_2O	0.15
0.500 - 0.425	9.74	K_2O	0.08
0.425 - 0.355	6.14	Al_2O_3	0.39
0.355 - 0.180	15.06	Fe_2O_3	0.43
0.180 - 0.106	10.49	LOI	42.43
0.106 - 0.000	17.75	d_{50}: 0.43 mm	

The size distributions of the lignite, cotton residue and limestone together with their calculated Rosin-Rammler function parameters are given in Appendix C.

CHAPTER 5

RESULTS AND DISCUSSION

The assessment of the accuracy of the comprehensive system model extended to incorporate N_2O formation and reduction mechanisms in the scope of this thesis study was carried out by comparing the predicted O_2, CO_2, CO, SO_2, NO and N_2O concentration and temperature profiles throughout the combustor with the experimental data obtained in METU 0.3 MW_t ABFBC Test Rig fired with lignite only, lignite with limestone addition and lignite with limestone and cotton residue at 30 and 41 wt. % shares, respectively. Predictive performance of the present system model was tested with the axial species concentrations and temperatures along the combustor and carry over ash particle size distributions. Emission performance of the system model was also tested for all combustion tests performed experimentally.

The input data required by the model includes the following:

- Configuration and dimensions of the test rig and its internals
- Air, fuel and bed drain flow rates and Ca/S ratio
- The chemical and physical characteristics of the fuels and the sorbents
- All solid and gas properties
- Fuel partitioning into char nitrogen and volatile nitrogenous compounds
- Size distribution functions of feed fuels, feed limestone and bottom ash deduced from sieve analyses
- Inlet temperature of air, cooling water and feed solids

The measured and predicted PSDs, temperatures and concentrations are compared in the following sections.

5.1 Particle Size Distribution

The comparisons of measured and predicted size distributions of carry over ash particle for all tests under consideration are shown in the Figure 5.1. As the figure illustrates, the measured and predicted size distributions of particles in carry over stream are found to be in favorable agreement. The deviation between the coarse end of the measured and predicted size distributions is considered to be due to the entrained coarse particles due to bubble eruption.

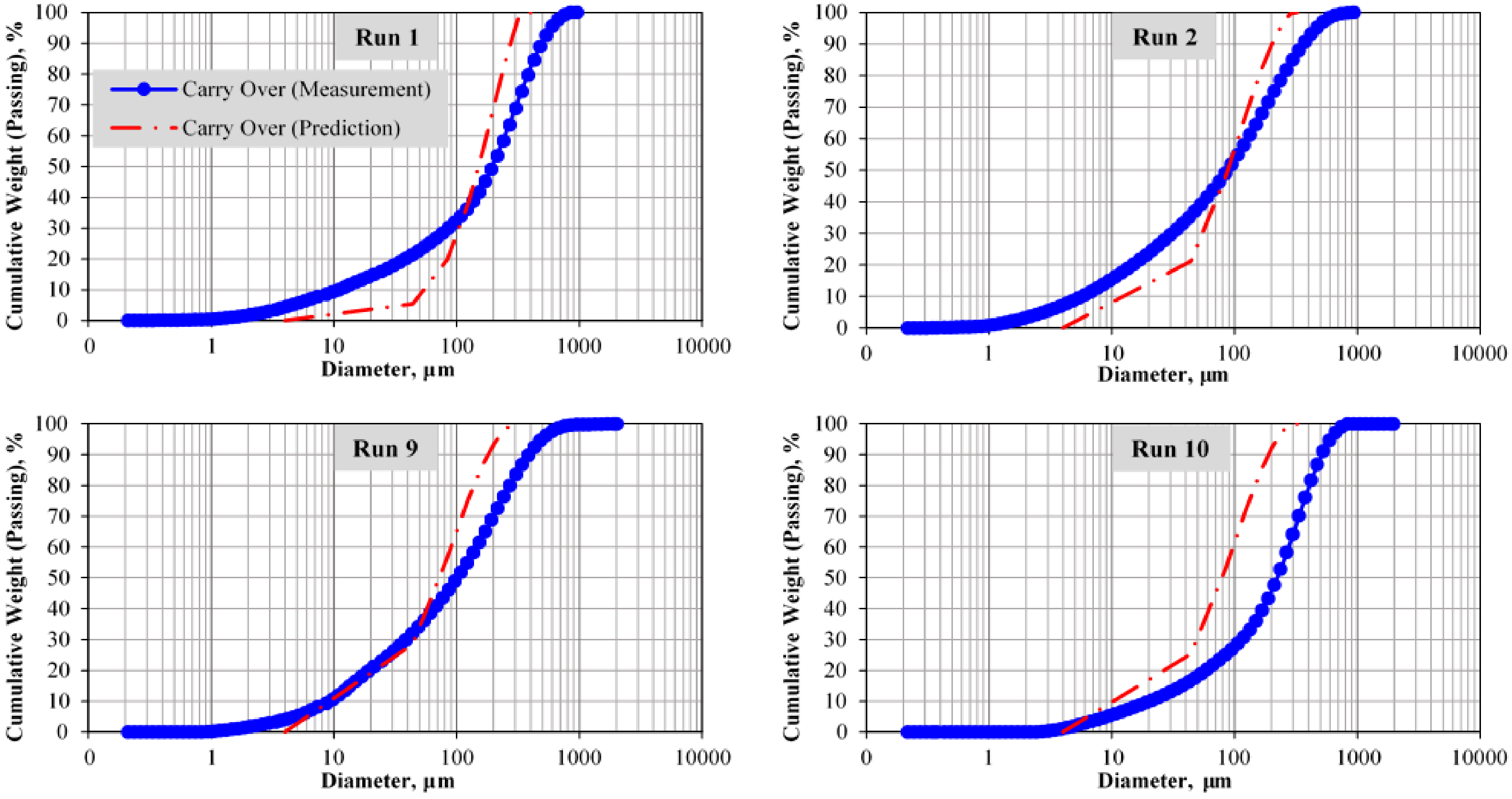

Figure 5.1 Measured and predicted size distributions of carry over ash particles for all tests under consideration

5.2 Temperature Profiles

Figure 5.2 compares the predicted and measured temperature profiles throughout the combustor for all combustion tests. Favorable comparison is achieved between the measured and predicted profiles. Addition of limestone reduces the temperatures slightly due to its calcination via endothermic reaction. It can be noted that temperature is the lowest in Run 2 where the limestone feed rate is the highest. Due to the presence of the cooler module at the exit of combustor, the temperatures fall suddenly toward the combustor exit.

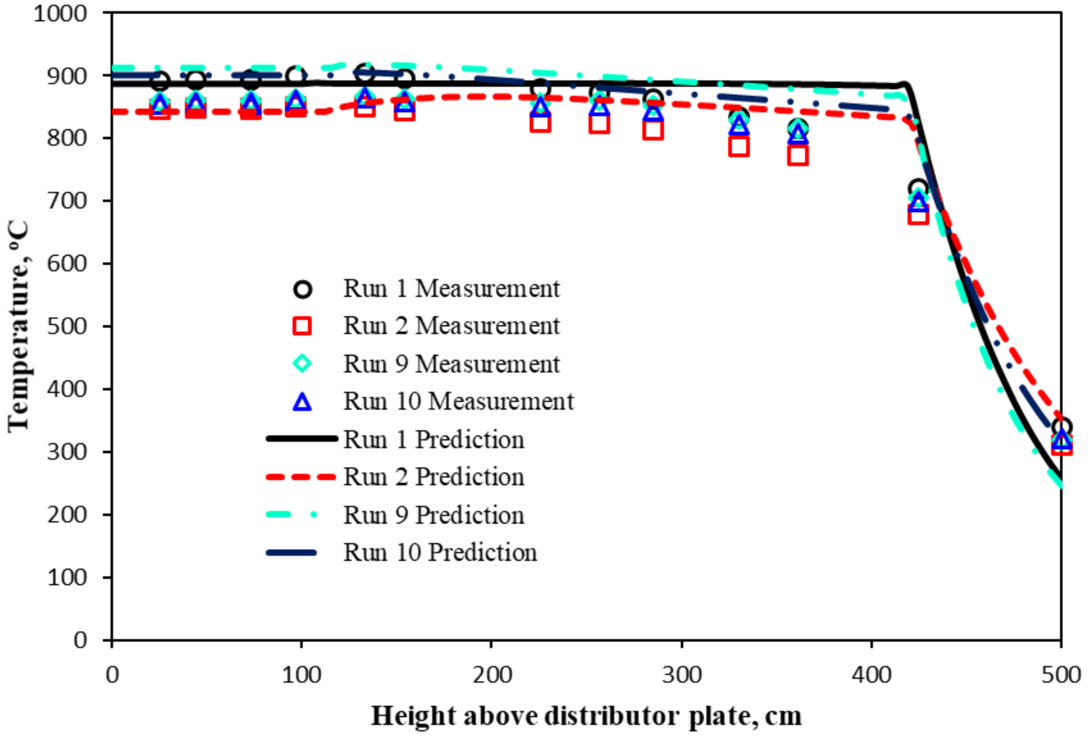

Figure 5.2 Measured and predicted temperature profiles for all tests under consideration

5.3 O_2, CO_2 and CO Concentration Profiles

In Figure 5.3, the measured and predicted concentrations of the species O_2, CO_2 and CO are compared for all tests under consideration. The predicted and measured concentrations of these three species are found to be in reasonable agreement. As can be seen from the figure, O_2 concentrations decrease drastically along the bed section and continue to decrease in the freeboard with a much lower slope whereas the concentrations of CO_2 display an opposite trend as expected. CO concentrations, on the other hand, show maxima in the bed section and suddenly decrease at the freeboard entrance due to rapid mixing of O_2-rich and O_2-lean phases. The concentration profiles of these three species reveal that the majority of the combustibles are burned in the bed section owing to the fact that char and volatile combustion primarily take place in the bed section by virtue of improved residence times of particles provided by under-bed feeding system. On the other hand, still a considerable amount of combustion takes place in the freeboard due to entrained particles and unburnt volatiles escaping from the bed.

Addition of limestone slightly increases the CO_2 concentrations throughout the combustor due to rapid CO_2 release during calcination of limestone. The effect of limestone on O_2 and CO concentrations are found to be insignificant. Addition of cotton residue, on the other hand, does not significantly influence exit concentrations of these three species.

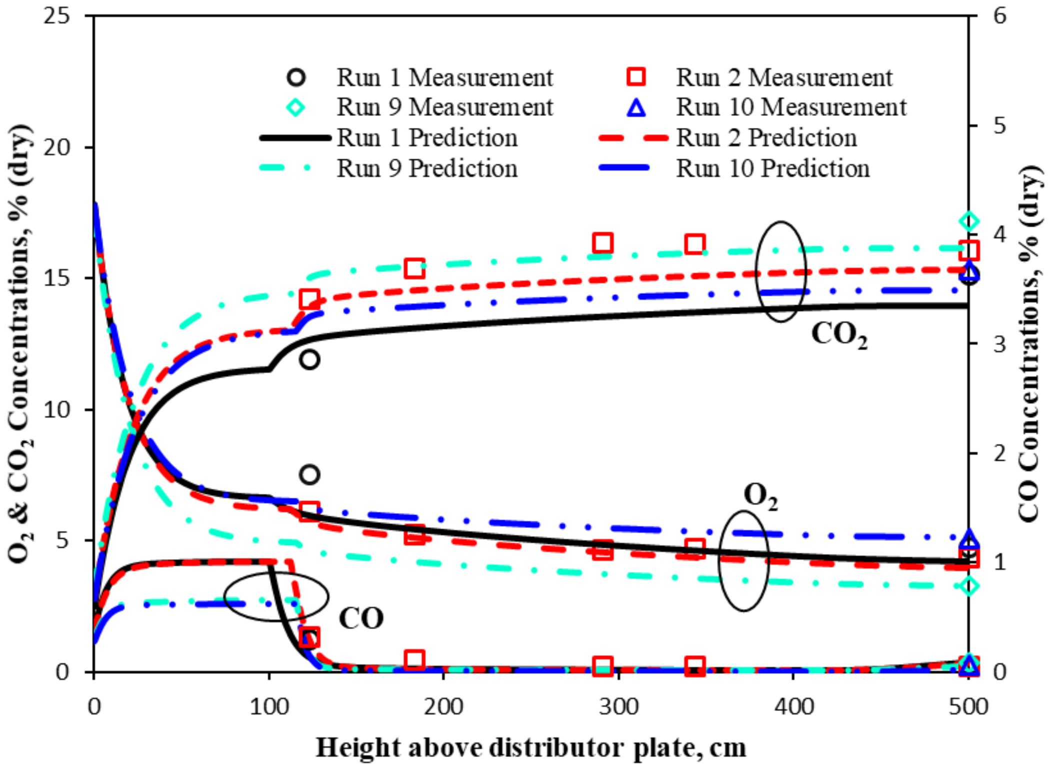

Figure 5.3 Measured and predicted O_2, CO_2 and CO concentrations for all tests under consideration

5.4 SO_2 Concentration Profiles

Figure 5.4 shows the comparison between predicted and measured concentrations of SO_2 along the combustor for all combustion tests. SO_2 concentrations increase drastically in bed region owing to the fact that major proportion of combustible sulfur is burned in that region. As for the freeboard section, the SO_2 concentrations continue to increase with a lower slope due to gradual release of combustible sulfur in the freeboard region. SO_2 concentrations are the highest in Run 1 due to combustion of high sulfur content lignite in the absence of limestone. However, addition of limestone in Run 2 reduces SO_2 concentrations significantly, as expected. Moreover, addition of cotton residue in co-firing runs reduces SO_2 concentration further due to low sulfur content of cotton residue. Slight discrepancy between measured SO_2 concentrations of Run 9 and Run 10 at the exit of the combustor is considered to be due to feeding problems of low sulfur content cotton residue encountered before the start of Run 9.

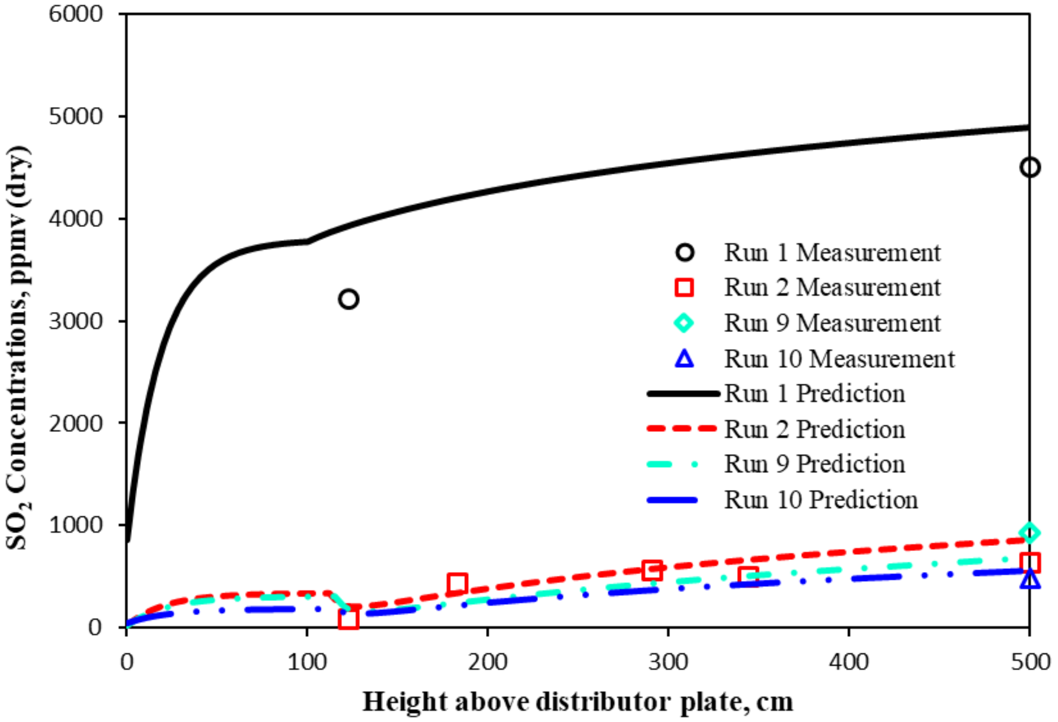

Figure 5.4 Measured and predicted SO_2 concentrations for all tests under consideration

5.5 NO and N_2O Concentration Profiles

Comparisons between the predicted and measured NO and N_2O concentrations along the combustor are demonstrated in Figure 5.5. As can be seen from the figure, NO and N_2O concentrations rise steeply along the bed section, go through maxima and decrease gradually along the freeboard. Steep rise in concentrations of NO and N_2O in the bed section where devolatilization and char combustion are rapid reveals the significant influence of heterogeneous reactions on the formation of NO and N_2O.

Addition of limestone to lignite in Run 2 does not significantly influence concentrations of NO and N_2O. This finding is also depicted by the previous studies [70–72]. On the other hand, addition of cotton residue increases the concentrations of total nitrogenous species due to the higher nitrogen content of cotton residue (~ 4.1 %

as received basis). Increasing the share of cotton residue raises the total nitrogen content of the fuel blend. As the amount of nitrogenous species rises, the reaction between two nitrogenous species, which preferentially forms reduced species such as N_2 and N_2O, becomes predominant rather than formation of NO by oxidation of nitrogenous species [24,56,124]. Therefore, the major impact is observed in the increase in the net formation of N_2O.

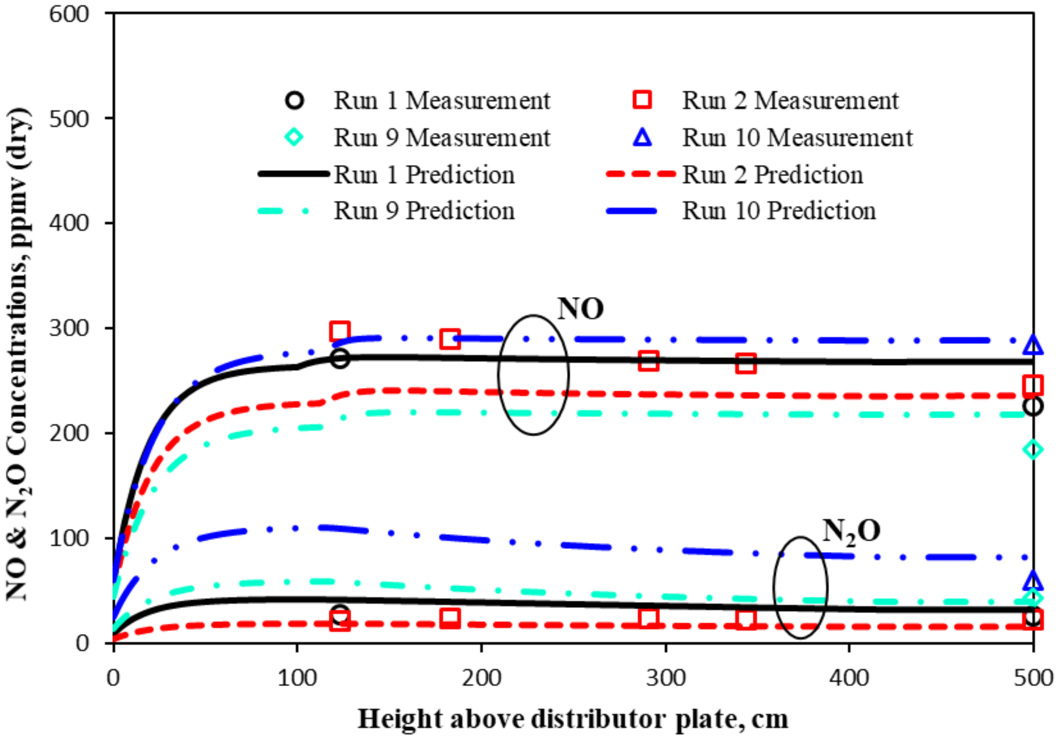

Figure 5.5 The measured and predicted NO and N_2O concentration profiles for all tests under consideration

In Figure 5.6, the comparison between the contributions of each chemical reaction on the net formation or reduction of NO and N_2O is performed by investigation of reaction rates for all combustion tests under consideration. A general inspection on the figure implies that the major source for the formation of NO is the char nitrogen oxidation (R10). In addition, ash-catalyzed oxidation of NH_3 (R20) and HCN oxidation (R15) also contribute to the formation of NO considerably. On the other hand, the dominating reduction mechanism of NO in bed section is the char-catalyzed reduction of NO with CO (R18). Moreover, reaction of NO with char nitrogen (R11) to produce N_2O remarkably influences NO concentrations especially in Run 9 and Run 10 where co-combustion of lignite with limestone and cotton residue takes place. Although gas phase reduction of NO with NH_3 (R13) seems insignificant among the NO reduction reaction, it is responsible for gradual decrease of NO in freeboard as only homogeneous NO and N_2O formation and reduction reactions are considered in freeboard section. Regarding N_2O formation and reduction reactions, reaction of NO with char nitrogen (R11) is the most dominant source for formation whereas HCN oxidation (R16) rate is found to be insignificant with the adopted reaction rate expressions. N_2O reduction over char surface (R23) is the overwhelming reduction mechanism for N_2O. In addition, thermal decomposition of N_2O (R25) takes place considerably.

Consequently, comparison between the contributions of each chemical reaction to formation and reduction of nitrogen oxides and the predictions of NO and N_2O concentration profiles along the combustor reveals that the partitioning of fuel nitrogen to char bound nitrogen and volatile nitrogen species and the distribution of volatile matters to bed and freeboard greatly influence NO and N_2O emissions in bubbling fluidized bed combustors due to both differences in the reaction paths of char nitrogen and volatile nitrogen and different catalytic solid concentrations in bed and freeboard section.

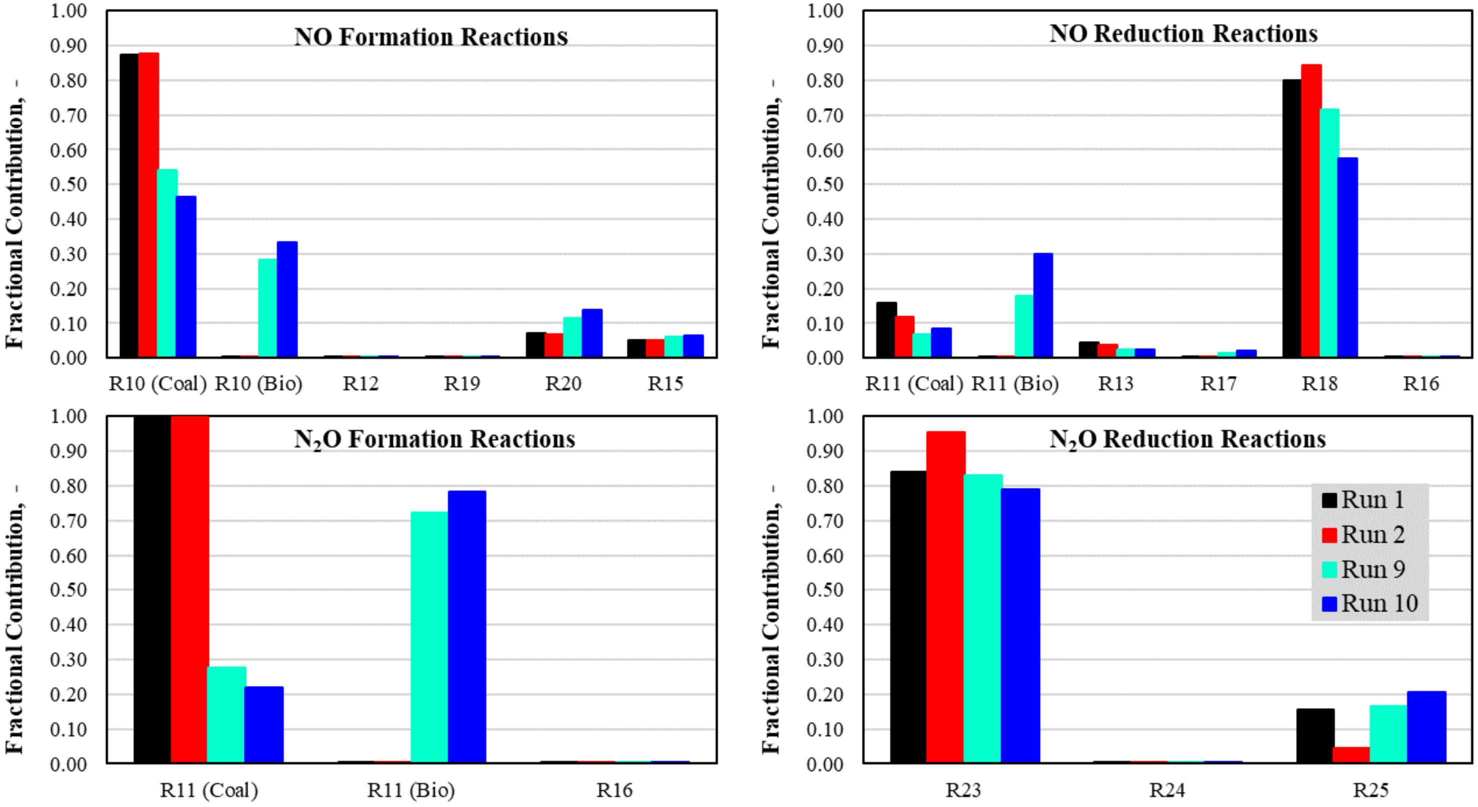

Figure 5.6 The partitioning of the chemical reactions on the formation and reduction of NO and N_2O

5.6 Model Sensitivity Analysis

In NO and N_2O modeling studies, partitioning of fuel nitrogen into char and volatiles and the distribution of volatile nitrogen species are important aspects for accurate prediction of NO and N_2O emissions. For this purpose, partitioning factor for lignite and cotton residue, $X_{N,Vol,lig}$ and $X_{N,Vol,CR}$, the fraction of N_2 in the volatile nitrogen of lignite and cotton residue, $X_{N_2,lig}$ and $X_{N_2,CR}$, the fraction of NH_3 in the volatile nitrogen of lignite and cotton residue, $X_{NH_3,lig}$ and $X_{NH_3,CR}$, and the fraction of HCN in the volatile nitrogen of lignite and cotton residue, $X_{HCN,lig}$ and $X_{HCN,CR}$, are determined based on experimental measurements. The determination of those parameters is explained in detail in Chapter 3.2.6 and the corresponding values of those parameters utilized in the model calculations are presented in Figure 3.3. In this section, sensitivity analysis of NO and N_2O concentrations of Run 10, where lignite is co-fired with limestone and cotton residue, on each of those parameters by varying one parameter at a time is carried out.

In many of NO and N_2O modeling studies, the partitioning factor, $X_{N,Vol}$, of coals and biomasses are estimated based on either pyrolysis experiments or correlations based on operational temperatures or fuel properties as it was discussed in section 2.3.1. Figure 5.7 (a) and (b) illustrates the influence of partitioning factor of lignite and cotton residue, respectively, on the concentrations of NO and N_2O for Run 10 where lignite is co-fired with limestone and cotton residue. As can be seen from the figure, poor agreement between the predicted and measured NO and N_2O concentrations is obtained unless the partitioning factors, estimated as 0.35 for lignite based on fuel properties and as 0.82 for cotton residue based on pyrolysis experiments, are utilized.

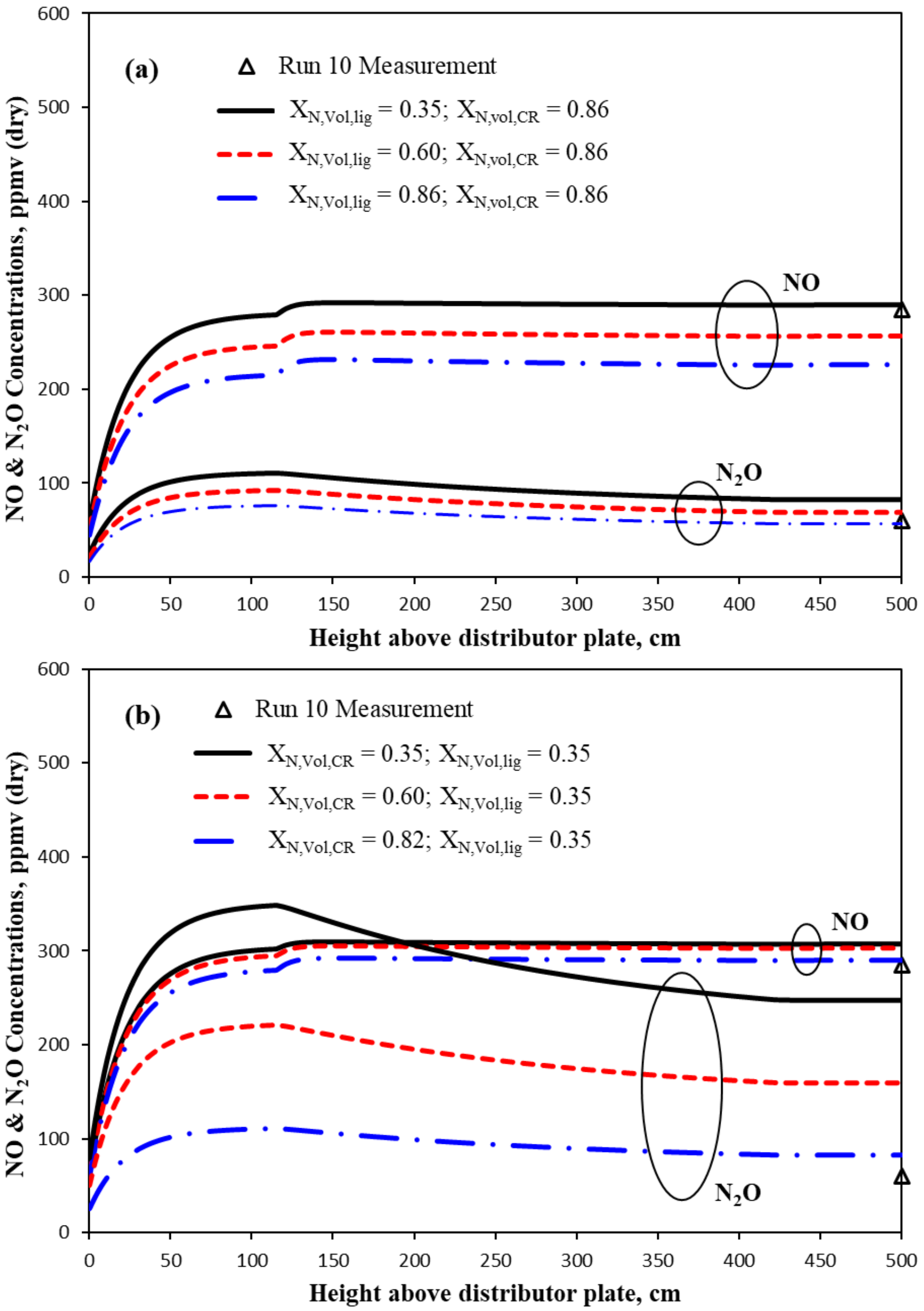

Figure 5.7 The influence of partitioning factor, $X_{N,Vol}$ (a) of lignite (b) of cotton residue on the concentrations of NO and N_2O of Run 10 where lignite is co-fired with limestone and cotton residue ($X_{N_2,lig}$ = 0.80, $X_{NH_3,lig}$ = 0.1, $X_{HCN,lig}$ = 0.1, $X_{N_2,CR}$ = 0.95, $X_{NH_3,CR}$ = 0.025, $X_{HCN,CR}$ = 0.025)

Another parametric study is performed to investigate the influence of the fraction of N_2 released in the volatile nitrogen, X_{N_2}, during devolatilization of lignite and cotton residue on NO and N_2O emissions of Run 10 (Figure 5.8). As illustrated in the figure, the concentrations of NO and N_2O decrease as the amount of N_2 released during devolatilization increases. This can be attributed to the fact that molecular nitrogen, N_2, is not involved in NO and N_2O formation and reduction mechanism under the low temperatures prevailing in FBCs as it was discussed in Chapter 2. The observed effect of N_2 fraction in volatile nitrogen is more intense for cotton residue due to its high nitrogen content. Reasonable agreement between the predicted and measured NO and N_2O concentration when utilizing X_{N_2} values, 0.80 for lignite and 0.95 for cotton residue based on previous pyrolysis studies [51,52], reflects the proximity of the assumption to the reality.

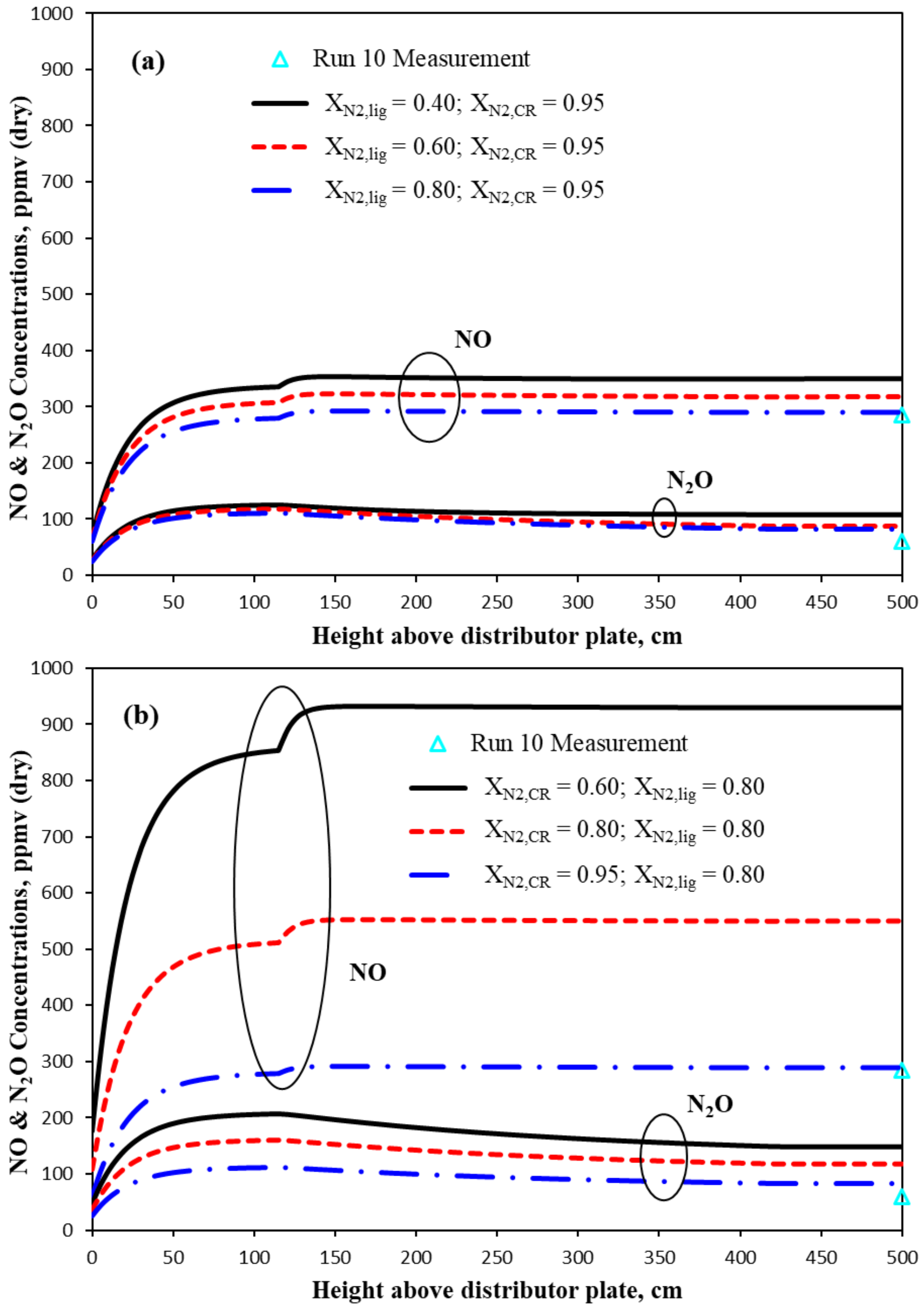

Figure 5.8 The influence of N_2 fraction in the volatile nitrogen, X_{N_2}, (a) for lignite (b) for cotton residue, on the concentrations of NO and N_2O of Run 10 where lignite is co-fired with limestone and cotton residue ($X_{N,vol,lig}$ = 0.35, $X_{NH_3,lig}$ = 0.1, $X_{HCN,lig}$ = 0.1, $X_{N,vol,CR}$ = 0.82, $X_{NH_3,CR}$ = 0.025, $X_{HCN,CR}$ = 0.025)

Furthermore, the influence of the distribution of NH_3 and HCN in volatile nitrogen for lignite and cotton residue on NO and N_2O formation and reduction in Run 10 is investigated in Figure 5.9 (a) and (b), respectively. As the fraction of NH_3 in the volatile nitrogen, X_{NH_3}, increases, concentration of NO and N_2O in the freeboard decreases owing to enhanced rate of homogenous NO reduction in the presence of ammonia (R13). Reasonable agreement is found between the predicted and measured NO and N_2O emissions when experimentally measured values of X_{NH_3}, 0.1 for lignite and 0.025 for cotton residue, and X_{HCN}, 0.1 for lignite and 0.025 for cotton residue, are utilized.

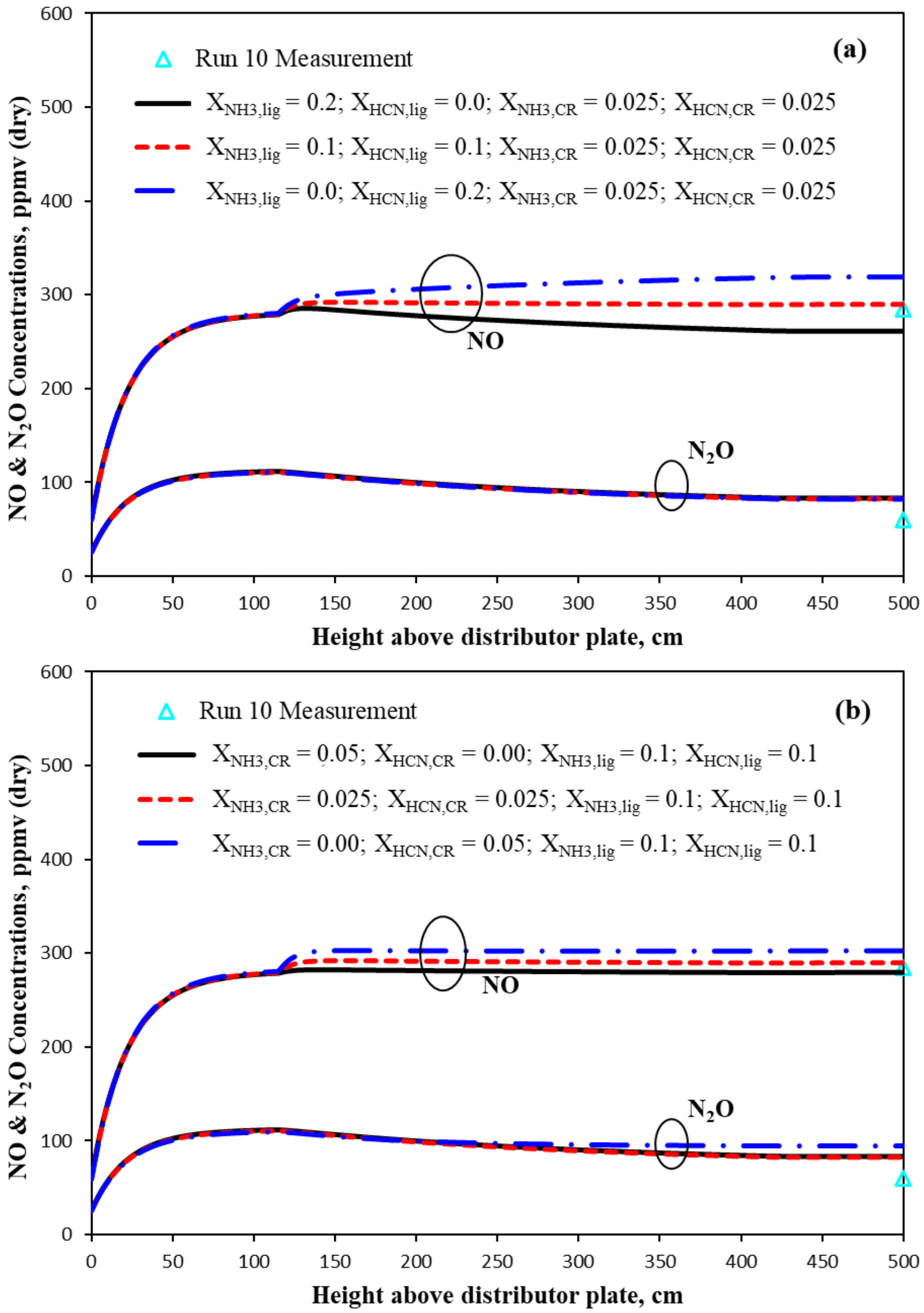

Figure 5.9 The influence of NH_3 and HCN fraction in the volatile nitrogen, X_{NH_3}, X_{HCN} (a) for lignite (b) for cotton residue on the concentrations of NO and N_2O of Run 10 where lignite is co-fired with limestone and cotton residue ($X_{N,vol,lig}$ = 0.35, $X_{N_2,lig}$ = 0.80, $X_{N,vol,CR}$ = 0.82, $X_{N_2,CR}$ = 0.95)

5.7 Gaseous Emissions

The gaseous emissions predictions and measurements are compared in Table 5.1. As depicted in the table, reasonable agreement is obtained between the measurements and predictions of gaseous emissions except CO emissions. This is considered to be due to deployment of a kinetic rate expression for CO oxidation developed for combustion of CO in gas phase only at high temperatures, as no kinetic rate expression for CO oxidation in the bed section of a fluidized bed combustor where lower temperatures and high concentrations of lignite and ash prevail, was available in the literature.

Table 5.1 Predicted and measured gaseous emissions for all tests under consideration

	O_2, %	**CO, %**	**CO_2, %**	**SO_2, ppm**	**NO, ppm**	**N_2O, ppm**
Run 1 Prediction	4.2	0.09	14.0	4892	269	32
Run 1 Measurement	4.8	0.05	15.2	4507	227	26
Relative Error, %	**13**	**80**	**8**	**8**	**19**	**23**
Run 2 Prediction	4.0	0.08	15.3	861	236	16
Run 2 Measurement	4.9	0.05	16.1	630	246	23
Relative Error, %	**18**	**60**	**5**	**36**	**4**	**30**
Run 9 Prediction	3.3	0.05	16.1	703	219	40
Run 9 Measurement	3.3	0.09	17.2	925	185	43
Relative Error, %	**0**	**44**	**6**	**24**	**18**	**7**
Run 10 Prediction	5.1	0.03	14.5	572	289	80
Run 10 Measurement	5.1	0.06	15.3	486	285	60
Relative Error, %	**0**	**50**	**5**	**18**	**1**	**33**

CHAPTER 6

CONCLUSION

Combustion of a typical Turkish lignite, having high VM/FC ratio, sulfur and ash contents, with and without limestone addition and co-combustion of Turkish lignite with limestone and cotton residue, with high nitrogen content, is investigated by extending a previously developed system model for co-firing of lignite and cotton residue for incorporation of N_2O formation and reduction mechanism. The system model accounts for bed and freeboard hydrodynamics, volatile release and combustion, char combustion, particle size distribution, heat transfer, sulfur retention and NO and N_2O formation and reduction. The assessment of the accuracy of the model is achieved by comparing its predictions against the experimental data obtained in METU 0.3 MW_t ABFBC where a typical Turkish lignite, with high VM/FC ratio (~ 1.2) and high ash content (~ 27 wt. %) and high sulfur content (~ 3.5 wt. %), with and without limestone is fired and Turkish lignite with limestone and cotton residue, with high nitrogen content (~ 4.1 wt. %), is co-fired in their own ashes.

On the basis of the experimental observations and comparisons of the model predictions with measurements, the following conclusions have been reached:

- Predictions of O_2, CO, CO_2, SO_2, NO and N_2O concentrations and temperature profiles are found to be in good agreement with the experimental data.
- NO and N_2O formation and reduction mechanism employed in this study sufficiently represents the NO and N_2O chemistry of lignite and cotton residue used in this study.
- Determination of fuel nitrogen partitioning into char and volatiles and distribution of volatile nitrogen species (NH_3, HCN, N_2) are essential for modeling of NO and N_2O emissions in fluidized bed combustors.

- Oxidation of char nitrogen in the emulsion phase dominates the formation of both NO and N_2O in the combustor.
- Addition of cotton residue increases emission of total nitrogenous species due to its high nitrogen content. The main effect is observed in the increase in the net N_2O formation.

6.1 Suggestions for Future Work

Based on the experience gained in this study, the following recommendations for a future study are suggested.

- A radiation model is required to be coupled to freeboard heat transfer model for a more a realistic approximation of the actual physical phenomena.
- Use of different volatile release sub-models in the literature in conjunction with the current system model is suggested.

REFERENCES

[1] "International Energy Agency (IAE) - Key World Energy Statistics 2017," accessed August 26, 2018, https://www.iea.org/publications/freepublications/publication/KeyWorld2017.pdf.

[2] "Republic of Turkey Ministry of Energy and Natural Resources – Coal," accessed August 26, 2018, http://www.enerji.gov.tr/en-US/Pages/Coal.

[3] "Turkish Statistical Institute (TSI)," accessed August 26, 2018, http://www.turkstat.gov.tr/PreTablo.do?alt_id=1001.

[4] Hocaoğlu, S. M., Haksevenler, H. G., Baştürk, İ., and Aydöner, C., 2015, Zeytin Sektörü Atıklarının Yönetimi, TÜBİTAK-MAM Project No: 5148602.

[5] "Turkish Ministry of Trade," accessed August 26, 2018, http://koop.gtb.gov.tr/data/5ad06bb9ddee7dd8b423eb23/2017FındıkRaporu.pdf.

[6] Sılgır, N., 2015, "An Investigation on the Determination of Nutrient Contents of Cottonseed Meals Produced in Çukurova Region," M.Sc. Thesis, Mustafa Kemal University, Hatay, Turkey.

[7] Selçuk, N., Degirmenci, E., and Gogebakan, Y., 2003, "Modeling of a Bubbling AFBC with Volatiles Release," J. Energy Resour. Technol., **125**(1), p. 72–81.

[8] Gogebakan, Y., and Selçuk, N., 2004, "Assessment of a Model with Char Attrition for a Bubbling Atmospheric Fluidized-Bed Combustor," Combust. Sci. Technol., **176**(5–6), pp. 799–818.

[9] Altindag, H., Gogebakan, Y., and Selçuk, N., 2004, "Sulfur Capture for Fluidized-Bed Combustion of High-Sulfur Content Lignites," Appl. Energy, **79**(4), pp. 403–424.

[10] Afacan, O., Gogebakan, Y., and Selçuk, N., 2007, “Modeling of NO_x Emissions from Fluidized Bed Combustion of High Volatile Lignites,” Combust. Sci. Technol., **179**(1–2), pp. 227–247.

[11] Kulah, G., Morali, E. M., and Selçuk, N., 2010, “Mathematical Modeling of a Bubbling Fluidized Bed Combustor Cofired with Lignite and Biomass,” Combust. Sci. Technol., **182**(7), pp. 600–612.

[12] Kulah, G., 2010, “Validation of a FBC Model for Co-Firing of Hazelnut Shell with Lignite against Experimental Data,” Exp. Therm. Fluid Sci., **34**(5), pp. 646–655.

[13] Gogebakan, Z., Gogebakan, Y., and Selçuk, N., 2008, “Co-Firing of Olive Residue with Lignite in Bubbling FBC,” Combust. Sci. Technol., **180**(5), pp. 854–868.

[14] Gogebakan, Z., and Selçuk, N., 2008, “Cofiring Lignite with Hazelnut Shell and Cotton Residue in a Pilot-Scale Fluidized Bed Combustor,” Energy Fuels, **22**(3), pp. 1620–1627.

[15] Gogebakan, Z., and Selçuk, N., 2009, “Trace Elements Partitioning during Co-Firing Biomass with Lignite in a Pilot-Scale Fluidized Bed Combustor,” J. Hazard. Mater., **162**(2–3), pp. 1129–1134.

[16] Selçuk, N., Gogebakan, Y., Harmandar, H., and Altindag, H., 2004, “Effect of Recycle on Fluidized-Bed Combustion and Emission Characteristics of High-Sulfur Lignite,” Combust. Sci. Technol., **176**(5–6), pp. 959–975.

[17] Sanger, M., Werther, J., and Ogada, T., 2001, “NO_x and N_2O Emission Characteristics from Fluidised Bed Combustion of Semi-Dried Municipal Sewage Sludge,” Fuel, **80**, pp. 167–177.

[18] Marias, F., Benzaoui, A., Vaxelaire, J., Gelix, F., and Nicol, F., 2015, “Fate of Nitrogen during Fluidized Incineration of Sewage Sludge. Estimation of NO and N_2O Content in the Exhaust Gas,” Energy Fuels, **29**(7), pp. 4534–4548.

[19] “United States Environmental Protection Agency (US EPA) - Overview of Greenhouse Gas (GHG) Emissions,” accessed August 26, 2018, https://www.epa.gov/ghgemissions/overview-greenhouse-gases.

[20] Hayhurst, A. N., and Lawrence, A. D., 1992, “Emissions of Nitrous Oxide from Combustion Sources,” Prog. Energy Combust. Sci., **18**, pp. 529–552.

[21] Selçuk, N., and Sivrioğlu, Ü., 1980, “Mathematical Modeling of Coal-Fired Fluidized Beds,” J. Therm. Sci. Tech-Jpn., **3**(1), pp. 31–38.

[22] Hayhurst, A. N., and Lawrence, A. D., 1996, “The Amounts of NO_x and N_2O Formed in a Fluidized Bed Combustor during the Burning of Coal Volatiles and Also of Char,” Combust. Flame, **105**(1), pp. 341–357.

[23] Williams, A., Jones, J. M., Ma, L., and Pourkashanian, M., 2012, “Pollutants from the Combustion of Solid Biomass Fuels,” Progr. Energy Combust. Sci., **38**(2), pp. 113–137.

[24] Glarborg, P., Jensen, A. D., and Johnsson, J. E., 2003, “Fuel Nitrogen Conversion in Solid Fuel Fired Systems,” Progr. Energy Combust. Sci., **29**(2), pp. 89–113.

[25] Konttinen, J., Kallio, S., Hupa, M., and Winter, F., 2013, “NO Formation Tendency Characterization for Solid Fuels in Fluidized Beds,” Fuel, **108**, pp. 238–246.

[26] Tian, F. J., Yu, J., McKenzie, L. J., Hayashi, J. I., and Li, C. Z., 2007, “Conversion of Fuel-N into HCN and NH_3 during the Pyrolysis and Gasification in Steam: A Comparative Study of Coal and Biomass,” Energy Fuels, **21**(2), pp. 517–521.

[27] Yuan, S., Zhou, Z. J., Li, J., and Wang, F. C., 2012, “Nitrogen Conversion during Rapid Pyrolysis of Coal and Petroleum Coke in a High-Frequency Furnace,” Appl. Energy, **92**, pp. 854–859.

[28] Abelha, P., Gulyurtlu, I., and Cabrita, I., 2008, “Release of Nitrogen Precursors from Coal and Biomass Residues in a Bubbling Fluidized Bed,” Energy Fuels, **22**(1), pp. 363–371.

[29] Aho, M. J., Hämäläinen, J. P., and Tummavuori, J. L., 1993, “Importance of Solid Fuel Properties to Nitrogen Oxide Formation through HCN and NH_3 in Small Particle Combustion,” Combust. Flame, **95**, pp. 22–30.

[30] Friebel, J., and Köpsel, R. F. W., 1999, “Fate of Nitrogen during Pyrolysis of German Low Rank Coals - a Parameter Study,” Fuel, **78**(8), pp. 923–932.

[31] Wu, Z., and Ohtsuka, Y., 1996, “Remarkable Formation of N_2 from a Chinese Lignite during Coal Pyrolysis,” Energy Fuels, **10**(6), pp. 1280–1281.

[32] Levendis, Y. A., Joshi, K., Khatami, R., and Sarofim, A. F., 2011, “Combustion Behavior in Air of Single Particles from Three Different Coal Ranks and from Sugarcane Bagasse,” Combust. Flame, **158**(3), pp. 452–465.

[33] Gogebakan, Z., 2007, “Co-Firing Biomass with Coal in Bubbling Fluidized Bed Combustors,” Ph.D. dissertation, Middle East Technical University, Ankara, Turkey.

[34] Liu, Z., and Balasubramanian, R., 2014, “A Comparative Study of Nitrogen Conversion during Pyrolysis of Coconut Fiber, Its Corresponding Biochar and Their Blends with Lignite,” Bioresour. Technol., **151**, pp. 85–90.

[35] Tan, L. L., and Li, C.-Z., 2000, “Formation of NO_x and SO_x Precursors during the Pyrolysis of Coal and Biomass. Part II. Effects of Experimental Conditions on the Yields of NO_x and SO_x Precursors from the Pyrolysis of a Victorian Brown Coal,” Fuel, **79**(15), pp. 1891–1897.

[36] Hayashi, J., Kusakabe, K., Morooka, S., Nielsen, M., and Furimsky, E., 1995, “Role of Iron Catalyst Impregnated by Solvent Swelling Method in Pyrolytic Removal of Coal Nitrogen,” Energy Fuels, **9**(6), pp. 1028–1034.

[37] Di Nola, G., 2007, “Biomass Fuel Characterization for NO_x Emissions in Co-Firing Applications,” Ph.D. dissertation, Delft University of Technology, Delft, The Netherlands.

[38] Sun, Z., Shen, J., Jin, B., and Wei, L., 2010, “Combustion Characteristics of Cotton Stalk in FBC,” Biomass Bioenergy, **34**(5), pp. 761–770.

[39] El-Sayed, S. A., and Mostafa, M. E., 2014, “Pyrolysis Characteristics and Kinetic Parameters Determination of Biomass Fuel Powders by Differential Thermal Gravimetric Analysis (TGA/DTG),” Energ. Convers. Manage., **85**, pp. 165–172.

[40] Zhu, D., Yang, H., Chen, Y., Li, Z., Wang, X., and Chen, H., 2017, “Fouling and Slagging Characteristics during Co-Combustion of Coal and Biomass,” BioRes., **12**(3), pp. 6322–6341.

[41] Zhuang, H., Niu, Y., Gong, Y., Zhang, Y., Zhang, Y., and Hui, S., 2017, “Influence of Biomass Reburning on NO_x Reductions during Pulverized Coal Combustion,” Energy Fuels, **31**(5), pp. 5597–5602.

[42] Thomas, K. M., 1997, “The Release of Nitrogen Oxides during Char Combustion,” Fuel, **76**(6), pp. 457–473.

[43] Molina, A., Eddings, E. G., Pershing, D. W., and Sarofim, A. F., 2000, “Char Nitrogen Conversion: Implications to Emissions from Coal-Fired Utility Boilers,” Progr. Energy Combust. Sci., **26**(4), pp. 507–531.

[44] Yuan, S., Zhou, Z. J., Li, J., Chen, X. L., and Wang, F. C., 2010, “HCN and NH_3 Released from Biomass and Soybean Cake under Rapid Pyrolysis,” Energy Fuels, **24**(11), pp. 6166–6171.

[45] Ren, Q., and Zhao, C., 2015, “Evolution of Fuel-N in Gas Phase during Biomass Pyrolysis,” Renew. Sust. Energ. Rev., **50**, pp. 408–418.

[46] Becidan, M., Skreiberg, Ø., and Hustad, J. E., 2007, “NO_x and N_2O Precursors (NH_3 and HCN) in Pyrolysis of Biomass Residues,” Energy Fuels, **21**(2), pp. 1173–1180.

[47] Leppälahti, J., and Koljonen, T., 1995, “Nitrogen Evolution from Coal, Peat and Wood during Gasification: Literature Review,” Fuel Process. Technol., **43**(1), pp. 1–45.

[48] Svoboda, K., Cermak, J., and Trnka, O., 2000, “Chemistry and Emissions of Nitrogen Oxides (NO, NO_2, N_2O) in Combustion of Solid Fuels I. Heterogeneous Reactions - NO + NO_2,” J. Chem. Pap., **54**(2), pp. 104–117.

[49] Solomon, P. R., Serio, M. A., and Suuberg, E. M., 1992, “Coal Pyrolysis: Experiments, Kinetic Rates and Mechanisms,” Progr. Energy Combust. Sci., **18**(2), pp. 133–220.

[50] Hannes, J. P., 1996, “Mathematical Modelling of Circulating Fluidized Bed Combustion,” Ph.D. dissertation, RWTH, Aachen, Germany.

[51] Wu, Z., and Ohtsuka, Y., 1997, “Key Factors for Formation of N_2 from Low-Rank Coals during Fixed Bed Pyrolysis: Pyrolysis Conditions and Inherent Minerals,” Energy Fuels, **11**(4), pp. 902–908.

[52] Yuan, S., Chen, X. L., Li, W. F., Liu, H. F., and Wang, F. C., 2011, “Nitrogen Conversion under Rapid Pyrolysis of Two Types of Aquatic Biomass and Corresponding Blends with Coal,” Bioresour. Technol., **102**(21), pp. 10124–10130.

[53] Bassilakis, R., Zhao, Y., Solomon, P. R., and Serio, M. A., 1993, “Sulfur and Nitrogen Evolution in the Argonne Coals: Experiment and Modeling,” Energy Fuels, **7**(6), pp. 710–720.

[54] Zhan, H., Yin, X., Huang, Y., Yuan, H., Xie, J., Wu, C., Shen, Z., and Cao, J., 2017, “Comparisons of Formation Characteristics of NO_x Precursors during Pyrolysis of Lignocellulosic Industrial Biomass Wastes,” Energy Fuels, **31**(9), pp. 9557–9567.

[55] Chen, H., Wang, Y., Xu, G., and Yoshikawa, K., 2012, “Fuel-N Evolution during the Pyrolysis of Industrial Biomass Wastes with High Nitrogen Content,” Energies, **5**(12), pp. 5418–5438.

[56] Winter, F., Wartha, C., and Hofbauer, H., 1999, "NO and N_2O Formation during the Combustion of Wood, Straw, Malt Waste and Peat," Bioresour. Technol., **70**(1), pp. 39–49.

[57] Johnsson, J. E., 1994, "Formation and Reduction of Nitrogen Oxides in Fluidized-Bed Combustion," Fuel, **73**(9), pp. 1398–1415.

[58] Desroches-Ducarne, E., Dolignier, J. C., Marty, E., Martin, G., and Delfosse, L., 1998, "Modelling of Gaseous Pollutants Emissions in Circulating Fluidized Bed Combustion of Municipal Refuse," Fuel, **77**(13), pp. 1399–1410.

[59] Liu, H., and Gibbs, B. M., 2002, "Modelling of NO and N_2O Emissions from Biomass-Fired Circulating Fluidized Bed Combustors," Fuel, **81**, pp. 271–280.

[60] Nikolopoulos, A., Malgarinos, I., Nikolopoulos, N., Grammelis, P., Karrelas, S., and Kakaras, E., 2014, "A Decoupled Approach for NO_x-N_2O 3-D CFD Modeling in CFB Plants," Fuel, **115**, pp. 401–415.

[61] Zhong, W., Xie, J., Shao, Y., Liu, X., and Jin, B., 2015, "Three-Dimensional Modeling of Olive Cake Combustion in CFB," Appl. Therm. Eng, **88**, pp. 322–333.

[62] Gungor, A., and Eskin, N., 2008, "Two-Dimensional Coal Combustion Modeling of CFB," Int. J. Therm. Sci., **47**(2), pp. 157–174.

[63] Gungor, A., 2009, "Simulation of NO_x Emission in Circulating Fluidized Beds Burning Low-Grade Fuels," Energy Fuels, **23**(5), pp. 2475–2481.

[64] Glarborg, P., Johnsson, J. E., and Dam-Johansen, K., 1994, "Kinetics of Homogenous Nitrous Oxide Decomposition," Combust. Flame, **99**, pp. 523–532.

[65] Johnsson, J. E., Åmand, L.-E., Dam-Johansen, K., and Leckner, B., 1996, "Modeling N_2O Reduction and Decomposition in a Circulating Fluidized Bed Boiler," Energy Fuels, **10**(4), pp. 970–979.

[66] Chen, Z., Lin, M., Ignowski, J., Kelly, B., Linjewile, T. M., and Agarwal, P. K., 2001, “Mathematical Modeling of Fluidized Bed Combustion. 4: N_2O and NO_x Emissions from the Combustion of Char,” Fuel, **80**(9), pp. 1259–1272.

[67] Goel, S. K., Morihara, A., Tullin, C. J., and Sarofim, A. F., 1994, “Effect of NO and O_2 Concentration on N_2O Formation during Coal Combustion in a Fluidized-Bed Combustor: Modeling Results,” 25th Symp. (Int.) on Combustion, The Combustion Institute, Irvine, California, pp. 1051–1059.

[68] Winter, F., Wartha, C., Löffler, G., and Hofbauer, H., 1996, “The NO and N_2O Formation Mechanism during Devolatilization and Char Combustion under Fluidized-Bed Conditions,” 26th Symp. (Int.) on Combustion, The Combustion Institute, Napoli, Italy, pp. 3325–3334.

[69] Goel, S., Sarofim, A., Kilpinen, P., and Hupa, M., 1996, “Emissions of Nitrogen Oxides from Circulating Fluidized-Bed Combustors: Modeling Results Using Detailed Chemistry,” 26th Symp. (Int.) on Combustion, The Combustion Institute, Napoli, Italy, **26**(2), pp. 3317–3324.

[70] Selçuk, N., Batu, A., and Oymak, O., 2003, “NO_X Emissions from Combustion of High Sulfur Lignite in an ABFBC Test Rig,” 17th Int. Con. on FBC, ASME, Jacksonville, Florida USA, pp. 1–6.

[71] Shimizu, T., Tachiyama, Y., Kuroda, A., and Inagaki, M., 1992, “Effect of SO_2 Removal by Limestone on NO_x and N_2O Emissions from a Bubbling Fluidized-Bed Combustor,” Fuel, **71**, pp. 841–844.

[72] Wojtowicz, M. A., Pels, J. R., and Moulijn, J. A., 1993, “Combustion of Coal as a Source of N_2O Emission,” Fuel Process. Technol., **34**, pp. 1–71.

[73] Mann, M. D., Collings, M. E., Dakota, N., and Box, P. O., 1992, “Nitrous Oxide Emissions in Fluidized Bed Combustion: Fundamental Chemistry and Combustion Testing,” Progr. Energy Combust. Sci., **18**, pp. 447–461.

[74] Löffler, G., Andahazy, D., Wartha, C., Winter, F., and Hofbauer, H., 2001, “NO_x and N_2O Formation Mechanisms - A Detailed Chemical Kinetic Modeling Study on a Single Fuel Particle in a Laboratory-Scale Fluidized Bed,” J. Energy Resour. Technol., **123**(3), pp. 228-235.

[75] Zhou, W., Zhao, C. S., Duan, L. B., Chen, X. P., and Liang, C., 2011, “Two-Dimensional Computational Fluid Dynamics Simulation of Nitrogen and Sulfur Oxides Emissions in a Circulating Fluidized Bed Combustor,” Chem. Eng. J., **173**(2), pp. 564–573.

[76] Sung, L. Y. J., 1995, “NO_x and N_2O Emissions from Circulating Fluidized Bed Combustion,” M.Sc. Thesis, University of British Columbia, Vancouver, Canada.

[77] Goel, S. K., Beer, J. M., and Sarofim, A. F., 1996, “An Emission Model for a Bubbling FBC Using Detailed Chemical Kinetics: Significance of Destruction Reactions,” J. Instit. Energy, **69**, pp. 201–213.

[78] Löffler, G., Wargadalam, V. J., and Winter, F., 2002, “Catalytic Effect of Biomass Ash on CO, CH_4 and HCN Oxidation under Fluidised Bed Combustor Conditions,” Fuel, **81**(6), pp. 711–717.

[79] Chan, L. K., Sarofim, A. F., and Beer, J. M., 1983, “Kinetics of the NO-Carbon Reaction at Fluidized Bed Combustor Conditions,” Combust. Flame, **52**, pp. 37–45.

[80] Furusawa, T., Tsunoda, M., Tsujimura, M., and Adschiri, T., 1985, “Nitric Oxide Reduction by Char and Carbon Monoxide Fundamental Kinetics of Nitric Oxide Reduction in Fluidized-Bed Combustion of Coal,” Fuel, **64**, pp. 1306–1309.

[81] Svoboda, K., Cermak, J., and Hartman, M., 2000, “Chemistry and Emissions of Nitrogen Oxides (NO, NO_2, N_2O) in Combustion of Solid Fuels II. Heterogeneous Reaction - N_2O,” J. Chem. Pap., **54**(2), pp. 118–130.

[82] Johnsson, J. E., and Dam-Johansen, K., 1991, "Formation and Reduction of NO_x in a Fluidized Bed Combustor," 11th Int. Con. on FBC, ASME, New York USA, pp. 1389–1396.

[83] Li, Y. H., Lu, G. Q., and Rudolph, V., 1998, "The Kinetics of NO and N_2O Reduction over Coal Chars in Fluidised-Bed Combustion," Chem. Eng. Sci., **53**(1), pp. 1–26.

[84] Rodriguez-Mirasol, J., Ooms, A. C., Pels, J. R., Kapteijn, F., and Moulijn, J. A., 1994, "NO and N_2O Decomposition over Coal Char at Fluidized-Bed Combustion Conditions," Combust. Flame, **99**(3–4), pp. 499–507.

[85] Johnsson, J. E., 1989, "Modeling of NO_x Formation in Fluidized Bed Combustion," Fluidization VI: Proceedings of the 6th Int. Conf. on Fluidization, Engineering Foundation, New York, USA, pp. 435–442.

[86] Jensen, A., Johnsson, J. E., and Dam-Johansen, K., 1996, "Nitrogen Chemistry in FBC with Limestone Addition," 25th Symp. (Int.) on Combustion, The Combustion Institute, Irvine, California, pp. 3335–3342.

[87] Zhou, H., Flamant, G., Gauthier, D., and Flitris, Y., 2003, "Simulation of Coal Combustion in a Bubbling Fluidized Bed by Distinct Element Method," Chem. Eng. Res. Des., **81**(9), pp. 1144–1149.

[88] Zhou, H., Flamant, G., and Gauthier, D., 2004, "DEM-LES of Coal Combustion in a Bubbling Fluidized Bed. Part I: Gas-Particle Turbulent Flow Structure," Chem. Eng. Sci., **59**(20), pp. 4193–4203.

[89] Gungor, A., 2010, "Simulation of Emission Performance and Combustion Efficiency in Biomass Fired Circulating Fluidized Bed Combustors," Biomass Bioenergy, **34**(4), pp. 506–514.

[90] Gungor, A., 2013, "Simulation of Co-Firing Coal and Biomass in Circulating Fluidized Beds," Energ. Convers. Manage., **65**, pp. 574–579.

[91] Krzywanski, J., Rajczyk, R., Bednarek, M., Wesolowska, M., and Nowak, W., 2013, “Gas Emissions from a Large Scale Circulating Fluidized Bed Boilers Burning Lignite and Biomass,” Fuel Process. Technol., **116**, pp. 27–34.

[92] Xie, J., Zhong, W., Jin, B., Shao, Y., and Liu, H., 2014, “Three-Dimensional Eulerian-Eulerian Modeling of Gaseous Pollutant Emissions from Circulating Fluidized-Bed Combustors,” Energy Fuels, **28**(8), pp. 5523–5533.

[93] Xie, J., Zhong, W., Shao, Y., Liu, Q., Liu, L., and Liu, G., 2017, “Simulation of Combustion of Municipal Solid Waste and Coal in an Industrial-Scale Circulating Fluidized Bed Boiler,” Energy Fuels, **31**(12), pp. 14248–14261.

[94] Yu, G., Chen, J., Li, J., Hu, T., Wang, S., and Lu, H., 2014, “Analysis of SO_2 and NO_x Emissions Using Two-Fluid Method Coupled with Eddy Dissipation Concept Reaction Submodel in Circulating Fluidized Bed Combustors,” Energy Fuels, **28**(3), pp. 2227–2235.

[95] Lu, L., Ismail, T. M., Jin, Y., Abd El-Salam, M., and Yoshikawa, K., 2016, “Numerical and Experimental Investigation on Co-Combustion Characteristics of Hydrothermally Treated Municipal Solid Waste with Coal in a Fluidized Bed,” Fuel Process. Technol., **154**, pp. 52–65.

[96] Field, M. A., Gill, D. W., Morgan, B. B., and Hawksley, P. G. W., 1967, *Combustion of Pulverized Coal,* British Coal Utilization Research Association Leatherhead, England.

[97] Adánez, J., De Diego, L. F., García-Labiano, F., Abad, A., and Abanades, J. C., 2001, “Determination of Biomass Char Combustion Reactivities for FBC Applications by a Combined Method,” Ind. Eng. Chem. Res., **40**(20), pp. 4317–4323.

[98] Hottel, H. C., Williams, G. C., Nerheim, N. M., and Schneider, G. R., 1965, “Kinetic Studies in Stirred Reactors: Combustion of Carbon Monoxide and Propane,” 10th Symp. (Int.) on Combustion, The Combustion Institute, Cambridge, England, pp. 111–121.

[99] Duo, W., Dam-Johansen, K., and Østergaard, K., 1992, "Kinetics of the Gas-phase Reaction between Nitric Oxide, Ammonia and Oxygen," Can. J. Chem. Eng., **70**(5), pp. 1014–1020.

[100] Loirat, H., Caralp, F., Destriau, M., and Lesclaux, R., 1987, "Oxidation of CO by N_2O between 1076 and 1228 K: Determination of the Rate Constant of the Exchange Reaction," J. Phys. Chem., **91**(26), pp. 6538–6542.

[101] Bonn, B., Pelz, G., and Baumann, H., 1995, "Formation and Decomposition of N_2O in Fluidized Bed Boilers," Fuel, **74**(2), pp. 165–171.

[102] Mori, S., and Wen, C. Y., 1975, "Estimation of Bubble Diameter in Gaseous Fluidized Beds," AIChE J., **21**(1), pp. 109–115.

[103] Davidson, J. F., and Harrison, D., 1963, *Fluidized Particles*, Cambridge University Press, New York.

[104] Gogolek, P. E. G., and Becker, H. A., 1992, "Calculation of the Expansion of a Bubbling Fluidised Bed of Coarse Particles," Powder Technol., **71**(1), pp. 107–110.

[105] Ergun, S., 1952, "Fluid Flow through Packed Columns," Chem. Eng. Prog., **48**(2), pp. 89–94.

[106] Jung, K., and La Nauze, R. D., 1983, "Sherwood Numbers for Burning Particles in Fluidized Beds," 4th Conf. (Int.) on Fluidization, Engineering Foundation, Koshikojima, Japan, pp. 427–434.

[107] Incropera, F. P., and DeWitt, D. P., 1990, *Fundementals of Heat and Mass Transfer*, 3rd ed., John Wiley & Sons, Inc., New York.

[108] Kunii, D., and Levenspiel, O., 1969, *Fluidization Engineering*, Wiley, New York.

[109] Choi, J. H., Chang, I. Y., Shun, D. W., Yi, C. K., Son, J. E., and Kim, S. D., 1999, "Correlation on the Particle Entrainment Rate in Gas Fluidized Beds," Ind. Eng. Chem. Res., **38**(6), pp. 2491–2496.

[110] Kunii, D., and Levenspiel, O., 1992, “Heat Transfer between Fluidized Beds and Wall Surfaces,” 7th Conference (International) on Fluidization, Engineering Foundation, Brisbane, Australia, pp. 47–58.

[111] Denloye, A. O. O., and Botterill, J. S. M., 1978, “Bed to Surface Heat Transfer in a Fluidized Bed of Large Particles,” Powder Technol., **19**(2), pp. 197–203.

[112] Sleicher, C. A., and Rouse, M. W., 1975, “A Convenient Correlation for Heat Transfer to Constant and Variable Property Fluids in Turbulent Pipe Flow,” Int. J. Heat Mass Tran., **18**(5), pp. 677–683.

[113] Grace, J. R., and Clift, R., 1974, “On the Two-Phase Theory of Fluidization.,” Chem. Eng. Sci., **29**(2), pp. 327–334.

[114] Grace, J. R., and Harrison, D., 1969, “The Behaviour of Freely Bubbling Fluidised Beds,” Chem. Eng. Sci., **24**(3), pp. 497–508.

[115] Hazlett, J. D., and Bergougnou, M. A., 1992, “Influence of Bubble Size Distribution at the Bed Surface on Entrainment Profile,” Powder Technol., **70**, pp. 99–107.

[116] Stubington, J. F., Chan, S. W., and Clough, S. J., 1990, “A Model for Volatiles Release into a Bubbling Fluidized-bed Combustor,” AIChE J., **36**(1), pp. 75–85.

[117] Anthony, D. B., and Howard, J. B., 1976, “Coal Devolatilization and Hydrogastification,” AIChE J., **22**(4), pp. 625–656.

[118] Değirmenci, E., 2000, “Dynamic Simulation of Fluidized Bed Combustors,” Ph.D. dissertation, Middle East Technical University, Ankara, Turkey.

[119] Kunii, D., and Levenspiel, O., 1991, *Fluidization Engineering,* 2nd ed., Butterworth-Heinemann, USA.

[120] Altindağ, H., 2003, “Mathematical Modeling of Sulfur Retention in Fluidized Bed Combustors,” M.Sc. Thesis, Middle East Technical University, Ankara, Turkey.

[121] Jensen, A., Johnsson, J. E., Andries, J., Laughlin, K., Read, G., Mayer, M., Baumann, H., and Bonn, B., 1995, "Formation and Reduction of NO_x in Pressurized Fluidized-Bed Combustion of Coal," Fuel, **74**(11), pp. 1555–1569.

[122] Afacan, O., 2005, "Mathematical Modeling of NO_x Emissions in Bubbling Fluidized Bed Combustors," M.Sc. Thesis, Middle East Technical University, Ankara, Turkey.

[123] Gogebakan, Z., Gogebakan, Y., Selçuk, N., and Selçuk, E., 2009, "Investigation of Ash Deposition in a Pilot-Scale Fluidized Bed Combustor Co-Firing Biomass with Lignite," Bioresource Technol., **100**(2), pp. 1033–1036.

[124] Vermeulen, I., Block, C., and Vandecasteele, C., 2012, "Estimation of Fuel-Nitrogen Oxide Emissions from the Element Composition of the Solid or Waste Fuel," Fuel, **94**, pp. 75–80.

APPENDICES

A. Freeboard Sulfation Rates

A.1. Sulfation Rates due to Sorbents Carried to Freeboard by Elutriation

In this study, the sulfation rate is assumed to be in first order in SO_2 concentration and reactive sorbent surface area, and it is expressed as:

$$r_{SO_2} = kC_{SO_2}S_0\sigma_{avg} \tag{A.1}$$

where total initial external surface area for spherical sorbent particles can be expressed as:

$$S_0 = \frac{6M_{CaO}}{\rho_{CaO}d_p} \tag{A.2}$$

M_{CaO}, which is hold-up of elutriated sorbent particles in freeboard, in Equation (A.2) can be defined by dividing the mass flowrate of elutriable sorbent particles to the residence time of particles.

$$M_{CaO} = \int_{r_{max}}^{r_{maxe}} \frac{F_{CaO}P_{bed,CaO}(r)}{\tau_{elut}}\,dr \tag{A.3}$$

Equation (A.4) can be rearranged by assuming that the fine particles rise at the superficial gas velocity.

$$M_{CaO} = \int_{r_{max}}^{r_{maxe}} \frac{F_{CaO}P_{bed,CaO}(r)(u_0 - u_t)}{H_f}\,dr \tag{A.4}$$

By combining Equations (A.1), (A.2) and (A.4), the overall sulfation rate for the fine sorbent particles carried by elutriation can be obtained:

$$r_{SO_2,elut} = kC_{SO_2}\frac{F_{CaO}}{\rho_{CaO}H_f}\left[\int_{r_{max}}^{r_{maxe}} \frac{P_{bed,CaO}(r)(u_0 - u_t)}{r_p}\,dr\right]\sigma_{avg} \tag{A.5}$$

A.2. Sulfation Rate due to Sorbents Carried to Freeboard by Bubble Eruption

For the coarse sorbent particles carried to freeboard due to bubble eruption, the sorbent hold-up can be defined by multiplying the volume occupied by CaO particles with the density of CaO particles:

$$M_{CaO} = V_f \rho_{CaO} \int_{r_{maxe}}^{r_{max}} \varepsilon_{CaO} P_{z,CaO}(r) dr \tag{A.6}$$

By combining Equations (A.2) and (A.6), the initial sorbent surface area of coarse particles carried by bursting bubbles can be expressed as,

$$S_0 = V_f \left[3 \int_{r_{maxe}}^{r_{max}} \frac{\varepsilon_{CaO} P_{z,CaO}(r)}{r_p} dr \right] \tag{A.7}$$

Finally, by combining Equations (A.1) and (A.7), the overall sulfation rate due to coarse particles carried by bubble eruption can be written as:

$$r_{SO_2,ent} = k C_{SO_2} V_f \left[3 \int_{r_{maxe}}^{r_{max}} \frac{\varepsilon_{CaO} P_{z,CaO}(r)}{r_p} dr \right] \sigma_{avg} \tag{A.8}$$

B. Nitrogen Partitioning into Char and Volatiles

The partitioning of fuel-N to char bound nitrogen and volatile nitrogen is estimated based on the dry basis mass fraction of char and volatile matter contents of the fuel for lignite, i.e., the ratio of char nitrogen to total nitrogen is equal to mass fraction of char in the parent fuel. The dry basis proximate analyses of the lignite used in the combustion tests are shown in the Table A1.

Table B.1 Proximate analyses of lignite, dry basis.

	Lignite			
	Run 1	Run 2	Run 9	Run 10
Proximate Analyses, dry basis				
Volatile Matter	35.61	37.18	37.34	38.10
Fixed Carbon	30.09	30.82	30.05	32.47
Ash	34.41	32.02	32.62	29.43
Char – VM Percentages, dry basis				
Volatile Matter	35.61	37.18	37.34	38.10
Char	64.39	62.84	62.68	61.90
Char-N/Fuel-N	0.65	0.63	0.63	0.62

C. Particle Size Distribution

C.1. Sieve Analyses

Table C.1 Sieve analyses of lignite and cotton residue [33]

Sieve opening (mm)	Weight (%)				
	Lignite				Cotton
	Run 1	Run 2	Run 9	Run 10	Residue
19.000 - 16.000	0.000	0.000	0.000	0.000	1.668
16.000 - 12.700	1.078	2.033	0.880	1.091	6.351
12.700 - 8.000	3.042	8.434	7.186	3.788	31.647
8.000 - 6.300	4.896	9.236	6.399	5.155	12.523
6.300 - 4.750	6.103	10.413	5.935	6.152	7.596
4.750 - 3.350	16.859	23.378	13.784	16.308	14.561
3.350 - 2.000	13.565	13.265	10.686	13.340	7.896
2.000 - 1.000	21.478	14.160	18.022	20.997	7.903
1.000 - 0.500	10.851	5.553	11.099	11.408	2.986
0.500 - 0.355	5.823	2.687	6.580	6.185	0.000
0.355 - 0.180	5.553	2.555	7.280	6.441	5.495
0.180 - 0.106	4.094	2.681	4.635	3.716	0.000
0.106 - 0.000	6.659	5.606	7.515	5.420	1.374

Table C.2 Size distribution of limestone [33]

Sieve opening (mm)	**Weight (%)**
1.180 - 1.000	14.795
1.000 - 0.850	5.286
0.850 - 0.710	6.257
0.710 - 0.600	10.657
0.600 - 0.500	3.837
0.500 - 0.425	9.738
0.425 - 0.355	6.135
0.355 - 0.180	15.060
0.180 - 0.106	10.487
0.106 - 0.000	17.748

Table C.3 Size distribution of bottom ashes [33]

Sieve opening (mm)	**Weight (%)**			
	Run 1	**Run 2**	**Run 9**	**Run 10**
8.000 - 6.300	0.003	0.580	1.013	0.866
6.300 - 4.750	0.123	1.458	2.340	2.671
4.750 - 3.350	4.140	9.269	10.147	10.960
3.350 - 2.000	6.572	11.480	9.530	9.775
2.000 - 1.000	47.066	36.110	25.887	26.182
1.000 - 0.500	37.191	31.478	37.141	42.894
0.500 - 0.355	4.578	8.795	13.400	5.964
0.355 - 0.180	0.102	0.550	0.371	0.244
0.180 - 0.106	0.048	0.089	0.036	0.127
0.106 - 0.000	0.176	0.189	0.196	0.318

C.2. Rosin-Rammler Size Distribution Functions

The size distribution of lignite, cotton residue and limestone were determined by sieve analysis and were expressed by the following Rosin-Rammler size distribution function in the system model:

$$P_0\left(d_p\right) = \exp(-b\, d_p^n) \qquad \text{(C.1)}$$

Parameter b and n in Equation (C.1) were calculated by carrying out non-linear regression using Microsoft Excel. Calculates values of the coefficients can be found in Table C.4

Table C.4 Rosin-Rammler function fitting results for solid feed streams

	n	***b***	**Correlation Coefficient**	**Standard Error**
Lignite Run 1	0.90	3.41	0.999	0.012
Lignite Run 2	1.09	2.55	0.996	0.042
Lignite Run 9	0.78	2.79	0.999	0.012
Lignite Run 10	0.91	3.36	0.999	0.010
Cotton Residue	1.40	1.43	0.996	0.031
Limestone	1.06	20.74	0.995	0.008
Bottom Ash Run 1	2.63	75.68	0.999	0.017
Bottom Ash Run 2	1.83	15.41	0.998	0.034
Bottom Ash Run 9	1.59	11.69	0.996	0.069
Bottom Ash Run 10	1.67	12.48	0.994	0.097

In Figure C.1 to Figure C.6 fitted Rosin-Rammler forms of lignite, cotton residue and limestone are present. As it can be observed from the figures, Rosin-Rammler function represents the size distribution accurately.

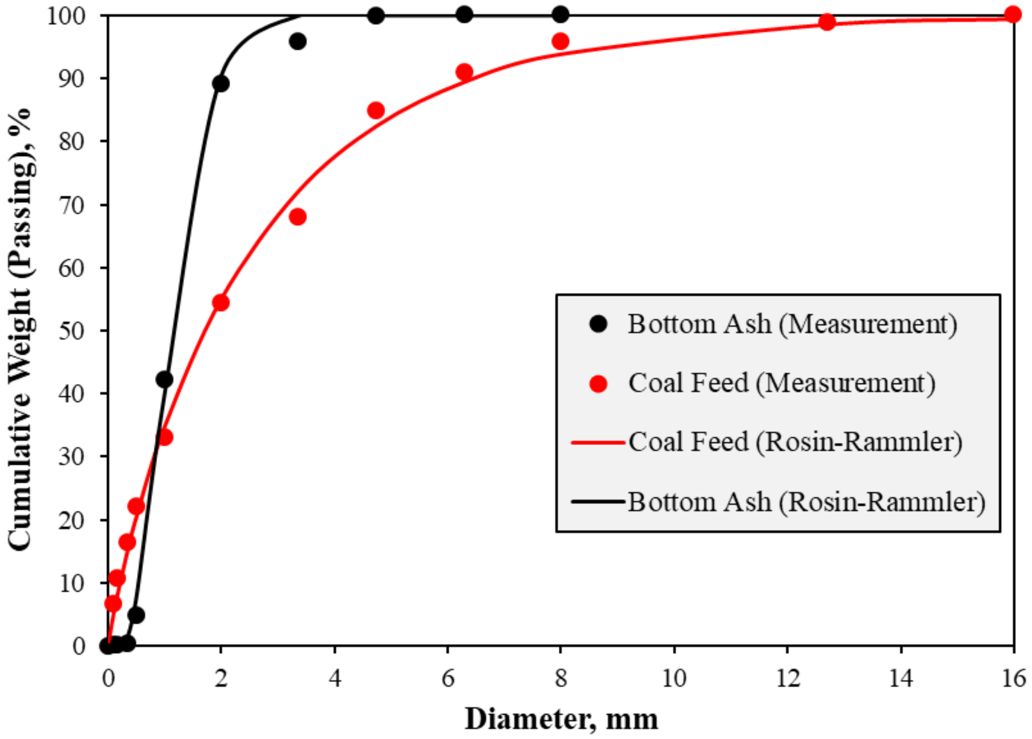

Figure C.1 Fitted Rosin-Rammler form of lignite and bottom ash (Run 1)

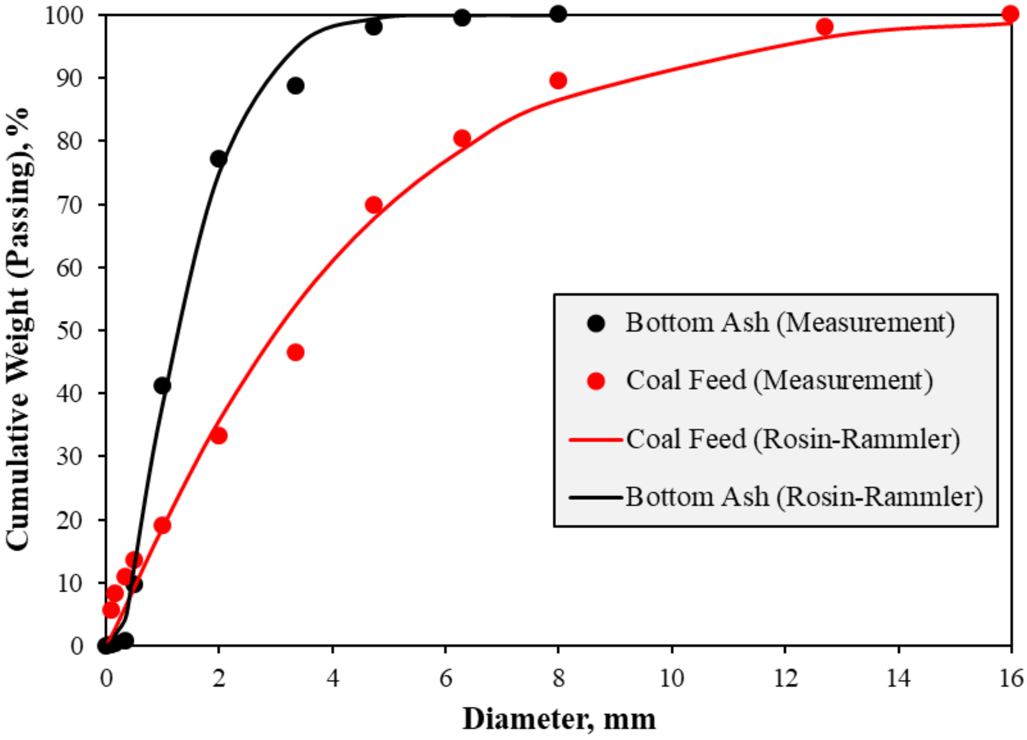

Figure C.2 Fitted Rosin-Rammler form of lignite and bottom ash (Run 2)

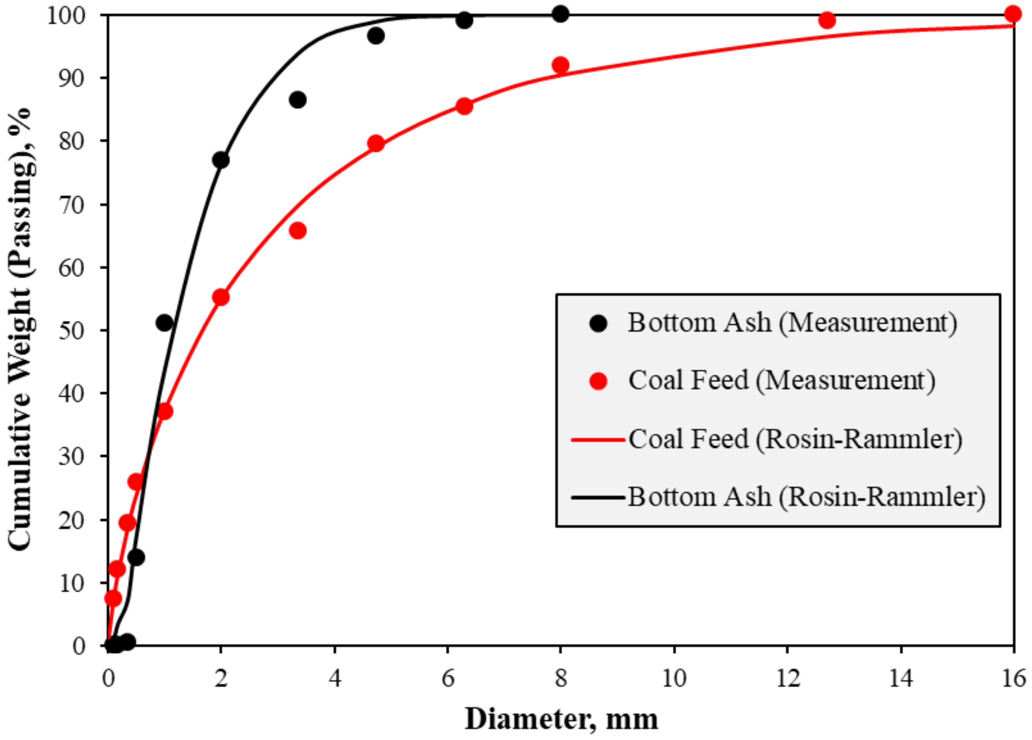

Figure C.3 Fitted Rosin-Rammler form of lignite and bottom ash (Run 9)

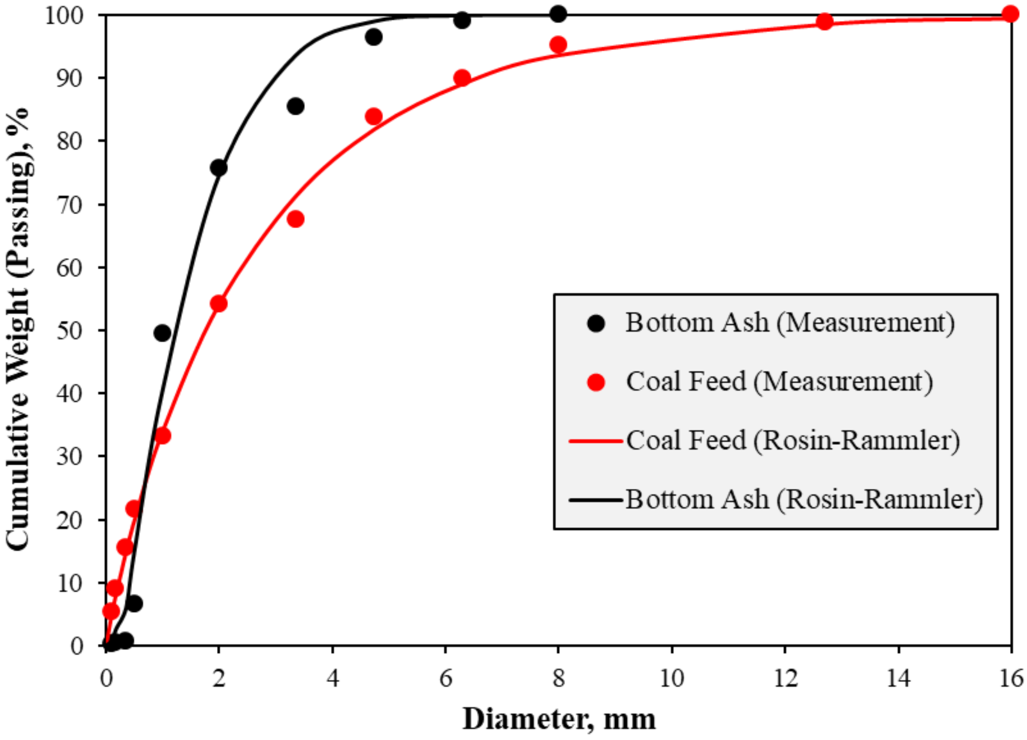

Figure C.4 Fitted Rosin-Rammler form of lignite and bottom ash (Run 10)

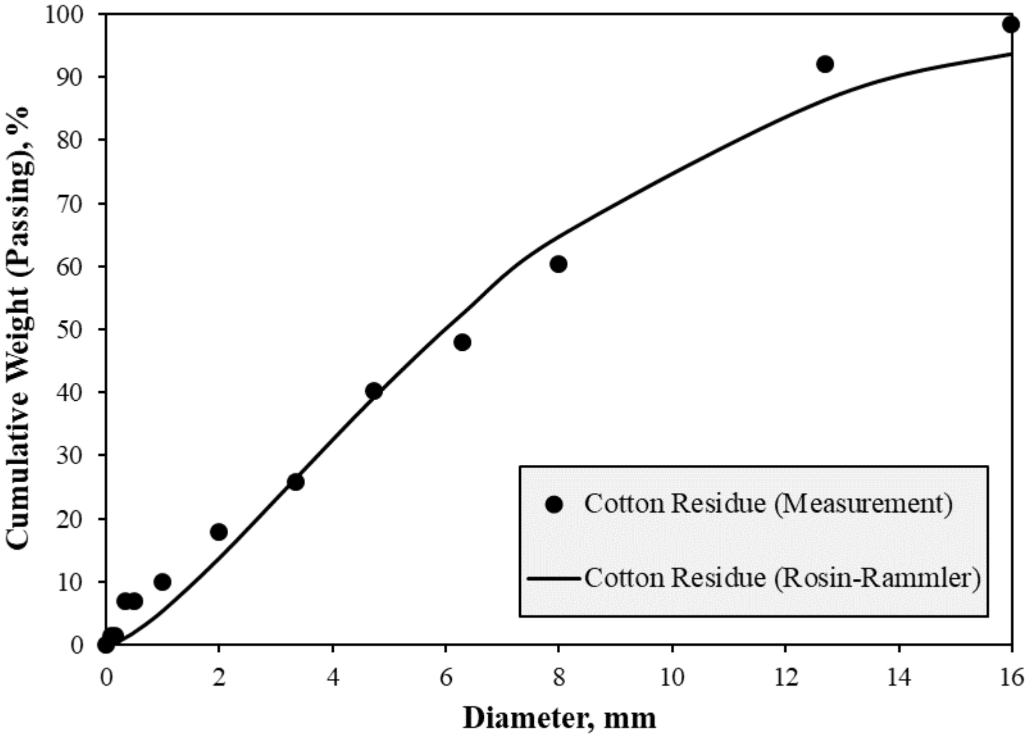

Figure C.5 Fitted Rosin-Rammler form of cotton residue

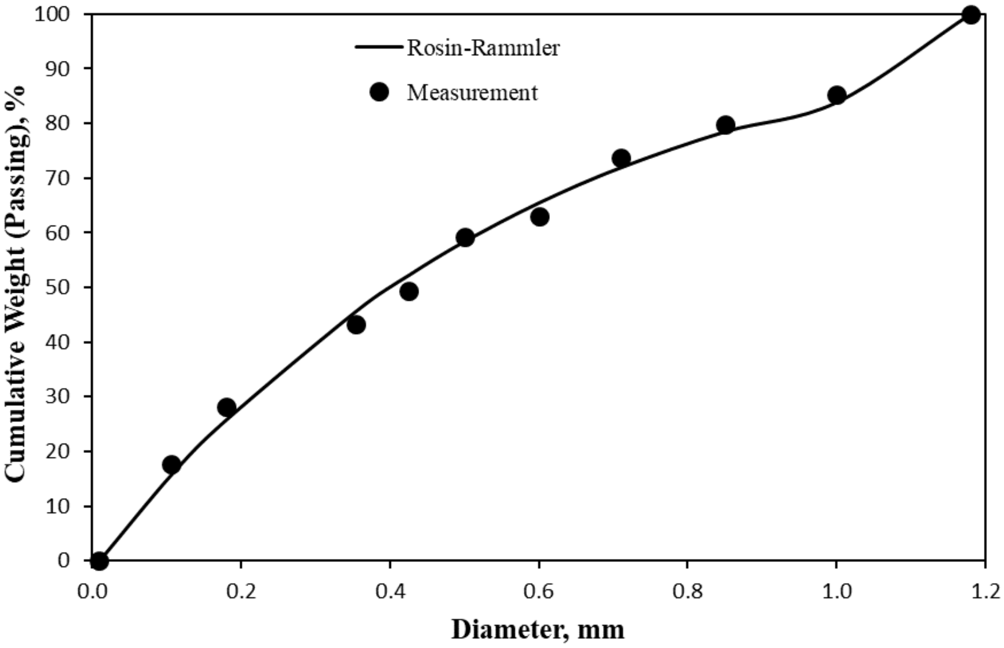

Figure C.6 Fitted Rosin-Rammler form of limestone